Topology Optimization for Damage Tolerance

A.J.J. Lagerweij

TU Delft

Topology Optimization for Damage Tolerance

Master of Science Thesis

For obtaining the degree of Master of Science in Aerospace Engineering
at Delft University of Technology

A.J.J. Lagerweij
4272080

May 7, 2019

Aerospace Structures and Materials · Faculty of Aerospace Engineering · Delft University of Technology

Delft University of Technology
Faculty of Aerospace Engineering
Department of Aerospace Structures and Materials

GRADUATION COMMITTEE

Graduation Date: May 17, 2019

Chair of the Committee: _____

dr.ir. S.R. Turteltaub

Daily supervisor: _____

dr.ir. C.D. Rans

Second daily supervisor: _____

dr.ir. J. Wu

Other committee members: _____

dr.ir. B. Chen

Acknowledgments

The master thesis in front of you was created because of a meeting with Calvin Rans. His introduction into optimization for damage tolerance objectives and the problems that can be encountered made me so excited that I wanted to make it my thesis topic. Back then, I did not know that it would take me more than fifteen months to complete this study about topology optimization for minimal fatigue crack growth. In this time, not only did I write a thesis that I am proud of, but I also learned much about computational modeling, programming and above all I learned about writing. I am happy to obtain these skills and am sure that they will benefit me in the future.

I wish to express my gratitude to everyone that helped me while writing this thesis. First and foremost my thanks go to my supervisor, Calvin Rans, who guided and helped me throughout the entire process. Being my supervisor is a difficult task. I would barge in on a daily basis just to talk, only sometimes I had actual questions or updates. Nevertheless, he was always there for me and managed to make me get back to work with renewed motivation. Secondly, I would like to show my appreciation to professors Jun Wu, Sergio Turteltaub and Boyang Chen. They were there to assist me with answers to questions about optimization, mathematics or finite element modeling. I am grateful to Gert-Jan Mulder and the other ASML lab technicians for the assistance they provided during my tests. Testing is harder than it seems, especially for someone with two left hands like me. Their guidance made sure that I did not damage the specimens, the machines or myself before completing the measurements.

Special thanks goes to all my friends and family, these people stuck with me, even during the difficult times that I encountered. Most important was Kyra van der Heijden who, besides living with me, had to read through everything that I have written. On numerous occasions did the mistakes in my miserably bad drafts make her feel sad or laugh to tears. Without her advice and support this thesis would not exist.

Bram Lagerweij
Delft, May 2019

Abstract

The aerospace industry has a lot of interest in additive manufacturing (AM). One of the reasons for this interest is caused by the complex topologies that can be produced with it. This means that it is possible to design parts that are lighter, which saves fuel, costs and reduces the environmental impact. The geometrical complexity that can be achieved translates into an increase in possible designs which causes difficulties in the designing process. The traditional design process might work well for simple constructions, but it is unable to grasp all the possibilities in a very large and complex design space. When the traditional process is used for AM parts, it is slow and the final design might not be the optimal one.

A design process with computational optimization will enable engineers to use the geometrical freedom offered by AM. These optimization algorithms will design a structure that performs most optimal within certain constraints. This study explores how topology optimization can be used to design structures that are fatigue tolerant. A structure that can sustain damage is called damage tolerant. Because of safety concerns damage tolerance is a requirement for aerospace structures. Damage tolerance can be related to crack propagation when fatigue is considered.

Two optimization algorithms for fatigue tolerance were developed in this thesis. One algorithm minimizes the stress intensity factor (SIF), whereas the other one maximizes the fatigue crack growth life (FCGL). The difference between the SIF minimization and FCGL maximization is that the first one considers the crack growth rate for a crack of a specific length, whereas the other considers the crack growth from the starting crack length until the final one. Both algorithms use a resource constraint to limit the total amount of material, an enriched finite element method to analyze the crack growth performance and the method of moving asymptotes to incrementally improve the design. The enriched finite element method was chosen, because it determines the stress intensity factor directly when solving the FE problem. This simplified the adjoint gradient calculation, which is required for the method of moving asymptotes.

The optimization algorithms were used to optimize three different types of structures:

- A discrete structure where the algorithm determines where to assign material and where not.
- An infill optimization case which is similar to the discrete one. However, here the material is added to an existing geometry. This existing geometry cannot be altered.
- A variable thickness plate structure with the local thicknesses as design variables. The algorithm reinforces a flat plate by distributing extra material.

Optimizing the SIF for discrete or infill structures resulted in designs that closed the crack tip. Closing the crack tip under loading means that the tip is compressed, which stops the fatigue propagation entirely. However, these designs cannot directly be used in structures, they are too susceptible to other failure modes.

Minimizing the SIF of the variable thickness plate showed more promising results. The SIF was reduced by 30 to 40 percent, with respect to a flat plate of the same weight. For 3D printed titanium this would reduce the crack growth rate by 80 to 90 percent. The actual gain in fatigue crack growth life is less, as that is also dependent on the performance at other crack lengths. Nevertheless, the FCGL maximization designed variable thickness plates with more than double the FCGL of a flat plate with similar weight. This was obtained from an algorithm that enforces a straight crack and which does not allow the thickness to change in elements along the crack path. It is believed that an algorithm with crack steering will result in even better performing structures.

List of Figures

List of Tables

Contents

Chapter 1

Introduction

Additive manufacturing (AM) is a group of manufacturing methods with unprecedented capabilities causing it to gain major interest of both the public and industry for over the past ten years [1]. Figure 1.1 shows what kind of complex geometries can be manufactured. These organic looking structures can incorporate the features of multiple traditional parts reducing the part count and the assembly costs. The complex parts are potentially lighter and can lead to reduce fuel costs in the aerospace industry. Hence, these manufacturing processes are promising for the aerospace industry [2].

An engineer has a great design freedom which allows for better performing structures, but it will also increase the difficulty of the designing process. Currently the engineer uses analytical approximations and gut feeling in the design process. From these equations the current performance can be determined and improvements can be identified. Iterative improvements are made until the engineer is satisfied with the performance. Then finite element methods (FEM) or tests are performed to verify and validate the performance.

Imagine that one has to design the parts in fig. 1.1 starting off with the left part. Using the traditional approach is unlikely to lead to the lightweight part at the right. The simplified analytical expression cannot capture the structural behavior which means that numerical methods such as FEM are required from the start. In contrasts to the analytical expressions do FEM do not tell how the design can be improved and due to the complexity it might be impossible to identify these improvements, even for experienced engineers.

It has been acknowledged that an optimization driven design process can enable the entire geometrical freedom offered by the AM techniques [4, 5]. Topology optimization (TO) is a method that finds the optimal material distribution of a problem [6]. Various objectives can be optimized with this method. Examples are; (end)compliance, strength, heat conduction or antenna gain [6–9]. Some topology optimization formulations are tailored to consider the maneuverability with AM processes [10, 11].

One of the main problems in the aerospace industry is that of fatigue resistance. This needs to be tackled with a damage tolerant approach due to safety requirements. This approach recognizes that failure

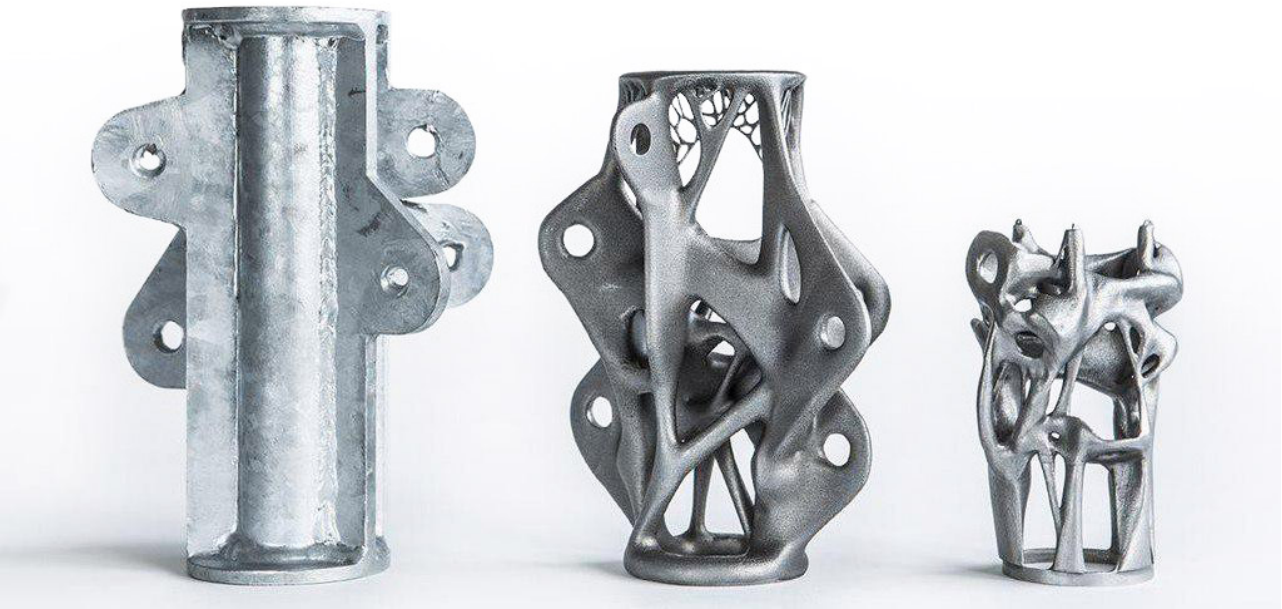

Figure 1.1: Optimized organic designs for additive manufacturing [3].

cannot entirely be avoided. Damage tolerant parts are designed such than even in the case of failure the mission can safely be fulfilled due to alternative load paths. Regular inspections are required to detect and repair the failed parts.

Few tolerant fatigue optimizations have been found in literature. A study of J. Lu, N. Kashaev and N. Huber [12], developed an algorithm that optimizes the crenelation pattern for fatigue crack growth life of a stiffened plate. Here they assume a pre-existing crack as well. However these studies use search methods such as genetic or biological algorithms. This is less efficient than gradient based versions.

An attempt that used gradient methods was made by Z. Kang, P. Liu and M. Li [13]. They developed a bi-criteria optimization that minimizes both the compliance and strain energy release rate of a structure with an existing crack. Minimizing the strain energy release rate reduces the crack growth rate, resulting in an increased fatigue crack growth life. This method does not optimize the entire growth behavior, only the crack growth rate for the crack at one specific location and length.

The author of this thesis was motivated by these two methods to develop a fatigue crack growth life maximization that uses a gradient method. The objective of this thesis was to explore optimizations that increase the fatigue tolerance. For that purpose two algorithms where developed, one that minimizes the crack growth rate and another that maximizes the fatigue crack growth life.

The crack growth rate minimization similar to the strain energy release rate minimization of Z. Kang [13], because it does only conciser the crack growth speed at one moment in time. The difference lies in the use of stress intensity factors instead of the strain energy release rate. Because of the enrichment FE method the stress intensity is obtained directly from the FEA. This makes the formulation more direct. Hence, the algorithm can be expanded more easily, so that it can optimize more complex problems.

The second algorithm is an example of such an expansion, it is a fatigue crack growth life maximization algorithm. This algorithm maximizes the amount of cycles the crack requires to grow to a maximum length. This is, to the author's knowledge, the first fatigue crack growth life topology optimization in existence.

This report is divided in three parts, a literature study, the development and presentation of the algorithm and a conclusion. To identify and specify the research topics a literature study was performed, part I contains the summary of this study. It examines the fatigue processes, gives an overview of topology optimization and discusses existing damage tolerance optimizations. This literature study is concluded in chapter 5, where the thesis scope is specified, the objective is formulated and the methodology which is used in the rest of the thesis is presented.

Part II discusses the mathematical definition and implementation of both algorithms in detail. It presents the validation of the FE method and explores capabilities of the algorithm by optimizing different example problems.

The thesis concludes in part III with the results, conclusions, recommendations and future work. The recommendations describe readily available methods to improve the algorithms in speed and capabilities. Whereas, the future work discusses promising new research topics which could assist in the development and adaptation of damage tolerant optimization algorithms.

Part I

Literature Study

Chapter 2

Fatigue of structures

Fatigue is a phenomena that causes material to weakening due to cyclic loading. Because, repeated load cycles are required before the damage becomes critical the fatigue failure mode is most commonly observed in structures with repeated use. Examples of cyclic loading can be found in the transportation, petrol and machine sector due to waves, pressure cycles, accelerations, shocks and others.

Fatigue can cause failure at loads magnitudes below the static failure limit. The failure can occur without any warning and little plastic deformation. This means that testing a part at the expected load once, as is done to test mechanical overload failure, is not sufficient, the test needs to be repeated, thousands or even millions of times before the fatigue becomes critical. These fatigue tests are time-consuming and expensive which can cause problems during the design and certification of a structure.

Most of the time the fatigue process is invisibly small, only at the end of the fatigue life, just before failure, a macroscopic crack can be observed. Predicting exactly when fatigue becomes critical is near impossible because of the probabilistic nature of the process and the amount of variables that play a role in it. The only way to ensure safety is to regularly inspect the fatigue critical locations. The interval between inspections should be smaller than the time required for the barely visible crack to grow until failure.

Cost related to structural failure, of which fatigue is a significant part, are enormous. Research indicates that around 4% of the GDP is spent on structural failure related costs (USA: $199bn per year 1982 [14], EU: ±4% GDP/year in 1991 [15]). These costs are caused by:

- repair or replacement,
- loss of revenue while unavailable,
- replacement because of unavailability,
- consequential damage,
- prevention (for example recalls),
- sub-optimal operations (overdesign),
- inspection/maintenance,
- testing, and
- other implications (loss of confidence/image).

Fatigue life can be split in three phases, crack initiation period, crack growth period and final failure. The last phase, final failure, will not be considered in this chapter. The first section, section 2.1, will discuss how cracks initiate, what processes and variables play a role in it and most importantly how it is predicted. The second section, section 2.2, discusses the fatigue crack growth phase.

2.1 Crack initiation period

The fatigue initiation period is the phase of crack nucleation and micro cracking. Initiation is influenced by surface and micro structural effects.

The time, or amount of cycles, required for crack initiation can be significant in terms of fatigue life [16, sec. 2.5]. This is surprising because the cracks are smaller, less than 0.5 mm, then those observed at final failure [17]. This means that the most significant impact on the fatigue life can be made by designing structured with a prolonged initiation period.

2.1.1 Mechanical drivers

Research into a railway accident in 1842 showed that a locally increased surface stress could reduce the fatigue life. At these stress raisers, such as notches and cutouts, the stresses are locally increased due to the geometrical. At these locations the stresses can be a multitude of the far field stresses and at these locations fatigue will initiate.

That the cracks initiate at these stress raisers is logical, as cyclic slip requires a certain amount of stress to occur. This cyclic slip starts the initiation is caused by cyclic plastic dislocations in the crystal structure. Another feature that increases the likelihood of initiation is the presence of a free surface, as that is where the grains are less constrained causing the slip to occur at lower stresses.

Cracks are nucleated due to a repeatedly slipping. After a slip, a new surface is exposed to the environment. Oxidation and strain hardening cause this to be irreversible. Over time and after a many slipping actions a notch starts to appear with higher stresses at the tip causing the process to speed up.

This micro crack growth is still depended on surface properties and grain boundaries. Just by crossing a boundary the crack growth can slow down, and sometimes even stop.

Shortly, the following influences the crack initiation:

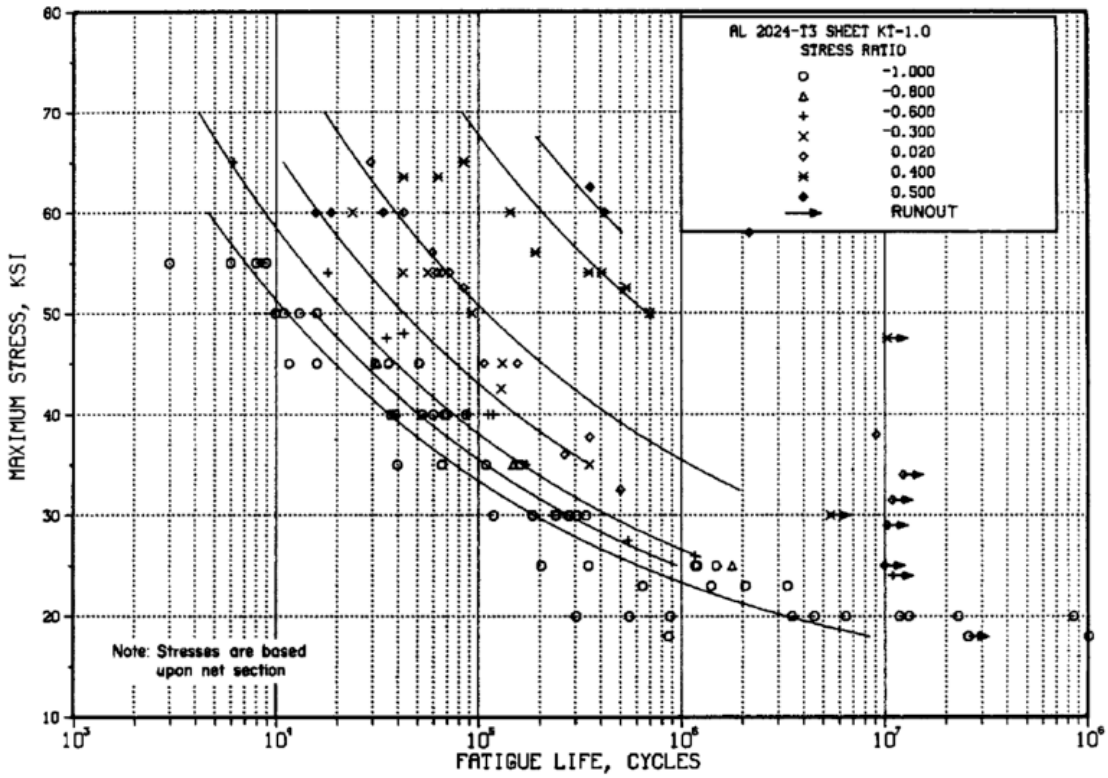

Figure 2.1: Best-fit S/N curves for unnotched sheets of Al 2024-T3 [19, Fig. 3.2.3.1.8(a)].

Load: magnitude and amplitude can cause the local stress field to change wile frequency and shape of the loading can cause the impact of the environment to change.

Geometric: features can cause the local stress to be higher than the stresses in the far field, this is related to the stress concentration.

Surface: properties play an effect such as, roughness and surface treatments. Cracks initiate faster on rough surfaces. Several surface treatments influence the initiation phase, most notably shot peeling which causes the surface to be under compression and reduce the speed of microscopic growth [18].

Environment: such as corrosion and fretting can roughen the surface and speed op the initiation phase.

(Micro) Material: properties such as the orientation of the slip planes, strength, toughness, grain size and boundary can cause changes in the crack nucleation phase.

2.1.2 Prediction of initiation

Initiation is treated as a probabilistic process. Determining moment of initiation exactly is impossible because there is little understanding of the physical processes. Even laboratory samples that are carefully processed in the same manner can show significant differences in the amount of load cycles required to initiate a crack.

With extensive measurements *S-N* (Wöhler) curves can be made, they link stress to fatigue life. The specimens used are designed such that final failure happens shortly after initiation. Hence, these diagrams relate the amount of cycles required for a crack to initiate. The load amplitude plays an important role in the initiation process, to capture this, the test are performed not only at different stress levels, but also at multiple load ratios ($R = S_{\min}/S_{\max}$). In the end statistical methods are used to best fit curves through the data. An example of the resulting curves can be found in fig. 2.1.

Generating these *S, R-N* curves is however costly. Many experiments are required while the results can only be used in specify situations. Take for example fig. 2.1. It required 107 specimens to determine the relation:

$$\log(N) = 11.1 - 3.97 \log\left(S_{\max}(1-R)^{0.56} - 15.8\right)$$

where the fit parameter is only $R^2 = 82\%$. The equation is only applicable to longitudinal oriented Aluminum (2024-T3) sheets with an eloctro-chemical polished surface in a standard laboratory environment (dry, ±21°C etc.). For other materials, surface treatments, environment and sheet orientation new tests need to be performed.

Some of the samples used to create fig. 2.1 never failed. For these so called runouts, noted by '→', the tests were stopped because of time limitations. From these *S-N* curves one can derive that some materials do not experience fatigue underneath a certain load, the so-called fatigue limit. When designing the

structure such it is assumed that no fatigue should occur when the local maximum stress stays below this limit.

The *S-N* curves shown in the example are based on unnotched specimens, specimens without stress raisers. A designer should be aware that their structures have stress raisers. The stresses of the critical location should be used for fatigue initiation predictions.

Better understanding of the physical phenomenons in crack initiation is required for more accurate predictions. Currently no better models available. Lack of physical understanding/models cause even larger uncertainties when more complicated problems are being solved. For example the models used to predict variable amplitude fatigue, are based on more statistics and best fit parameters. This causes more (unexplained) scatter and thus uncertainties.

2.1.3 Preventing crack initiation

As mentioned before, crack initiation can be prevented by designing such that the peak surface stress stays below the fatigue limit. There are however drawbacks when doing so. The fatigue limit is significantly below the yield stress the design becomes heavier than those that only take mechanical overloads in account. Besides the fatigue limit is not only influenced by the material but also by the surface conditions, such as fretting and corrosion, which are difficult to take in account. This makes it hard to ensure that fatigue will never occur.

Aerospace engineering requires lightweight structures. This means that overdesigning structures to avoid fatigue initiation is not possible. Therefore, the aerospace industry does not try to prevent fatigue initiation. Instead, it focuses on ensuring safety of structures that do fatigue. This is done by damage tolerance also named safety by inspection. Damage tolerant parts are designed such than even in the case of failure the mission can safely be fulfilled due to alternative load paths. Regular inspections are required to detect and repair parts that show fatigue damage.

Various methods are used to extend the fatigue initiation life. A combination of proper surface treatments, material selection and geometric designs improve the fatigue performance. When designing notches, the geometries are chosen such that the stresses are raised least.

Some optimization methods claim that the optimal design is one which has equal stresses everywhere. This means that all stress raisers are removed and that the fatigue life is thus optimal. However, these designs cause problems for inspections as fatigue cracks can initiate everywhere. Not having any critical regions would require inspectors to investigate every location increasing the amount of work and the related costs.

2.2 Crack growth period

The crack growth period starts when the crack is fully initiated, i.e. when the growth rate becomes independent of the surface and micro-structural effects. The two periods are treated separately because the mechanics behind are different. Although some physical understanding of the crack growth exists, the methods used to describe it are based on curve fitting. The models used in this thesis are based on linear elastic fracture mechanics, which is discussed in section 2.2.2.

This crack growth period will, in general, be a lot shorter than the crack initiation period. The crack will propagate faster when compared to the first phase, and will eventually result in failure.

This does not mean that the crack growth period is less important. As the crack becomes visible during this phase the inspection interval is linked to the time required by the crack to grow from (barley) visible to final failure. Especially for hard to reach cracks extending the crack growth phase could result in a larger inspection interval, reducing work, unavailability and costs. Besides the importance for inspection the crack path is required for a good damage tolerant design. To properly predict what the impact of part failure is, one is required to know how the part fails. For fatigue critical cases one needs to know what path the crack will take and how long the crack is before final failure.

2.2.1 Mechanical drivers

Crack tips are some type of stress raisers, the will cause the local stresses to increase. Compared to the crack initiation phase the stresses are even higher.

The crack will cause the stress field to become different from that of the uncracked part. When the crack growths it will change the stresses even more. Because the stress field is related to the crack growth rate the growth speed does also change with crack growth.

Shortly the following influences the crack nucleation:

Load: magnitude and amplitude can cause the local stress field to change wile frequency and shape of the loading can cause the impact of the environment to change.

Geometric: features can cause the stress state severity at the crack tip to change and can thus be related to the crack propagation speed.

Environment: properties can influence the crack growth rate. From experiments, it was observed that corrosive environments increase the crack growth rate.

Material: properties influence the crack growth rate.

2.2.2 Prediction of crack growth

Linking crack growth rate to tip stress, as is done for the initiation phase, is difficult as the tip stresses go towards infinity in linear elastic mechanics. The stresses go to infinity because it is assumed the crack tip is infinity sharp. Infinite stresses do not exist in reality, it is caused by the assumption that the material is linear elastic.

Instead of stresses at the tip, stress intensity factors are used. These factors are indications for the severity of the stress field around the crack, i.e. how fast the stresses go to infinity. In a two-dimensional space two stress intensity factors exist, K_I and K_{II} for mode I and mode II opening respectively.

The theory of stress intensity factors was developed by G.R. Irwin [20]. He proposed to describe the intensity of the stresses at the crack tip with $K_I = \lim_{r\to 0} \sqrt{2\pi r}\sigma_{yy}(r, 0)$. For the problem shown in fig. 2.2 the stress equations derived are:

$$\sigma_{xx} = \frac{K_I}{\sqrt{2\pi r}} \cos\frac{\theta}{2}\left(1 - \sin\frac{\theta}{2}\sin\frac{3\theta}{2}\right) - S \qquad (2.1)$$
$$\sigma_{yy} = \frac{K_I}{\sqrt{2\pi r}} \cos\frac{\theta}{2}\left(1 + \sin\frac{\theta}{2}\sin\frac{3\theta}{2}\right)$$
$$\tau_{xy} = \frac{K_I}{\sqrt{2\pi r}} \cos\frac{\theta}{2}\sin\frac{\theta}{2}\cos\frac{3\theta}{2}$$

In the value of K_I both the load and the are geometry considered.

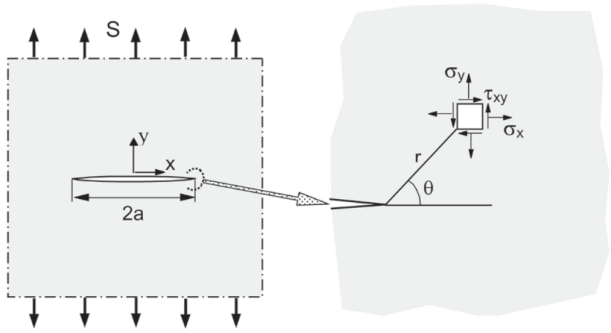

Figure 2.2: Infinite sheet with center crack, axis system definitions [16].

P. Paris, M. Gomez and W. Anderson [21] observed that for similar cases, with a constant $\Delta K = K_{max} - K_{min}$, the crack growth rate was constant. P. Paris and P. Erdogan [22] observed that plotting crack growth rate (da/dN) versus stress intensity (ΔK) in a log-log space results in linear lines. Therefore, they proposed a fit equation,

$$\frac{da}{dN} = C\,\Delta K^m \qquad (2.2)$$

understanding as the relation between crack growth rate and the stress intensity cycle.

Because the method is based on curve fitting, the variables C and m need to be obtained experimentally. The values of C and m are assumed to be constant for 'similar' cases. This means that experiments need to be performed for new materials, environments and load cycles (R or frequency).

The unit if the constant C is dependent on the magnitude of the power m [23]. This can create difficulties when converting[1] the units. For conversions within the metric system unruly factors have to be used. This thesis will use the following units for eq. (2.2),

$$\left[\frac{\text{mm}}{\text{cycle}}\right] = C\ [\text{MPa}\sqrt{\text{mm}}]^{[-]} \qquad (2.3)$$

even if constants are obtained from literature they will be converted to this system first.

2.2.3 Stress intensity factors

The stress intensity factor which describes the severity of the stress state around the crack contains information about both the geometry and the loading. For simple cases the stress intensity can be described with $K_I = \sigma\beta\sqrt{\pi a}$ [MPa$\sqrt{\text{mm}}$], here σ is the far-field stress, a the crack length and β an unitless geometry correction factor.

There exist three main methods to determine the stress intensity factor function of a geometry, algabraic determination β using for example the Westergaard function method, empirically fitting K_I as a function of load and geometric parameters or a finite element analysis.

The case of an infinite plate with a center crack can be approached with the Westergaard stress equations and results in a $\beta = 1$. Similar derivation, as shown by H. Tada [24], can be made for other geometries such as those of a finite width plate with a center crack where;

$$\beta = \sqrt{\frac{1}{\cos\left(\frac{\pi a}{W}\right)}} \qquad (2.4)$$

is a function of geometry only.

For more complex geometries empirical equations, where for example the far-field stress is undefined, are fitted to experiments or FEA. An example of such an empirical equation is the stress intensity calculation used for a flat compact tension (CT) specimens as proposed by the ASTM standard [25]:

$$K_I = \frac{P}{B\sqrt{W}} \frac{2 + \frac{a}{W}}{\left(1 - \frac{a}{W}\right)^{3/2}}\left[0.886 + 4.64\left(\frac{a}{W}\right) - 13.32\left(\frac{a}{W}\right)^2 + 14.75\left(\frac{a}{W}\right)^3 - 5.6\left(\frac{a}{W}\right)^4\right] \qquad (2.5)$$

this equation allows for quick calculation of stress intensity factors.

When working with arbitrary geometries FEA is the fastest way of obtaining a stress intensity value.

[1] A unit converter can be found at Zentech.

These calculations require a converged FE problem with a stress and displacement field that can handle the singularities that occur at crack tips. Four different extraction methods will be discussed, Stress extrapolation, displacement extrapolation, J-Integral and element enrichment.

Because the stress intensity is defined as a function of the stresses approaching the tip,

$$K_I = \lim_{r \to 0} \left[\sigma_{yy}(r, 0) \sqrt{2\pi r} \right] \tag{2.6}$$

the stress field around the crack tip can be used to extrapolate the stress intensity value [26, 27]. FEA calculates the displacements from which stresses can be obtained. The step of calculating stresses can be avoided by using the displacement field directly. It is derived from an integration of the strains related to the stress field around the tip, with $k = 3 - 4\nu$ for plain strain and $k = (3-\nu)/(1+\nu)$ for plain stress [28, pp. 569]. This means that along $\theta = \pi$ the stress intensity factor can be extrapolated as,

$$K_I = \lim_{r \to 0} \left[\frac{2G}{k+1} \sqrt{\frac{2\pi}{r}} u_y(r, \pi) \right] \tag{2.7}$$

The accuracy of both extrapolation methods is depended on the accuracy of the stress/displacement field around the crack tip. To model the displacement field at the crack tip special singularity elements must be used, an example for this is the quarter node element. These quarter node elements must be combined with local mesh refinement to obtain accurate results. When the crack growths and the location of the crack tip changes, the location of the crack tip elements and refinement needs changes as well. Hence, remeshing is required which reduces the efficiency of the algorithms.

A method that can be used without mesh refinement is based on the energy release rate, J. This energy release rate can be linked to both the deformation field and the stress intensity factor. The integral required to calculate J is path independent. That means that taking an arbitrary integral around the crack tip leads to the same result. The following equations depend on k, where $k = E$ for plane stress and $k = E/(1-\nu^2)$ for plain strain. Details on the other variables can be found in the papers from G.P. Cherepanov and J.R. Rice [29, 30].

$$J = \frac{1}{k} K_I^2 \tag{2.8}$$

$$J = \int_\Gamma \left(W dy - T \cdot \frac{\partial \boldsymbol{u}}{\partial x} \mathrm{d}s \right) \tag{2.9}$$

This method is more accurate than both extrapolation methods because it is not so dependent on the local stress and displacement field. However, the other methods allow the user to use the residual of the equation used for the extrapolation as a simple check to see whether the results are consistent [26].

The last method proposed is one that considers enriching the crack tip elements. The method used was developed by S. E. Benzley [31] and improved by L. N. Gifford [32]. It uses a linear summation of a continuous displacement field and a near crack tip displacement field capturing both the discrete behavior at the crack tip and the continuous one around it. The discrete solution was derived with the Westergaard function method [33]. This type of tip element enrichment allows accurate predictions of stress intensity directly from the FEA without any post processing as it can be found in the displacement vector.

The main benefits of this method are that:

- The stress intensity factors can be derived from the final displacement vector in the FEA. No post-processing is required.
- The resulting K_I and K_{II} are relatively insensitive to the mesh size. A relative course mesh can be used due to the high order of the tip element.
- An extension into 3D is readily available, developed by P.D. Hilton [34].
- An XFEM version exists which allows the cracks to propegate through the elements, described by X.Y. Liu, X.Z. Xiao and B.L. Karihaloo [35].

Drawbacks exist as well most notably that the method requires an element to be positioned at the crack tip exactly, when simulating growing cracks remeshing is required.

Chapter 3

Topology optimization

Structural optimization is a major topic in this communication. Proper understanding of it is required before a fatigue life optimization algorithm can be developed. This chapter will provide the reader with a basic insight into topology optimization. The optimization algorithm developed is based on the topology optimization.

Several structural optimization methods exist most notably; topology, shape and sizing optimization. This research focuses on topology optimization (TO) as it is the most general of the three methods. Sizing and shape optimization work with predefined geometries and cannot change the topology of the design anymore while TO can alter the layout of the structure. Within a design space it tries to distribute a limited amount of material such that a certain objective is maximized or minimized. This design space is limited by; the size of the design region, a material constrain, boundary conditions and others.

This chapter will introduce TO. It will discuss the formulation of a basic algorithm and the problems that can be encountered. It will provide the reader the basic grasp that is required before a change in optimization objective can be discussed. Therefore, section 3.1 will introduce a basic example of the TO algorithm that minimizes the global compliance, and thus maximizes stiffness. After which common problems such as non-uniqueness and mesh refinement will be discussed. If a solution for these problems is available they will be explained in section 3.2. The algorithm developed in this thesis does not try to maximize stiffness therefore section 3.3 discusses how to change objectives.

3.1 Global compliance TO

To introduce topology optimization a basic example algorithm is presented in this section. By explaining this basic algorithm the background of topology optimization can be comprehended. This knowledge will be applicable to other topology optimization examples as well and should be informative to anybody who wants a concise and clear introduction in topology optimization.

This type of TO tries to minimize the global compliance. It will be the main example algorithm as it has been researched and documented extensively among others by the TopOpt group at the Technical University of Denmark (DTU) [6, 7, 36–38]. The goal of the method is to minimize the compliance by distributing the assigned mass. It has to satisfy certain constraints, the volume constrain V limits the amount of mass available and the structure should be in equilibrium. If required, more constraints can be formulated. One can limit the size of the finest features and take manufacturing limitations in account or introduce a local density constraint to create porous structures which ensures structural stability [39].

Different implementations of global compliance TO exist, but only one will be presented here. It is based on a gradient method and thus requires a continuous expression for the compliance as a function of the mass/density distribution. Therefore, it must allow elements with density values that are between 0 and 1 and it uses a proportional stiffness with penalization method (SIMP) to approximate a discrete 0-1 problem. Other methods such as solving the discrete problem with genetic algorithms will not be shown. Maore information on those methods can be found

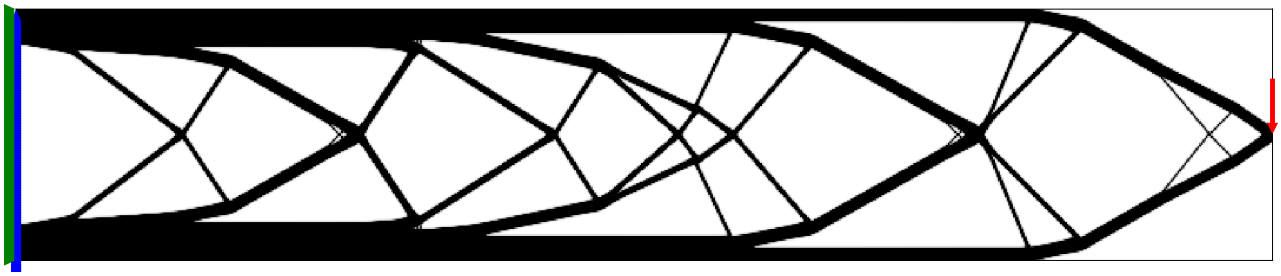

Figure 3.1: A 2D cantilever beam with minimized compliance.

in the paper of T. Chen and Y. Chiou or M. Beckers [40, 41].

The algorithm developed for the literature study[1] was derived from the MatLab codes developed by the TopOpt group at the DTU [6, 7] and an object oriented Python code written by Li-Yi Wei from the University of Hong Kong [43]. Care was taken to make the code readable and flexible. This will reduce the development time of future versions that can optimize for other objectives such as the damage tolerance. All examples used are generated by this code[2]. For example fig. 3.1, which is a 2D cantilever beam that was subjected to a point load at the tip (red arrow) and constrained in x and y direction at the end, show by the respective green and blue triangles.

This section will start with a presentation of the optimization objective and its formulation in a continuum form. In section 3.1.2 the spatially discretized formulation is shown. This will include the penalization scheme used to allow for a smooth density function. Then the basics of the computational implementation is shown in section 3.1.3. Followed by a explanation of an efficient FEA solver for this specific problem (section 3.1.4). Lastly a discussion of the sensitivity analysis, method of moving asymptotes (MMA) and the update scheme in section 3.1.5.

3.1.1 Continuum formulation

The linear elastic optimization for small deformation as presented by N. Olhoff and J.E. Taylor [44] is used. It considers a design region Ω that is in $\boldsymbol{R}^2$ or $\boldsymbol{R}^3$ of which a subregion Ω^m is filled with material [36]. The optimal topology is reached when the optimal stiffness tensor $\boldsymbol{E}_{ijkl}(\boldsymbol{x})$ is found.

As all space within Ω^m is filled an equation of the mass distribution X can be formulated as a discrete function,

$$X(\boldsymbol{x}) = \begin{cases} 1 & \text{if } \boldsymbol{x} \in \Omega^m \\ 0 & \text{if } \boldsymbol{x} \in \Omega \backslash \Omega^m \end{cases} \tag{3.1}$$

This can be used to define the stiffness tensor,

$$\boldsymbol{E}_{ijkl}(\boldsymbol{x}) = X(\boldsymbol{x}) \overline{\boldsymbol{E}}_{ijkl} \tag{3.2}$$

in terms of this mass distribution function and the constant rigidity tensor $\overline{\boldsymbol{E}}_{ijkl}$. The constant rigidity tensor is function of the material properties only. As X is a discrete function all admissible tensors are discrete and thus the optimization problem has a discrete valued parameter function.

The amount of work due of the deformation $\boldsymbol{u}$ can be calculated by eq. (3.3). With the standard linearized strain formulation this results in,

$$l(\boldsymbol{u}) = \int_\Omega \boldsymbol{f}\boldsymbol{u} \, \mathrm{d}\Omega + \int_{\Gamma_T} \boldsymbol{t}\boldsymbol{u} \, \mathrm{d}\Gamma_T \tag{3.3}$$

[1] The python code is available at GitHub [42].

[2] A database with the simulation settings of each figure is available at OSF to improve the reproducibility [90].

A bi-linear energy equation with virtual work $a(\boldsymbol{u}, \hat{\boldsymbol{u}})$ is formulated,

$$a(\boldsymbol{u}, \hat{\boldsymbol{u}}) = \int_\Omega \boldsymbol{E}_{ijkl} \boldsymbol{\varepsilon}_{kl}(\boldsymbol{u}) \boldsymbol{\varepsilon}_{ij}(\hat{\boldsymbol{u}}) \, \mathrm{d}\Omega \tag{3.4}$$

$\hat{\boldsymbol{u}}$ is an arbitrary kinematically admissible deformation. Equilibrium is ensured when $l(\hat{\boldsymbol{u}}) = a(\boldsymbol{u}, \hat{\boldsymbol{u}})$ is satisfied for all admissible deformations $\hat{\boldsymbol{u}}$.

As minimizing the work, due to the traction forces for a given load, minimizes the deformation of a structure the problem can be formulated as:

$$\begin{aligned} \min_{\Omega^m} \; & l(\boldsymbol{u}) \\ \text{s.t. :} \; & a(\boldsymbol{u}, \hat{\boldsymbol{u}}) = l(\hat{\boldsymbol{u}}) \\ & \int_\Omega X(\boldsymbol{x}) \mathrm{d}\Omega \; = \; \mathrm{Vol}(\Omega^m) \; \leq \; V \end{aligned} \tag{3.5}$$

3.1.2 Discretization

To solve the continuum problem of the previous section it is discretized into a finite element analysis with N elements:

$$\begin{aligned} \min_{X_1, X_2, \ldots, X_N} \; & c = \boldsymbol{f}^T \boldsymbol{u} \\ \text{s.t. :} \; & \boldsymbol{K}\boldsymbol{u} = \boldsymbol{f} \\ & \sum_{e=1}^{N} v_e X_e \; \leq \; V \\ & X_e \in \{0, 1\} \quad \forall \quad e \in \{1, 2, \ldots, N\} \\ \text{where :} \; & \boldsymbol{K} = \sum_{e=1}^{N} \boldsymbol{K}_e(X_e, \overline{E}) \end{aligned} \tag{3.6}$$

it shows that the element stiffness matrix $\boldsymbol{K_e}$ depends on the element material value X_e and the material stiffness $\overline{E}$. The problem becomes unstable towards the element type and mesh when the discrete formulation of eqs. (3.1) and (3.2) are used. Such a distribution problem generally has no solution [45, 46]. Iterative search methods would not work because they require the calculation of gradients. Therefore, the problem is changed so that the density becomes a continuous equation ranging from 0 to 1.

$$0 \leq X_e \leq 1 \tag{3.7}$$

This method would result in a design with intermediate values. Although this makes sense for variable thickness plate design, see the work of M.P. Rossow and J.E. Taylor [47], for discrete topology design loses its direct physical representation. There is either material or there is not, intermediate values are meaningless. Changing eq. (3.2) with a penalization that reduces the effectiveness of intermediate values results in a formulation that suppresses these intermediate values. The method used here, developed by E. Andreassen [38], is derived from the classical penalized proportional stiffness method (SIMP) [6, 36]. Here $E_{\min}$ is a small artificial stiffness used to avoid elements with zero stiffness as that could make the FEA unstable.

$$\boldsymbol{E}_{ijkl}(\boldsymbol{x}) = \boldsymbol{E}_{ijkl,\min} + X(\boldsymbol{x})^p \left(\overline{\boldsymbol{E}}_{ijkl} - \boldsymbol{E}_{ijkl,\min} \right) \tag{3.8}$$

When $p > 1$ the intermediate density values are less effective as there stiffness is low in comparison to the volume occupied. When p is sufficiently large, generally $p \geq 3$, the design converges to a solution that is close to a discrete (0-1) design.

3.1.3 Computational implementation

The iterative implementation of topology optimization as proposed by M. Beckers, [41] or M.P. Bendsøe and O. Sigmund [6] are similar. It exists out of three parts, initialization, optimization and post processing. The flowchart for the methods used in this communication can be found in fig. 3.2.

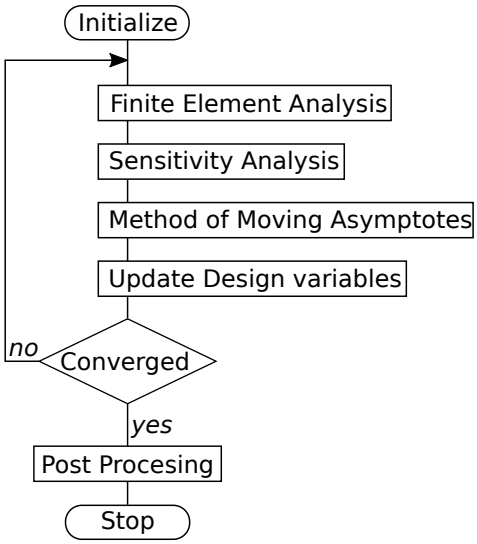

Figure 3.2: Basic flowchart for compliance minimization [6].

In the initialization phase the problem is set up. It defines the design domain, the loading conditions, the initial design and generates the finite element mesh that will be used in the optimization phase.

The optimization phase is the iterative method that solves the topology problem. It will analyze the current design with a FEA. After which it will calculate the sensitivity of the global compliance to the density of each element, this is the local gradient of which the calculation is discussed in section 3.1.5. The Method of Moving Asymptotes (MMA), developed by K. Svanberg [48], is used to formulate a simplified convex approximation of the problem which is optimized to formulate the updated design. These steps are performed in a loop until the design is converged, i.e. when the change in design between two iterations becomes negligible.

Post processing is required to remove the last elements with intermediate values and generate a shape out of the design, for example a CAD or STL file. This literature study will not contain a detailed analysis of the post processing steps. The code used in this communication simply plots the final shape and load case.

3.1.4 Efficiently FEA formulation

The most computational time is spent on the finite element analysis. The FE problem consists of assembling the global stiffness matrix and inverting it. The code for assembling becomes more efficient when a regular grid is used. The location of a degree of freedom can be calculated if the location of the element is known. Then the most time is spend on solving the linear problem $\boldsymbol{f} = \boldsymbol{K}\boldsymbol{u}$ where the displacement vector is the unknown. This section will discuss how characteristics of a multigrid preconditioned conjugate gradient (MG-cg) solver can be used to reduce computational costs. The method presented here was descirbed by O. Amir, N. Aage and B. Lazarov [49].

Multigrid methods have a theoretical convergence rate that is independent of the mesh size. This is an improvement over other methods such as a conjugate gradient method. It is a multiresolution method which means that it uses different mesh sizes to improve convergence with relaxation techniques. It iterates over smoothing, coarsing and interpolation cycles to solve the linear problem. Beside good convergence the method can be paralyzed which allows it to run even more efficient on modern hardware [50].

There is one major drawback of MG solvers, the amount of iterations required to solve the problem depends on the contrast of the matrix, the higher this contrast the slower the solver. In the case of topology this can be linked to $\overline{E}/E_{\text{min}}$ which is high in general. It was proven that a contrast of more than 10^6 barely effects the amount of iterations required while the method was still faster than an incomplete Cholesky preconditioned conjugate gradient method [49].

Some properties of the TO can be used to improve the efficiency of the solver. The first property utilized is connected to the filter radius (see section 3.2.2). These filters smoothen the problem, reducing the amount or impact of high frequency modes. To ensure that the solver errors propagate into smoothed regions as efficiently as possible a relation between the filter size and the amount of MG-cg levels was developed [49, sec. 3.1]. The second improvement is about the required accuracy of the linear approximation. This improvement can be made with any type of iterative solver and stops the iterations when an accurate enough solution is obtained. As the design update scheme is based on the sensitivities, see section 3.1.5, the only requirement is that the sensitivities are calculated accurate enough [51, 52]. An exact formulation of both ideas can be found in the paper of O. Amir, N. Aage and B. Lazarov [49].

3.1.5 Sensitivity analysis and MMA

The main focus on developing a robust and stable algorithm is the update scheme. The MMA scheme was chosen as it proofed to be very effective for this type of optimization [6]. MMA is an efficient method

meant for non-linear non-convex problems that approaches those problems by generating purely convex sub-problems, based on the gradient information. It can be used to iterative solve the optimization problem.

The gradient of one element in the discretized form is $\partial c/\partial X_e$. This derivative does not have to be explicitly calculated as the problem is self adjoint. This is used by the following proof. It starts with a new formulation of the work, the difference is the zero term at the end. Again $\hat{\boldsymbol{u}}$ is any arbitrary admissible deformation [6].

$$c = \boldsymbol{f}^T\boldsymbol{u} - \hat{\boldsymbol{u}}^T(\boldsymbol{K}\boldsymbol{u} - \boldsymbol{f}) \tag{3.9}$$

taking the derivative to the density leads to:

$$\frac{\partial c}{\partial X_e} = \left(\boldsymbol{f}^T - \hat{\boldsymbol{u}}^T\boldsymbol{K}\right)\frac{\partial \boldsymbol{u}}{\partial X_e} - \hat{\boldsymbol{u}}^T\frac{\partial \boldsymbol{K}}{\partial X_e}\boldsymbol{u} \tag{3.10}$$

when $\hat{\boldsymbol{u}}$ satisfies the adjoint equation it becomes:

$$\frac{\partial c}{\partial X_e} = -\hat{\boldsymbol{u}}^T\frac{\partial \boldsymbol{K}}{\partial X_e}\boldsymbol{u} \quad \text{when} \quad \boldsymbol{f}^T - \hat{\boldsymbol{u}}^T\boldsymbol{K} = 0 \tag{3.11}$$

Satisfying this adjoint equation is simple, just choose $\hat{\boldsymbol{u}} = \boldsymbol{u}$. The derivative of the stiffness matrix to the density of an element can be derived leading to the final expression of the gradient:

$$\frac{\partial c}{\partial X_e} = -pX_e^{p-1}\boldsymbol{u}^T\boldsymbol{K}_e\boldsymbol{u} \tag{3.12}$$

MMA approaches the problem with multiple convex approximations around the expansion point (current iteration). The goal here is to find the optimal density distribution of the current iteration where the influence of the densities is approximated with a convex function. This approximation is based on the sensitivity and some information of previous iterations. Solving these convex equation can be done by various basic algorithms. The obtained optimum is not the real optimum of the optimization problem as the convex function used is only an approximation of the real problem. However, it is a step into the direction of the real optimum. The obtained density distribution is then used as an input of the next iteration [6, p.19-21]. The optimization of this local problem must meet all the constraints. This means that the updated design has to meet the global volume constraint.

The approximation, at iteration k, made by the MMA algorithm is described in eq. (3.13). Here X^k is a vector with the densities of all elements at the current iteration. A description on the calculations of U_e and L_e follows later. The method was developed by K. Svansberg [48].

$$c \approx c^k + \sum_{e=1}^{N}\left(\frac{r_e}{U_e - X_e} + \frac{s_e}{X_e - L_e}\right) \tag{3.13}$$

$$\text{where:} \quad r_e = \begin{cases} 0 & \text{if } \frac{\partial c}{\partial X_e} \le 0 \\ \left(U_e - X_e^k\right)^2\frac{\partial c}{\partial X_e} & \text{if } \frac{\partial c}{\partial X_e} > 0 \end{cases}$$

$$s_e = \begin{cases} 0 & \text{if } \frac{\partial c}{\partial X_e} \ge 0 \\ -\left(X_e^k - L_e\right)^2\frac{\partial c}{\partial X_e} & \text{if } \frac{\partial c}{\partial X_e} < 0 \end{cases}$$

That all the density sensitivities are negative can be derived from eq. (3.12). This simplifies the expression and resulted in:

$$c \approx c^k + \sum_{e=1}^{N} -\frac{\left(X_e^k - L_e\right)^2}{X_e - L_e}\frac{\partial c}{\partial X_e} \tag{3.14}$$

Then the optimization, on X_e, used in this iteration is defined as:

$$\min_{X_1, X_2, \ldots, X_N} \; c^k - \sum_{e=1}^{N}\frac{\left(X_e^k - L_e\right)^2}{X_e - L_e}\frac{\partial c}{\partial X_e} \tag{3.15}$$

$$\text{s.t. :} \quad \sum_{e=1}^{N} v_e X_e \le V$$

$$0 \ge X_e \ge 1 \quad \forall \quad e \in \{1, 2, \ldots, N\}$$

here the moving asymptote, L_e, can be varied and is chosen to improve convergence and stability, choosing this wisely is important. In general the goal is to stabilize the process when it is oscillating, i.e. moving the asymptote closer. Or to relax the problem when it is monotone, i.e. moving the asymptote further and thus causing larger steps to be taken at that iteration. This can be done by including the behavior of previous iterations or calculating the second derivative of the optimization objective to the design variables. Several implementations exist, they are tuned to work for specific problems [48, 53].

The update scheme minimizes the local approximation to decide on the new densities. Starting with the minimalization of the Lagrange function:

$$\mathcal{L} = c^k - \sum_{e=1}^{N}\frac{\left(X_e^k - L_e\right)^2}{X_e - L_e}\frac{\partial c}{\partial X_e} + \Lambda\left(\sum_{e=1}^{N} v_e X_e - V\right) + \sum_{e=1}^{N}\lambda_e^-(X_e - 0) + \sum_{e=1}^{N}\lambda_e^+(1 - X_e) \tag{3.16}$$

This separable and purely convex problem can be solved by a range of algorithms. It can easily be changed into a formulation with other or more constraints.

3.2 Complications with TO

The TO algorithm as described in the previous section has some problems. To be able to use the algorithm, interpret its results or alter its formulation an understanding of these complications and there influence on the results is required. Here these problems will be discussed and if possible a solution will be presented. Some of the problems have no solution. It is important to keep them in mind when discussing the results of the optimizations.

First the issues of the local minima and non-uniqueness (section 3.2.1) are discussed. They are caused by the gradient method and the nature of the optimization problem. They make clear that the solution obtained might not be the only one possible nor

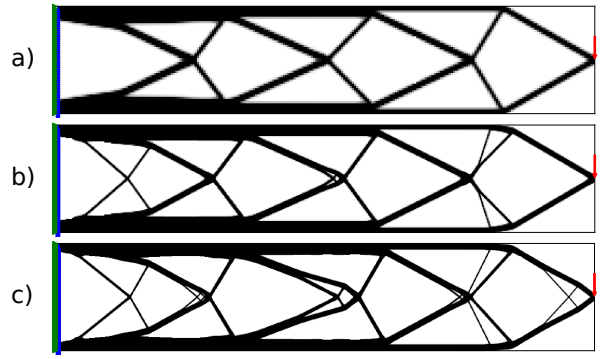

Figure 3.3: Optimized cantilever beams at resolution, a) 250x50, b) 500x100 and c) 1000x200. A sensitivity filter of $r_{min} = 1.25$ is used to avoid checkerboard patterns.

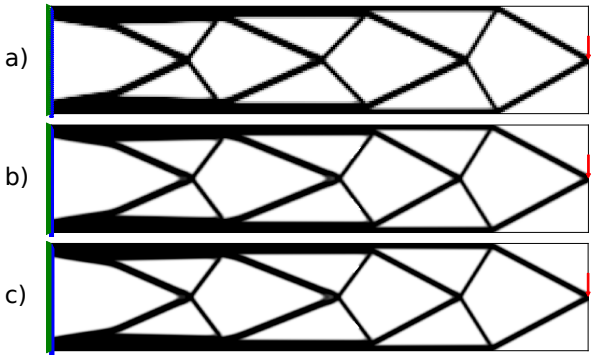

Figure 3.4: Sensitivity filtered optimized cantilever beams at resolutions an filters, a) 250x50 $r_{min} = 1.25$, b) 500x100 $r_{min} = 2.50$ and c) 1000x200 $r_{min} = 5.00$.

might it be the real optimum. There are no solutions available to solve these issues. Then mesh refinement and checkerboard patterns will be explained, sections 3.2.2 and 3.2.3. These problems are caused by the FEA and will be solved in the same way.

3.2.1 Local minimum

The MMA as a gradient decent method searches for a local minimum. This means that the solution converges to a design that might not be the global optimum in the design space. The final design is depended on the starting design. Avoiding this problem is only possible when another optimization algorithm is used that can search for a global optimum such as a genetic algorithm.

One could try several different starting designs to see if noticeable differences appear. This does not necessary lead to a global optimum but to multiple local optima. It is nearly impossible to proof that the converged design is a global optimum. One could use engineering sense and experience to judge the design. While methods that can solve for global optima are to inefficient (genetic algorithms) or not applicable to this non-linear non-convex problem.

TO algorithm presented in this communication uses a distributed starting design. This means that when the volume constrain is 30% the initialization density set to $X_e = 0.3$ for all elements.

Even solving for one global optimum might not result in the requested result, as multiple designs might have the same stiffness. A clear example of that would be a design space under uni-axial tension [54]. One thick bar would perform the same as a group of thinner bars with the same total thickness. This does not only mean that different designs can have the same performance but that even several equally optimal solutions can exist. One design might be better due to manufacturing, maintenance or other reasons. These topics are not considered by the algorithm and in contrast to genetic algorithms [55, 56] the user cannot be asked for their opinion.

3.2.2 Mesh refinement

Every reliable FEA requires a mesh convergence check to verify whether the results obtained are the correct ones. Commonly this is done by comparing the FE results run on different mesh sizes. Yet running the TO algorithm on different resolutions does result in different designs as is shown in fig. 3.3. This is logical, a finer mesh allows for finer features which can result in a better performance. This is unwanted for several reasons. Checking mesh convergence is impossible and the smallest features that appear in the optimization might be smaller than those that can be manufactured.

Several solutions exist, they try to limit the appearance of fine features. Examples are constraining the perimeter of all internal holes, reducing the design space to one that excludes these small features or filtering the sensitivities or densities in every iteration. Different regularization methods are compared by O. Sigmund [57]. The algorithm of this thesis will use filtering of the densities or sensitivities.

Filtering the sensitivities was proposed by O. Sigmund [58, p.72-75]. The method is derived from image processing and uses a normalized convolution filter to blur the figure. The density distribution X_e and the gradient can be interpreted as a figure with gray scale pixels. The gradient itself is not filtered, but the gradient multiplied by the densities is filtered before the update scheme decides on the densities of the next iteration [54, 59].

The sensitivity filter can be described as,

$$\widehat{\frac{\partial C}{\partial X_k}} = \frac{1}{X_k \sum_{i=1}^{N} H_i} \sum_{i=1}^{N} H_i X_i \frac{\partial l(\boldsymbol{u})}{\partial X_i} \tag{3.17}$$

$$H_i = \begin{cases} r_{min} - \text{dist}(k,i) & \text{if} \quad \text{dist}(k,i) < r_{min} \\ 0 & \text{if} \quad \text{dist}(k,i) \geq r_{min} \end{cases}$$

where k is the element to be filtered. The value of the filtered compliance density gradient at element i is depended on three main things, the density, density gradient and the distance to the surrounding nodes

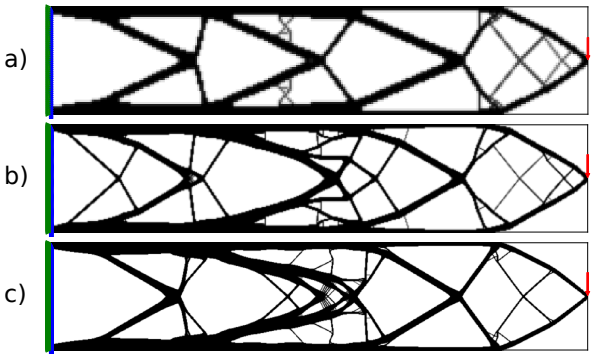

Figure 3.5: Optimized cantilever beams at resolution, a) 250x50, b) 500x100 and c) 1000x200. With a density filter of $r_{min} = 1.25$ to avoid checkerboard patterns.

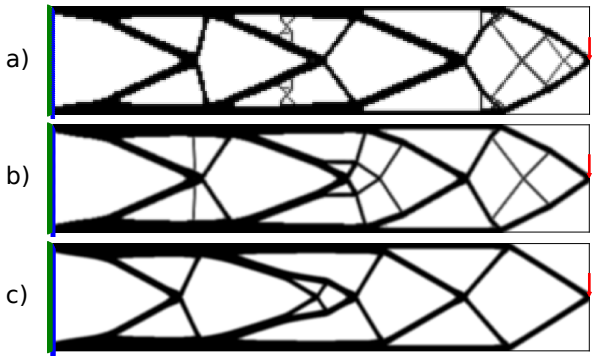

Figure 3.6: Density filtered optimized cantilever beams with resolution and filters, a) 250x50 $r_{min} = 1.25$, b) 500x100 $r_{min} = 2.50$ and c) 1000x200 $r_{min} = 5.00$.

i. All nodes that fall within radius r_{min} are contributing but the further the node is the lower its contribution. Note that the filter is normalized by dividing it by $\sum \hat{H}_i$. There is limited understanding why this filter works, there is no physical or theoretical basis for it. From experience, it was simply observed that it works well.

Figures 3.3 and 3.4 show the same simulations. The only difference is that the simulations in fig. 3.4 are filtered. It was observed that scaling the filter size r_{min} with the resolution results in similar designs. The main difference between the designs is that higher resolution simulations result in a smoother structure. But filtering this way leads to less discrete designs. Larger filters cause more pixels to have intermediate density values. Three solutions do exist; lowering the filter size for the last couple of iterations, increasing the SIMP penalty factor or applying extra post processing steps.

Another filter that can be considered is the linear density filter which was proposed by T.E. Bruns, D.A. Tortorelli and B. Bourdin [60, 61]. Here the blur filter,

$$\widehat{X_e} = \frac{1}{\sum_{i=1}^{N} H_i} \sum_{i=1}^{N} H_i X_i \tag{3.18}$$

$$H_i = \begin{cases} r_{min} - \text{dist}(k,i) & \text{if} \quad \text{dist}(k,i) < r_{min} \\ 0 & \text{if} \quad \text{dist}(k,i) \geq r_{min} \end{cases}$$

is applied directly on the densities. These filtered densities, $\widehat{X_e}$, are used in the FEA and SA. This means that the design variables X_e lose there physical meaning as the FEA gives it the relation to reality, therefore the final geometry should be based on the filtered densities [57].

A comparison between fig. 3.5 and fig. 3.6 shows that filtering the densities suppresses the finer features well. Comparing the performance difference of the sensitivity and density filters is difficult. Many criteria can be used such as, computational effort, how discrete the final design is, the magnitude of the final compliance and whether the volume constrained is still maintained. A small comparison was made by O. Sigmund [57]. The performance of the filters depends greatly on the design case used. The paper clearly shows that better filters exist then those presented in this communication however as the density and sensitivity filters are computational efficient and simple to implement they were chosen as the basic filters used in the code.

3.2.3 Checkerboard patterns

A common issue to appear it topology optimization results is the appearance of checkerboard patterns. An example of these patterns is shown in fig. 3.7. They do not appear due to beneficial micro-structural patterns but because of artificial stiffness created due to the FE analysis.

The 2D four node quadrilateral elements that are used can only deform linearly. First assume a patch of four elements (2x2), with a checkerboard pattern, and load the structure bi-axially. Even though the structure is unsymmetrical, it will deform symmetrically, the outer edges will stay straight. If quadratic elements (8 or 9 nodes) where used this would not happen, there stresses will peak in the corner where the corners of two filled elements meet. This will result in a more realistic deformation pattern. Using higher order elements suppresses the problem, however this results in a large increase of the computational effort. Therefore, other methods have been sought.

To ilustrate why these checkerboard patterns are preferred by the optimization a biaxial loading case is shown. For this case it is known that filling the inside with 50% volume causes checkerboard patters. The ideal solution would be a perfect distribution of the volume as every element is loaded the same way. This is also what comes out of a simulation with the penalty factor p set to one. The final design has a compliance of 12380, but the goal was to obtain discrete designs. Hence, p is increased to three, resulting in the pattern shown in fig. 3.7. Note that the compliance of the checkerboard result is only 7.7% more than that of the uniformly distributed case.

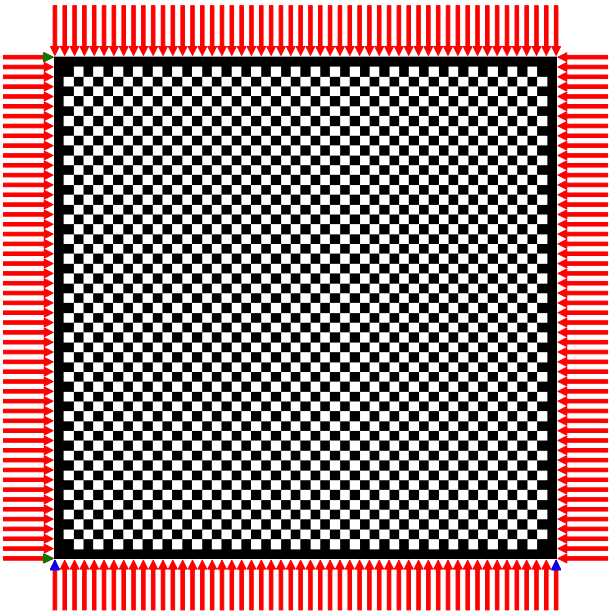

Figure 3.7: A biaxial compression case resulting in a checkerboard pattern. The border is forced to be totally filled. The compliance is 13334.

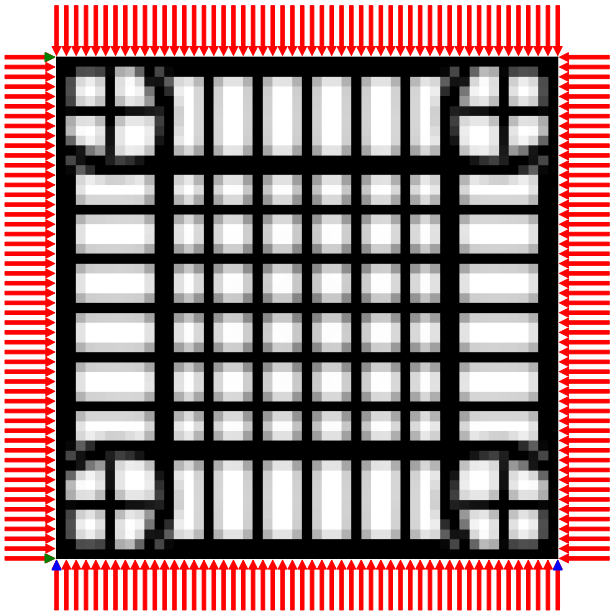

Figure 3.8: A biaxial compression case with sensitivity filtering. The compliance $c = 22181$ when the filter size $r_{\text{min}} = 1.15$.

Whereas forcing the structure out of these artificial patterns (fig. 3.8) causes a great increase, nearly 80%, in compliance.

Other patterns exist for other elements or optimization targets. In general these patterns occur when the structure is more optimal for artificial reasons than for physical ones. Under some circumstances even higher order elements might show artificial patterns (for high penalty factors p) [62]. When optimizing any structure for any goal one should review whether the method could create solutions that are only optimal because of artificial reasons.

This is where the filters proposed in the section about mesh refinement (section 3.2.2) help. These filters are used to remove fine features so that the FEA can capture the physical behavior properly. As checkerboard patterns are caused by the artificial stiffness created by a structure on element size they disappear when the small features are removed.

Other methods do exist, but they are more difficult to implement or require a higher computational effort. Some of these methods are described in the monologue written by O. Sigmund and M.P. Bendsøe [6].

3.3 Other objectives

Topology optimization can be used for several objectives; classical examples are, truss structure design, antenna/microphone design, heat convection problems [6, 63] and MEMS actuator designs [6, 7, 64, 65]. In general all these TO algorithms approach the optimization as a material distribution problem within a design space with a resource constraint witch is solved with an iterative gradient method.

When changing the objective and/or problem one should start with a formulation of the problem which consists of the objective, variables and constraints. Then the changes should be made in the calculation of the objective and sensitivity. Important therefor is the method used to link the optimization variables to the objective, in the case of compliance minimization it consists of the variables to density formulation (SIMP eq. (3.8)) and the FEA that links stiffness to compliance. Beneficial would be a (self) adjoint formulation because it allows for an efficient calculation of the sensitivities. The parts of the method that are unlikely to change are; the overall methodology, described in fig. 3.2, the method of moving asymptotes and its update scheme.

Sometimes optimization objectives are formulated in the form of several sub objectives resulting in multi objective optimization formulations. Optimizing for multiple objectives or load cases at once is common. For most structures several considerations, such as costs, weight and strength are taken in account. In addition do most structures experience multiple load-cases during their life. Several TO algorithms have been developed for this purpose. The most basic methods will be discussed here.

The method sets up multiple FEA as shown in fig. 3.9. Then the total objective will be linked to sub objectives. For instance the goal might be to minimize the compliance due to n load cases. One could formulate the total objective (O) as the weighted sum of the compliance of all load cases,

$$O = \sum_{i=1}^{n} w_i c_i \tag{3.19}$$

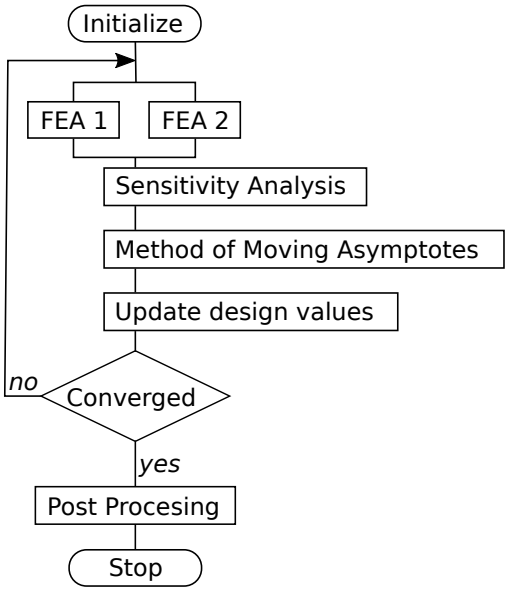

Figure 3.9: Flowchart of the multi loadcase compliance minimization algorithm [6].

resulting in a gradient function that can be formulated as,

$$\frac{\partial O}{\partial X_e} = \sum_{i=1}^{n} w_i \frac{\partial c_i}{\partial X_e} \tag{3.20}$$

Another example can be made with a similar method. Assume that adding up the objective is not what is wanted but that the goal is to prohibit two different failure modes. Hence, the design update is based on the most critical case resulting in objective,

$$O = \max(o_1, o_2, \ldots, o_n) \tag{3.21}$$

An example of such a formulation can be found in the TO based damage tolerance optimization algorithm presented by Z. Kang, P. Liu and M. Li [13, sec. 4.4]. Where they optimize geometries for the most cricital crack in every iteration. The sensitivities can then be formulated as:

$$\frac{\partial O}{\partial X_e} = \sum_{i=1}^{n} s_i \frac{\partial o_i}{\partial X_e} \tag{3.22}$$

$$\text{where} \quad s_i = \begin{cases} 1 & \text{if} \quad o_i = O \\ 0 & \text{if} \quad o_i \neq O \end{cases}$$

These basic multiple load case algorithms can be summarized in the flowchart shown in fig. 3.9. In general the FEA requires most of the computational time therefore the method as shown here is computationally inefficient. More advanced algorithms have been developed but these are outside the scope of this communication [66, 67].

Chapter 4

Optimization for fatigue and damage

Optimizing for damage (tolerance) and fatigue is not new. Several studies have been performed, which will be discussed in this chapter. A short summary of the reference studies can be found in table 4.1.

Optimizing fatigue (crack growth) life of structures is not uncommon in the field of shape optimization. Studies performed at the Monash University [68, 69] show that maximizing fatigue life can be achieved with a biological shape optimization algorithm. R. Jones D. Peng, D. Abramson et al. treat problems of hole and fillet shapes by moving the shape boundary [68]. Their first code is derived from a biological stress equalizing algorithm. It assumes that the optimal geometry is one that has equal hoop stresses at all points along the hole circumference. They extended the problem to one of equal stress intensity by assuming (small) cracks at all nodes around the hole. By using a finite element alternating technique, they avoided the need of a full FEA per crack. Ultimately a fatigue life optimization was developed. Which again considered cracks at all nodes around the hole, while their propagation was modeled with the Erdogan-Paris rule.

For these biological algorithms, two assumptions where made. Firstly that the most optimal design is one that has equal performance at all areas. This might actually be unwanted as it would mean that the likelihood to failure is equal everywhere, this means that the entire part needs to be inspected. Currently inspections are performed at the weakest locations only, greatly reducing the amount of work and time required for an inspection. The second assumption is that locally adding material improves the performance locally. This means that at the locations that perform below average, material is added and at those that perform well material is removed. This simplifies the development as no gradient information is required, but limits the flexibility of the problem formulation. Complicated objectives and problems do generally not allow one to formulate such a rule. Compliance maximization is for example a global parameter, making it difficult to express what the local performance is. Optimizing structural topology for fatigue life with this method might be impossible because, local performance can influence local behavior at other locations. Besides the fact that adding material at underperforming locations may or may not improve efficiency, as softening around the crack tip can result in fatigue life improvements [70].

Another group of optimization method that can be used, are genetic algorithms (GA), which search through the design space with a metaheuristic method. The method is inspired by the theory of evolution and selection, which allows one to search through the 'entire' design space without trying all options. It is also more likely to result in the global optimum, compared to the other methods considered. Because the GA only requires the objective calculations of every design it is known for its low development time and can easily be adopted to optimize complex problems. However, this comes at the cost of increased computational requirements and a major risk, as predicting the influence of the optimization settings onto the result is near impossible due to the stochastic nature of GA, making it into a kind of black box.

J. Lu, N. Kashaev and N. Huber [12] developed such an algorithm to design a variable thickness plate with the objective to maximize its fatigue crack growth life. Genetic algorithms are initiated with many randomly generated designs. Which were repeatedly improved by the processes of natural selection, mutation and crossover. Their method used a FEA to calculate the fatigue crack growth life, while many generations needed to be analyzed before convergence. This causes problems due to the computational requirements and as a result only 1D problems at low resolution can be run. Even considering these limitations, the increase of fatigue crack growth life was 10%, improving these algorithms can lead to significantly better structures.

B. Herremans [71] reduced the computational effort of this problem by replacing the FEA by an analytical stress intensity equation, which greatly simplifies the calculations required per design. This allowed them to optimize problems at a higher resolution. This thesis is inspired by these crenelations optimizations. It will explore the impact of a 2D problem, one where the local thicknesses of the plate are the design variables.

Another way of reducing the computational requirements is the use of gradient methods, especially those with an adjoint formulation. Examples of these methods are topology optimization algorithms that use the optimality criteria or method of moving asymptotes update schemes. These methods use the gradient information -how all the design vari-

ables impact the objective- to generate a simplified optimization problem, which is only valid close to the original design point. This simplified problem is solved in order to determine the updated design variables. Repeating this process should lead to a local minimum. Using the adjoint derivative formulation is an efficient method, as it allows the calculation of all derivatives with one equation. This method is in some ways similar to the biological methods used in shape optimization. However, the update scheme is more advanced and applicable to more complex processes. The drawback is that it requires the gradient calculation of which the derivations can be difficult.

Including damage (tolerance) in a topology optimization algorithm was done in 1998 by M.P. Bendsøe and A.R. Díaz [9]. They developed two algorithms. One that minimized the amount of damage due to yielding. While the other one was damage tolerance oriented, where the stiffness of a damage structure was maximized. Their work showed that damage tolerance considerations can be included in gradient based topology optimization.

A similar material failure optimization model was recently, 2018, presented by L. Li, G. Zhang and K. Khandewal [72]. Their formulation minimizes the weight, while requiring the structure to absorb a certain amount of energy and limiting the damage (yielding). This allowed them to design robust, lightweight and energy absorbing structures which can be used for crash structures.

Neither of these two algorithms or any of the comparable damage TO methods [73, 74] consider damage tolerance for propagating fatigue cracks. Optimizing for fatigue life has two major difficulties. The algorithm does not know where the crack initiates, as the initiation location is dependent on the design variables. Secondly, a propagating crack changes in the stress/displacement field, causing the original FEA to become invalid, resulting in path dependencies.

Closest to a working gradient based fatigue optimization is the algorithm written by Z. Kang, P. Liu and M. Li [13]. They assume the existence of a crack and minimize the sum of its energy release rate and compliance. A low energy release rate relates to a low crack growth, while the compliance was required to ensure realistic designs. The method requires a known initiation location, which is difficult to define before the geometry is known and only optimizes for one crack length. As cracks are propagating, they change the stress state at its tip. Therefore, the optimum design for this crack might be inefficient when the crack becomes longer. Adding information about the whole fracture process would be an improvement to the algorithm.

L. Xia, D. Da and J. Yvonnet [75] did exactly that. Though their research focused on monotonic brittle failure, which is different from fatigue, they showed how to consider the whole fracture process. Their algorithm maximizes the energy released of a structure composed of two materials by distributing materials in the optimal way. Maximizing the mechanical fracture energy is equivalent to fracture resistance, and the crack paths are dependent on the geometry, allowing the method to consider crack steering to increase its performance.

Their extended bidirectional evolutionary structural optimization (BESO) update scheme is related to biological methods but considers the derivatives when adding or removing material. This allows the implementation of global objectives while maintaining some simplicity of the biological methods. The algorithm uses a phase field model which diffuses the local and discrete behavior of the crack and is able to model the crack propagation. The method designs composite materials of arbitrary geometry, and there results cannot be manufactured with the current manufacturing methods making validation of their results impossible.

Optimizing fatigue life with a gradient implementation of TO has not been attempted before, but should be possible as the largest problems of it have been solved already. Z. Kang [13] showed that optimizing for crack growth is possible while L. Xia [75] and K. James [74] show that even the path dependency problem can be optimized for. Combining the strength of their methods should allow one to formulate a path dependent fatigue life maximisation method with a local damage model which can optimize the geometry under a material constraint.

Author		Objective	Update scheme	Constraint	Damage model	Remarks
M. P. Bendsøe	[9]	Min. damage	Optimality criteria	Max. material	Material softening	
M. P. Bendsøe	[9]	Min. compliance after damage	Optimality criteria	Max. material	Material softening	Damage constraint to separate damage load case.
R. Jones	[68]	Equalize stress	Biological	Max. hole dimensions	None	
R. Jones	[68]	Min. stress intensity	Biological	Max. hole dimensions	LEFM	Finite element alternating used to efficently model initial cracks.
R. Jones	[68]	Max. fatigue life	Biological	Max. hole dimensions	Paris law	Finite element alternating, cracks of initial size at all possible locations.
R. Das	[69]	Min. stress intensity	Biological	Max. hole dimensions	LEFM	3D finite element alternating used to efficently model initial cracks.
M. Jansen	[73]	Various	MMA	Max. material	Softening where damage is assumed	Damage of certain size with max impact on objective considered.
K.A. James	[74]	Min. weight	MMA	Max. compliance & Max. damage	Non-local continuum damage model	Solves path dependency problem.
J. Lu	[12]	Max. fatigue crack growth life	Genetic algorithm	Max. material	LEFM & Paris law	1D plate thickness design in low resolutions.
Z. Kang	[13]	Min. compliance + energy release rate	MMA	Max. material	LEFM with singularity elements	Initial crack assumption.
L. Li	[72]	Min. weight	MMA	Min. plastic work & Max. damage	Non local damage model	Energy absorbing structures.
L. Xia	[75]	Max. fracture resistance	Bidirectional Evolutionary Structural Optimization	Max. inclusion material	Phase field fracture model	Optimal inclusion distribution of composite, initial crack assumption, complete fracture model and solved path dependency problem.

Table 4.1: Damage (tolerance) optimization algorithms summary.

Chapter 5

Research scope

In the field of aerospace engineering damage tolerance is one of the main pillars used to ensure safety. Designing structures while considering the ability to sustain defects until the next inspection is hence commonly used. For fatigue failure this means that the focus is on the crack growth period, as those crack can be detected during inspections. Topology optimization for fatigue crack growth life could prove valuable addition assist in the design of these structures. To the author's knowledge, nobody develop an fatigue crack growth life maximization algorithm.

5.1 Objective and questions

Due to time constraints it is impossible to develop an algorithm that maximizes fatigue life and considers the entire fracture process. Thus, the scope was reduced and the objective of this thesis was specified as: "Explore the opportunity that TO offers to design fatigue crack growth reducing geometries by developing a TO algorithm that minimizes stress intensity and maximizes fatigue crack growth life and optimize example problems."

The simplified algorithm should be able to optimize the fatigue life while considering straight cracks only to avoid the path dependency problem. The formulation should be as concise and simple as possible to allow future researchers to formulate a three-dimensional version for arbitrary shaped crack surfaces. To develop such an algorithm the following research questions need to be answered:

1. What is the formulation of a TO algorithm that minimizes the crack growth rate?
   (a) Can the enriched crack tip FE method accurately calculate the stress intensity factors?
   (b) What is the adjoint sensitivity equation for the enriched crack tip element FE method?
   (c) What is the performance of the optimization results?
2. What is the formulation of a TO algorithm that maximizes the fatigue life?
   (a) What implementation of the Paris rule can calculate fatigue crack growth life?
   (b) What is the adjoint sensitivity equation for the fatigue crack growth life maximization?
   (c) What is the performance of the optimization results?

5.2 Hypothesis

It was hypothesized that stress intensity factors could accurately be calculated with the enriched crack tip FE method. This enrichment method would calculate the stress intensity factors directly as a degree of freedom in the FEA. Minimizing K_I is, in that sense, similar to end compliance minimization, simplifying the derivation of the sensitivities. Hypothesized is that the formulation of the adjoint and sensitivity equations for the stress intensity minimization are the same as those used in the end compliance minimization algorithms.

A fatigue crack growth life maximization is an extension of the stress intensity factor minimization. The amount of cycles required to grow a certain distance can be derived from the Paris-Erdogan rule. It would be dependent on an integral which consists of the stress intensity factors as a function of crack length. This integral can be approached by a summation,

$$N = \frac{1}{C} \sum_{l=1}^{L-1} \frac{\delta a_l}{\left(\frac{1}{2} \left(K_I^l + K_I^{l+1} \right) \right)^m} \tag{5.1}$$

which assumes that the crack growth between two locations of known stress intensity value is equal to their average. In this equation N is the fatigue life in cycles, C and m are constants of the Paris law and δa_l is the step size. The objective is the inverse of a summation of stress intensity factors meaning that the sensitivity equation is also some type of summation of the sensitivity to stress intensity values.

5.3 Methodology

To explore the possibilities of TO for damage tolerance two algorithms will be developed. It starts with the development of the optimization algorithms, of which the process is shown in fig. 5.1. Here the first step is the formulation of the problem for stress intensity minimization in the most general form. Followed by the development of a FE model that can capture the singular behavior at the crack tip. Then the stress intensity minimization algorithm will be explained. Which, in the end, will be expanded to a fatigue crack growth life maximization algorithm.

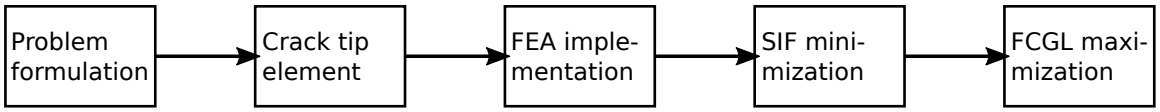

Figure 5.1: Optimization algorithm development process.

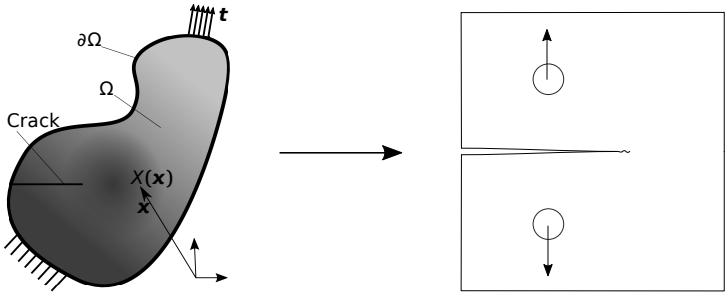

Figure 5.2: The general problem formulation and the compact tension specimen studied in this thesis.

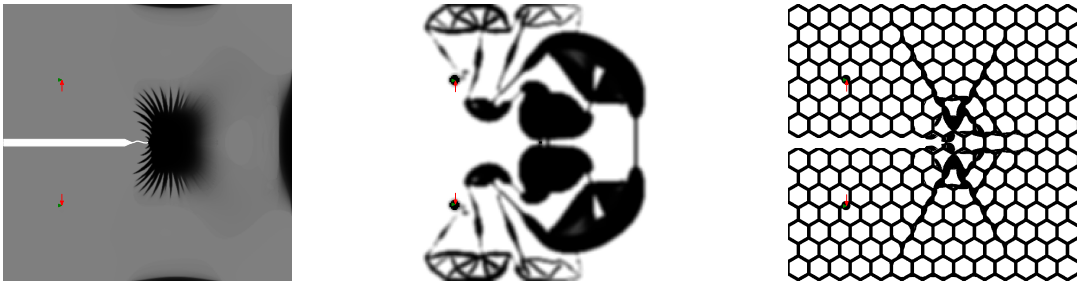

a) Variable thickness problem. b) Discrete problem. c) Honeycomb infill problem.

Figure 5.3: Three diferent types of optimizations are used for the evaluation and validation.

The implementation of both the stress intensity minimization and fatigue crack growth life maximization algorithms will be based on the compliance minimization example discussed in section 3.1. They will employ:

- an adjoint formulation of the sensitivities to reduce computational requirements,
- the method of moving asymptotes (MMA) as a local approximation to base the design variable updates on,
- density filtering to avoid checkerboard patterns and constrain a minimum feature size, and
- no post-processing steps as it is out of this thesis its scope.

The scope of the research is reduced, by constraining the general problem formulation to that of a compact tensions (CT) specimen. This is shown in fig. 5.2. This CT specimen is used to specify both the design domain and load case. It was chosen because of its simple geometry, load case and the availability of various test standards [25, 76, 77]. The standardized specimen consists of a rectangular flat plate with a manufactured crack. This crack is pulled open causing it to grow. The driving force increases steeply with the crack length because it is a combination of both tension and bending. This allows for measurement of crack growth rates at a large range of stress intensity factors.

The reference CT specimen is a flat plate, of course this is not the case for the optimization results. The optimization can add and/or remove material to improve the performance, which resulted in the typologies shown in fig. 5.3. The algorithms will be used to optimize three different types of problems:

- A variable thickness plate optimization where the design variables are the local thicknesses. The local thickness is constraint between a minimum and maximum while the total amount of mass is limited by the resource constraint. The result of such an optimization can be found in fig. 5.3a.
- A discrete optimization in which material is distributed throughout the design space. Here the SIMP penalization method is used to obtain a design that is discrete, as is shown in fig. 5.3b
- An infill optimization case which is similar to the discrete optimization problem. Here material is added to an existing geometry, while the existing geometry cannot be altered. Figure 5.3c shows how extra mass is distributed in a honeycomb base structure.

Before the algorithms can be evaluated and used it is important to validate the FE analysis and the assumptions that it is based on. The validation will be performed in two steps, a comparison of flat plates stress intensity factors to the known solutions and

the testing of optimized geometries.

The flat plate validation consist of a comparison between the stress intensity factors calculated with the enriched FE method and a known solution for the same geometry. For this validation the compact tension, double edge and single edge crack specimens are used. A mesh refinement study is performed for these specimens and the converged stress intensity factors are compared to the algebraic solution.

The second validation checks whether the optimization results perform as predicted. The difference with the first validation step is that it will consider plates with varying thickness. This is important as the optimization algorithm can come up with solutions where artificial patterns appear. The performance of these patterns is overestimated because the FE method cannot capture their behavior properly. This validation is performed by measuring the performance manufactured optimized design and comparing it to the FE results of the same geometry.

Finally, the performance of optimization results will be evaluated. This is done by performing optimizations and comparing them to the reference CT design. For the stress intensity minimization the variable thickness plate, discrete and infill design problems are examined. The study of the fatigue life maximization will be less extensive and focus on variable thickness plates only.

Part II

Algorithm development, Validation & Testing

Chapter 6

Stress intensity factor minimization

The objective of the research was to explore how topology optimization can be used to optimized for damage tolerance objectives such as fatigue crack growth rate. It was hypothesized that the difficulties would lay in the formulation an objective function and the adjoint equation. There formulation should be based upon linear fracture mechanics with the use of FEA. In this chapter the method behind the algorithm[1], will be presented. This algorithm will be used in the later chapters and there the results of the algorithm will be discussed. Therefore, understanding the method, its benefits, limitations and quirks, will allow for better interpretation of the results.

The chapter will be divided in five parts, the first one, section 6.1, will present the problem and its objective and constraints. Secondly, section 6.2 the enriched finite element implementation that is used to calculate the stress intensity factor will be derived. There are multiple methods to calculate the stress intensity factors but this method stood out for its simplicity, the FEA calculates the stress intensity values directly which simplies the formulation of the objective and adjoint equations significantly. In section 6.3 the method that minimizes the stress intensity is shown. It is based upon a compliant maximization method developed at the DTU. The last section, section 6.4 known limitations of the method are mentioned and if possible an indication of the severity or a solution to the problem are given.

6.1 Problem formulation

The problem formulation, required for optimization problems, should contain the optimization objective, its link to the design variables and the constraints. Because the goal is design a geometry with the lowest crack growth rate and the Paris-Erdogan law [22] minimizing stress intensity factor K_I was chosen as the objective. Due to this formulation the design geometry, topology, is the optimization variable.

Assuming a general problem, shown in fig. 6.1, which minimizes the stress intensity by changing the material distribution, $X(\boldsymbol{x})$ within the design domain Ω,

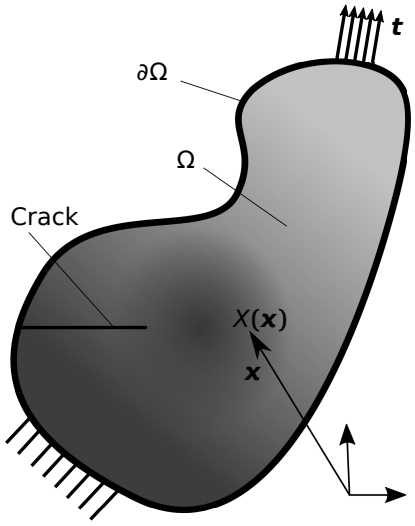

Figure 6.1: Design domain Ω with a crack, arbitrary boundary conditions and a density X which is dependent on the position vector $\boldsymbol{x}$.

the following mathematical formulation is proposed;

$$\min_{X(\boldsymbol{x})} \; K_I(X(\boldsymbol{x})) \tag{6.1}$$
$$\text{s.t. :} \quad a(\boldsymbol{u}(X(\boldsymbol{x})), \hat{\boldsymbol{u}}) = l(\hat{\boldsymbol{u}})$$
$$\int_\Omega X(\boldsymbol{x}) \, \mathrm{d}\Omega = \mathrm{Vol}(\Omega^m) \leq V$$
$$X_{\min} \leq X(\boldsymbol{x}) \leq X_{\max}$$

it enforces equilibrium with a virtual work method while the problem is subjected to a resource constraint. This constraint limits the volume within the design domain that can be filled with a material beside setting a minimum and maximum density value.

For any optimization a link between the objective and the design variables must be made. The method proposed here can be used for two cases, variable thickness plate and discrete material distribution. The honeycomb infill problem is a type of discrete material distribution and will not be discussed separately. In the first case the optimization variables X are interpreted as the local plate thickness. As the thickness influences the local stiffness properties it affects the stress intensity values at the crack tip. For this variable thickness sheet a linear relation,

$$\boldsymbol{E}_{ijkl}(\boldsymbol{x}) = \boldsymbol{E}_{ijkl,\min} + X(\boldsymbol{x})\left(\overline{\boldsymbol{E}}_{ijkl} - \boldsymbol{E}_{ijkl,\min}\right) \tag{6.2}$$

[1] The source code is available at GitHub [78].

between local stiffness and thickness is used. This equation was proposed by M.P. Rossow and J.E. Taylor [47] and discussed by O. Sigmund [79], and causes the stiffness to become twice as high when the thickness is doubled. Here $\overline{\boldsymbol{E}}_{ijkl}$ is a constant stiffness tensor related to the material it unity thickness while $\boldsymbol{E}_{ijkl,\min}$ a tensor is with very small stiffness. Which enforces the total stiffness to be larger than zero. One cannot allow the stiffness to become zero as it would cause the FEA to fail. This relation might be inaccurate due to out of plane effects at thickness changes and it will be necessary to measure under what circumstances this equation is invalid.

When the goal is to obtain a discrete design the density values can be either 0 (no material) or 1 (material). This however causes the objective equation to become discrete as well as the method used a gradient approach and requires a continuous function of density. To ensure a discrete final design while maintaining a continuous objective function a penalization method was implemented. The method used was based upon the penalized proportional stiffness method (SIMP),

$$\boldsymbol{E}_{ijkl}(\boldsymbol{x}) = \boldsymbol{E}_{ijkl,\min} + X(\boldsymbol{x})^p \left(\overline{\boldsymbol{E}}_{ijkl} - \boldsymbol{E}_{ijkl,\min}\right) \tag{6.3}$$

it causes designs to converge to a 0-1 solution when the penalty factor p is chosen sufficiently high. Values of $p \geq 3$ are required for designs to become discrete.

6.2 FE implementation

The previous section linked the design variables to the stiffness distribution no official formulation of the stress intensity factors in terms of design variables was made. This formulation is indirectly made through the equilibrium constraint of eq. (6.1) as stiffness distribution influences the stress/displacement field of the loaded part, these stress/displacement distribution can be related to the stress intensity factor. The original equilibrium equation is in a continuum formulation but to simplify the problem a discretized version will be solved using FEA.

To ensure a direct and efficient calculation of the stress intensity factor while using a finite element analysis an enrichment method was used for elements close to the crack tip. The method used was developed by S.E. Benzley [31] and improved by L.N. Gifford [32]. It uses a linear summation of a continuous displacement field and a near crack tip displacement field capturing both the discrete behavior at the crack tip and the continuous one around it. The discrete solution was derived with the Westergaard function method [33]. This type of tip element enrichment allows accurate predictions of stress intensity directly from the FEA without any post processing as it can be found in the displacement vector.

6.2.1 Element stiffness matrix

The method uses special elements around the crack tip of which the stiffness matrix needs to be derived. As these enriched elements based upon an addition of the continuous and singularity displacement field these are discussed separately at first.

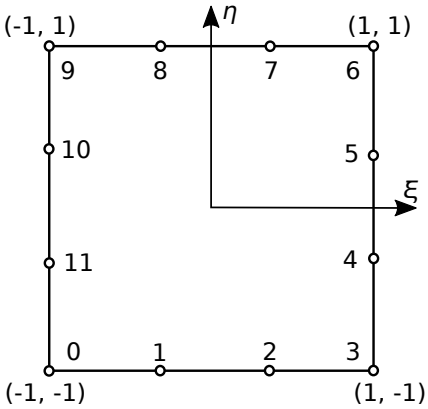

Figure 6.2: Nodal definition of the crack tip element.

The enrichment method shown here was based upon the crack tip element developed my L.N. Gifford [32]. Who based the enriched elements on a bicubic serendipity elements, see fig. 6.2. The algorithm presented here keeps the local coordinate system (ξ, η) as only a regular mesh with square elements will be used. For a more general element that can contain cracks under an angle and that transforms elements from (ξ, η) to (x, y) see the original paper [32].

The displacement field within the bicubic serendipity 12-node element can be described by:

$$\boldsymbol{u} = \sum_{i=0}^{11} N^i(\xi, \eta)\boldsymbol{u}^i \tag{6.4}$$

where the shape functions N^i are,

$$N^0 = \frac{1}{32}(1-\eta)(1-\xi)\left(9\eta^2+9\xi^2-10\right) \tag{6.5}$$
$$N^1 = \frac{9}{32}(1-\eta)(1-3\xi)\left(1-\xi^2\right)$$
$$N^2 = \frac{9}{32}(1-\eta)(1+3\xi)\left(1-\xi^2\right)$$
$$N^3 = \frac{1}{32}(1-\eta)(1+\xi)\left(9\eta^2+9\xi^2-10\right)$$
$$N^4 = \frac{9}{32}(1-3\eta)(1+\xi)\left(1-\eta^2\right)$$
$$N^5 = \frac{9}{32}(1+3\eta)(1+\xi)\left(1-\eta^2\right)$$
$$N^6 = \frac{1}{32}(1+\eta)(1+\xi)\left(9\eta^2+9\xi^2-10\right)$$
$$N^7 = \frac{9}{32}(1+\eta)(1+3\xi)\left(1-\xi^2\right)$$
$$N^8 = \frac{9}{32}(1+\eta)(1-3\xi)\left(1-\xi^2\right)$$
$$N^9 = \frac{1}{32}(1+\eta)(1-\xi)\left(9\eta^2+9\xi^2-10\right)$$

$$N^{10} = \frac{9}{32}(1+3\eta)(1-\xi)\left(1-\eta^2\right)$$
$$N^{11} = \frac{9}{32}(1-3\eta)(1-\xi)\left(1-\eta^2\right)$$

Added to this will be the crack tip singularity displacement field which derivation starts from the definition of stress intensity factors in a simplified 2D space,

$$K_I = \lim_{r\to 0}\sqrt{2\pi r}\sigma_{xx} \tag{6.6}$$
$$K_{II} = \lim_{r\to 0}\sqrt{2\pi r}\sigma_{xy}$$

and the crack tip stresses derived with the Westergaard method [33],

$$\begin{aligned}\sigma_{xx} =& \frac{K_I}{\sqrt{2\pi r}}\cos\frac{\theta}{2}\left(1-\sin\frac{\theta}{2}\sin\frac{3\theta}{2}\right) \\ &- \frac{K_{II}}{\sqrt{2\pi r}}\sin\frac{\theta}{2}\left(2+\cos\frac{\theta}{2}\cos\frac{3\theta}{2}\right) \\ \sigma_{yy} =& \frac{K_I}{\sqrt{2\pi r}}\cos\frac{\theta}{2}\left(1+\sin\frac{\theta}{2}\sin\frac{3\theta}{2}\right) \\ &+ \frac{K_{II}}{\sqrt{2\pi r}}\cos\frac{\theta}{2}\sin\frac{\theta}{2}\cos\frac{3\theta}{2} \\ \tau_{xy} =& \frac{K_I}{\sqrt{2\pi r}}\cos\frac{\theta}{2}\sin\frac{\theta}{2}\cos\frac{3\theta}{2} \\ &+ \frac{K_{II}}{\sqrt{2\pi r}}\cos\frac{\theta}{2}\left(1-\sin\frac{\theta}{2}\sin\frac{3\theta}{2}\right)\end{aligned} \tag{6.7}$$

which are accurate approximations of the stresses close to the crack tip, i.e. r is small. Figure 6.3 shows the axis system definition for the calculation around the crack tip. A formulation of the displacement field

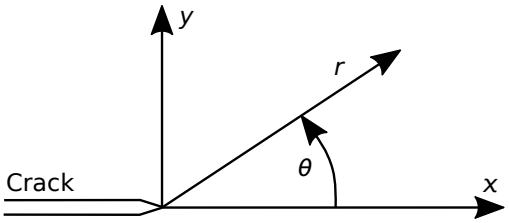

Figure 6.3: Definition of the axis systems around the crack tip.

can be found by integration leading to,

$$\begin{aligned}u_x =& K_I f_x(r,\theta) + K_{II} g_x(r,\theta) \\ =& \frac{K_I}{4G}\sqrt{\frac{r}{2\pi}}\left(-1+\gamma-2\sin^2\frac{\theta}{2}\right)\cos\frac{\theta}{2} \\ &+ \frac{K_{II}}{4G}\sqrt{\frac{r}{2\pi}}\left(1+\gamma+2\cos^2\frac{\theta}{2}\right)\sin\frac{\theta}{2} \\ u_y =& K_I f_y(r,\theta) + K_{II} g_y(r,\theta) \\ =& \frac{K_I}{4G}\sqrt{\frac{r}{2\pi}}\left(1+\gamma+2\cos^2\frac{\theta}{2}\right)\sin\frac{\theta}{2} \\ &+ \frac{K_{II}}{4G}\sqrt{\frac{r}{2\pi}}\left(1-\gamma+2\sin^2\frac{\theta}{2}\right)\cos\frac{\theta}{2}\end{aligned} \tag{6.8}$$

where $\gamma = (3-\nu)/(1+\nu)$ for plane stress and $\gamma = 3-4\nu$ for plane strain [28, pp.569]. When assuming linear fracture mechanics one can describe the displacement field of this element as summation of eqs. (6.4) and (6.8) resulting in:

$$\begin{aligned}u_x &= K_I f_x(r,\theta) + K_{II} g_x(r,\theta) + \sum N^i(\xi,\eta)u_x^i \\ u_y &= K_I f_y(r,\theta) + K_{II} g_y(r,\theta) + \sum N^i(\xi,\eta)u_y^i\end{aligned} \tag{6.9}$$

The singularity equations need to be transformed from the (r, θ) axis into the local (ξ, η) system. This transformation is dependent of the relative location of the crack tip to the local element axis system.

The enriched displacement functions, see eq. (6.9), can cause discontinuities at the border to normal elements, this can be repaired by multiplying the enrichment terms of the displacement function with an equation that is 1 at the crack tip and 0 at the border to non enriched elements [31]. It has however been reported that the effects of discontinuities are minor and this solution was therefore not implemented [32].

Following a definition of FE by Zienkiewicz [80] an element stiffness matrix can be calculated with,

$$\boldsymbol{K} = \int_{-1}^{1}\int_{-1}^{1} \boldsymbol{B}^T\boldsymbol{D}\boldsymbol{B}\ \det\boldsymbol{J}\ \mathrm{d}\xi\mathrm{d}\eta \tag{6.10}$$

where $\boldsymbol{D}$ the material stiffness matrix is, $\boldsymbol{J}$ the Jacobian of axis system transformation (ξ, η) into the global (x, y) axis system is and $\boldsymbol{B}$ the matrix is that converts displacement into strain. The integration was performed with a Gauss-Legendre quadrature function with 8x8 integration points as was found sufficient by L.N. Gifford [32].

For a standard bicubic serendipity element this $\boldsymbol{B}$ matrix is of shape (3, 24) however due to the enrichment it becomes (3, 26). Which results in a final stiffness matrix of (26, 26). Where

$$\boldsymbol{f} = \boldsymbol{K}\boldsymbol{u} = \begin{pmatrix} f_x^0 \\ \vdots \\ f_x^* \\ f_y^* \end{pmatrix} = \begin{bmatrix} \boldsymbol{k} & \vdots & \boldsymbol{k}_{12} \\ \dots & \vdots & \dots \\ \boldsymbol{k}_{21} & \vdots & \boldsymbol{k}_{22} \end{bmatrix} \begin{pmatrix} u_x^0 \\ \vdots \\ K_I \\ K_{II} \end{pmatrix} \tag{6.11}$$

Here $\boldsymbol{k}$ is similar to the stiffness matrix of a normal bicubic element, the enrichment is in the parts $\boldsymbol{k}_{12}$, $\boldsymbol{k}_{21}$ and $\boldsymbol{k}_{22}$. New terms do also appear in the force vector, where f_x^* and f_y^* are so-called singular loads. They describe the external forces applied on the crack boundary [31], in general these values are zero.

6.2.2 Meshing strategy

To reduce computational costs these enriched elements are only used at the crack tip and conventional linear elements are used throughout the rest of the mesh. It uses the hanging node method to connect the elements as can be seen in fig. 6.4.

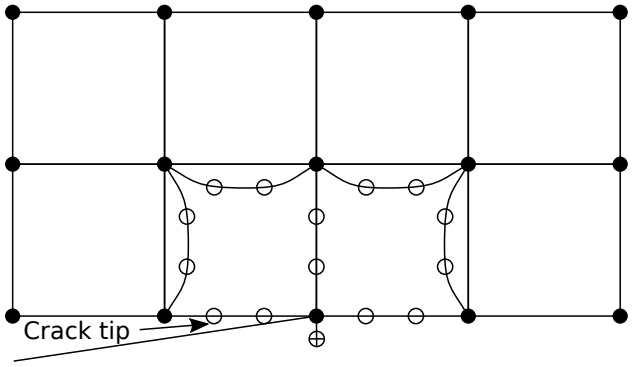

Figure 6.4: Top section of mesh around a crack tip, ⊕ is the enrichment node with K_I and K_{II}, while solid circles represent the linear ones and the open circle the higher order ones.

This mesh is not conform which can potentially cause the displacement field to become discontinuous. To avoid this one could use normal bicubic serendipity elements throughout the entire mesh which is computational inefficient. However, using a multi-resolution interpretation of topology optimization its performance might be improved [81].

Currently the linear system of the FEA, $\boldsymbol{f} = \boldsymbol{K}\boldsymbol{u}$, and the adjoint equation, $\boldsymbol{l} = \boldsymbol{K}\boldsymbol{\lambda}$, are solved with a complete Cholesky decomposition. A more efficient methods can be formulated with a Multi Grid Conjugate Gradient method as proposed by O. Amir [49].

6.3 Topology optimization

The optimization method that can efficiently solve the problem formulation of the previous section is based upon level-set topology optimization. The topology optimization algorithm used is derived from the compliant mechanism design code developed by Sigmund in the nineties [59]. The procedure for minimizing eq. (6.12) is presented in fig. 6.5.

This section explains the implementation of optimization in three subsections. One discusses the discretized objective, the objective sensitivities and adjoint equation. The second section treats the local approximation (MMA) and the update scheme while the last section handles filtering strategies used to create checkerboard free and mesh independent designs.

6.3.1 Discretization and sensitivities

As a spacial discretized method (FEA) was used to calculate the objective the problem formulation needs to become discretized as well. For a mesh of

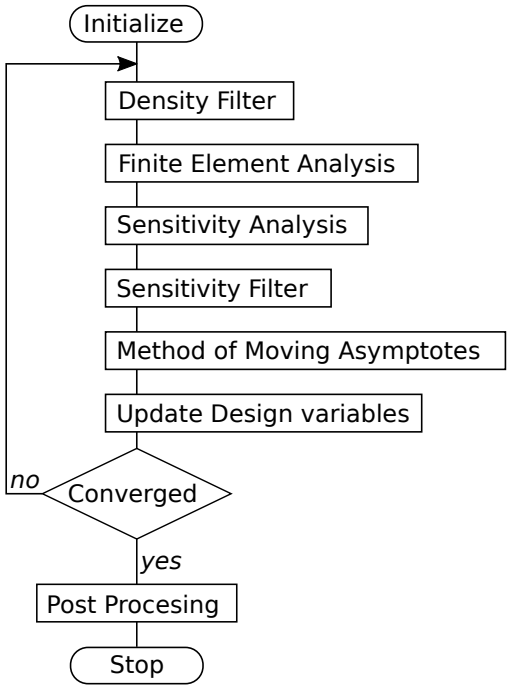

Figure 6.5: Topology optimization flowchart, either the density filter or the sensitivity filter is used [6].

N elements the optimization objective becomes;

$$\min_{X_1,X_2,\ldots,X_N} \quad K_I = \boldsymbol{l}^T\boldsymbol{u} \tag{6.12}$$

$$\text{s.t.} : \quad \boldsymbol{K}\boldsymbol{u} = \boldsymbol{f}$$

$$\sum_{e=1}^{N} v_e X_e \leq V$$

$$X_{\min} \leq X_e \leq X_{\max} \quad \forall \; e \in \{1, 2, \ldots, N\}$$

$$\text{where} : \quad \boldsymbol{K} = \sum_{e=1}^{N} \boldsymbol{K}_e(X_e, \bar{E})$$

and the terms have the exact same meaning as those of eq. (6.1), thus again it minimizes stress intensity by ensuring equilibrium and setting constraints to the density distribution. Here $\boldsymbol{u}$ is the enriched displacement vector, f the force vector and v_e is the (relative) element volume. $\boldsymbol{l}$ is zero vector except for the degree of freedom linked to the stress intensity factor, and the multiplication of $\boldsymbol{l}^T\boldsymbol{u}$ will return the stress intensity factor. This is similar to the compliant mechanism optimization mentioned by O. Sigmund [59] where the displacement of a specific degree of freedom is maximized.

As the problem of eq. (6.12) is non convex and unstable towards the mesh and element type an iterative solving method is selected. The iterative solver will attempt to improve the design of the current iteration by optimizing a simplified and convex approximation of the local problem repeatedly until the problem converges.

The local convex approximation requires the calculation of the sensitivity of K_I to a density change in any element. This can be measured by $\partial K_I/\partial X_e$, which can be calculated with the following steps and

starts with adding a zero term after the known function $K_I = \boldsymbol{l}^T\boldsymbol{u}$, where $\boldsymbol{\lambda}$ is an arbitrary vector:

$$K_I = \boldsymbol{l}^T\boldsymbol{u} - \boldsymbol{\lambda}^T(\boldsymbol{K}\boldsymbol{u} - \boldsymbol{f}) \tag{6.13}$$
$$\frac{\partial K_I}{\partial X_e} = \left(\boldsymbol{l}^T - \boldsymbol{\lambda}^T\boldsymbol{K}\right)\frac{\partial \boldsymbol{u}}{\partial X_e} - \boldsymbol{\lambda}^T\frac{\partial \boldsymbol{K}}{\partial X_e}\boldsymbol{u}$$

Now choosing a convenient vector for $\boldsymbol{\lambda}$ which causes $\boldsymbol{l}^T - \boldsymbol{\lambda}^T\boldsymbol{K}$ to be zero leads to the following expression for the sensitivity,

$$\frac{\partial K_I}{\partial X_e} = -\boldsymbol{\lambda}^T\frac{\partial \boldsymbol{K}}{\partial X_e}\boldsymbol{u} \tag{6.14}$$
$$\text{where:} \qquad \boldsymbol{l} = \boldsymbol{K}\boldsymbol{\lambda}$$

This means that $\boldsymbol{\lambda}$ can be calculated with the FEA, where $\boldsymbol{l}$ is seen as a sort force vector, by solving $\boldsymbol{l} = \boldsymbol{K}\boldsymbol{u}$. The sensitivity of $\boldsymbol{K}$ to the element density can be calculated but depends on what function is used to calculate the element stiffness, see eqs. (6.2) and (6.3).

6.3.2 MMA and update scheme

The local convex approximation is based upon the method of moving asymptotes (MMA) [48], as it proved to be an efficient for this specific type of optimization. MMA approximates K_I of the updated design by,

$$K_I \approx K_I^k + \sum_{e=1}^{N}\left(\frac{r_e}{U_e - X_e} + \frac{s_e}{X_e - L_e}\right) \tag{6.15}$$
$$\text{where:} \quad r_e = \begin{cases} 0 & \text{if } \frac{\partial K_I}{\partial X_e} \le 0 \\ \left(U_e - X_e^k\right)^2\frac{\partial K_I}{\partial X_e} & \text{if } \frac{\partial K_I}{\partial X_e} > 0 \end{cases}$$
$$s_e = \begin{cases} 0 & \text{if } \frac{\partial K_I}{\partial X_e} \ge 0 \\ -\left(X_e^k - L_e\right)^2\frac{\partial K_I}{\partial X_e} & \text{if } \frac{\partial K_I}{\partial X_e} < 0 \end{cases}$$

based upon a simplified convex and local approximation in iteration k. Here X_e^k are the densities at the current iteration while X_e is the optimization parameters and represents the density distribution belonging to the predicted K_I.

The name of the method is derived from U_e and L_e which are limiting the maximum density change in each element with their asymptotic behavior. The efficiency of the method is in choosing these asymtotes in a smart and adaptive way, when the optimization behaves stable they are spaced further apart to allow for larger steps, and they are closer together when oscillatory behavior is observed [48, 53].

To improve upon the current design the local approximation needs to be minimized resulting in the problem formulation,

$$\min_{X_1, X_2, \ldots, X_N} K_I^k + \sum_{e=1}^{N}\left(\frac{r_e}{U_e - X_e} + \frac{s_e}{X_e - L_e}\right) \tag{6.16}$$
$$\text{where:} \quad r_e = \begin{cases} 0 & \text{if } \frac{\partial K_I}{\partial X_e} \le 0 \\ \left(U_e - X_e^k\right)^2\frac{\partial K_I}{\partial X_e} & \text{if } \frac{\partial K_I}{\partial X_e} > 0 \end{cases}$$
$$s_e = \begin{cases} 0 & \text{if } \frac{\partial K_I}{\partial X_e} \ge 0 \\ -\left(X_e^k - L_e\right)^2\frac{\partial K_I}{\partial X_e} & \text{if } \frac{\partial K_I}{\partial X_e} < 0 \end{cases}$$
$$\text{s.t.:} \quad \sum_{e=1}^{N} = v_e X_e \ge V$$
$$X_{\min} \le X_e \le X_{\max} \;\; \forall \;\; e \in 1, 2, \ldots, N$$

As the approximation in eq. (6.15) was setup to be convex the optimization is straight forward and can be performed by a variety of methods. For this algorithm the primal-dual Newton method was implemented as proposed by K. Svansberg [53].

6.3.3 Filtering

Since a objective and method have been formulated an algorithm can be developed it however has a couple of problems such as mesh dependency and artifacts. The mesh convergence issue appears because finer meshes allow for finer features to be created. This can be unwanted as one might want to know wether the geometry obtained is an optimum on a finer mesh as well. Some types of features, such as checkerboard patterns, appear only because the FEM overestimates the stiffness of them because the structural details cannot be modeled at such course meshes. However when optimizing the problem at a finer mesh smaller version of these artifacts start to appear and will again have overestimated stiffness. To ensure that these features can not be created a limitation on the feature size has to be formulated. This can be done in several ways, of which two are implemented in the algorithm, the so-called sensitivity,

$$\widehat{\frac{\partial C}{\partial X_k}} = \frac{1}{X_k\sum_{i=1}^{I} H_i}\sum_{i=1}^{I} H_i X_i \frac{\partial l(\boldsymbol{u})}{\partial X_i} \tag{6.17}$$
$$H_i = \begin{cases} r_{min} - \text{dist}(k,i) & \text{if} \quad \text{dist}(k,i) < r_{min} \\ 0 & \text{if} \quad \text{dist}(k,i) \ge r_{min} \end{cases}$$

and density filtering,

$$\widehat{X_e} = \frac{1}{\sum_{i=1}^{I} H_i}\sum_{i=1}^{I} H_i X_i \tag{6.18}$$
$$H_i = \begin{cases} r_{min} - \text{dist}(k,i) & \text{if} \quad \text{dist}(k,i) < r_{min} \\ 0 & \text{if} \quad \text{dist}(k,i) \ge r_{min} \end{cases}$$

which where discussed in the literature study, section 3.2.2

The computationally most efficient formulation of both these filters is obtained when dedicated code to filter pictures is used. This simply generates a convolution matrix based upon the filter and applies it

to all pixels. This however, results in problems at the outer edges of the design space, which was noted by B. Bourdin [61]. As the convolution filter has a constant size it will try to filter a pixel at the edge partially based upon data that is outside the design region. No information about the densities or thickness is available there, this however is generally solved by extrapolating the figure. Simple examples of extrapolations are; repeating the data at the border pixels, reflecting along the border and setting a fixed value outside the design domain. It is assumed that the final design is barely affected by these settings when the filter size, r_{min}, is small compared to the resolution. However, features at the border might be influenced by it. The model uses reflection boundaries unless specified otherwise.

It was observed that scaling the filter size r_{min} linearly with the resolution results in similar designs. The main difference between the designs is that higher resolution simulations result in a smoother structure. But filtering this way leads to gray, undetermined, edges around discrete designs. Larger filters cause more pixels to have intermediate density values. This is unwanted when discrete optimization cases are coincided, three solutions do exist, lowering the filter size for the last couple of iterations, increasing the SIMP penalty factor or applying extra post processing steps.

6.4 Restrictions of the method

The method in its presented form has a couple of limitation, these can be caused by various sources and are separated based upon there origin.

An issue that comes from the problem formulation include assumption that the thickness to stiffness formula (eq. (6.2)) assumes that stresses are constant through the thickness. While examples of limitations are that the thickness of elements at the crack tip are not allowed to change and that the crack path needs to be determined in advance and the FE method implemented requires the cracks to be at along the edges elements. Lastly do problems exist that are related to topology optimization, such as non-uniqueness, local-minima and filter-objective interaction.

The limitation description will include an indication of the impact and if available a solution will be proposed.

6.4.1 Problem formulation

The first problem can be found in the formulation used for variable thickness plates. The equation that relates stiffness to the local optimization variable (thickness or density), see eq. (6.2), makes an incorrect assumption. It assumes that the stiffness increases linearly with the thickness and it completely neglects through thickness differences of the stresses and/or strains. This will cause problems at

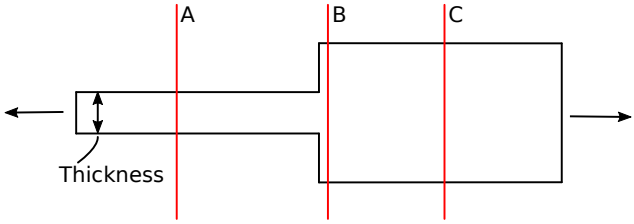

Figure 6.6: The variable thickness sheet under a uni-axial load, at cross-section A & C stress is constant while at B it varies through the thickness.

locations where the thickness changes, as depicted in fig. 6.6.

The stiffness approximation of the model assumes that, even at cross-section B, the stresses through the thickness are constant. This is untrue, the in-plane stresses at B will vary through the thickness. Hence, it is hypothesized that the stiffness equation for a variable thickness sheet is inaccurate for abrupt and large thickness changes. This means that the stiffness of areas with repeated large thickness changes could be overestimated. These problems might be solved with a large density filter which smoothens the thickness changes.

The assumption that the stiffness increases linearly with thickness or cross-sectional area is used extensively in literature. Not only in the field of variable thickness plate optimization [47, 79] but also for analytical expressions that predict stress intensity factors of stiffened plates [82, 83] and functional graded materials [84, 85]. When C.D Rans, R. Rodi and R.C. Alderliesten performed tests to verify their analytical stress intensity factor model it was observed that the difference between reality and the model is not too large and that the model predicts the overall behavior properly [82].

In the current algorithm it is assumed that the elements around the crack tip have a density/thickness of one. The current computational implementation cannot calculate the stiffness of the enriched elements with varying stiffenss ($\boldsymbol{K}(X_e)$). Allowing these elements to change could be achieved by deriving $\boldsymbol{K}(X_e)$ and $\partial \boldsymbol{K}/\partial X_e(X_e)$ for the enriched elements. Making the crack tip thickness variable might result in a stress intensity minimized geometry with no material at the tip, as it would reduce the stresses to 0. This is unwanted, as this solution would result in a structure with a hole at the crack tip. Hence, it is advised to set a minimum thickness constraint.

6.4.2 Finite element method

The finite element model has its own limitations, only those specific to the element enrichment method and implementation in this algorithm will be mentioned. It is assumed that the readers are familiar with common problems such as; inaccuracies around load introductions, element aspect ratio and non-linear behavior.

A limitation of the FEA enrichment is that the crack must be on the edge of the elements. This causes the current implementation to be limited to straight cracks only. With more advanced meshing one could model a curved crack as one that exists of multiple straight segments. This might cause new problems.

The FEA risks having a discontinuity in the displacement field there were the enriched elements touch the conventional ones because of the following two reasons:

- The enrichment function that contains the discrete displacement field can be non zero at these borders. One could multiply the enrichment equation with a term that goes to zero towards these borders and is equal to one at the crack tip. It was however observed that the impact is minimal [32].
- The non-conform mesh which is used, shown in fig. 6.4, does not constrain the location of the higher order nodes to be on the border of the linear elements. This means that a gap or overlap between elements might occur.

The best way to solve all these element enrichment problems is to use an XFEM method with direct stress intensity calculations. The formulations of XFEM allows for discontinuities within elements while maintaining continuity throughout the rest of the mesh. Accurate results can be obtained on coarse meshes and require minimal remeshing. This method was developed by T. Belytschko and T. Black [86]. Formulations of XFEM with direct evaluations of the stress intensity factors do exist. This means that implementing XFEM into the model work similar the enrichment method discussed in this thesis and is described by X.Y. Liu, X.Z. Xiao and B.L. Karihaloo [35]. Implementing this solution would be time expensive and was avoided due to the short development time of the algorithm.

6.4.3 Optimization strategy

The MMA searches for a local minimum with gradient decent method. This means that the solution converges to a design that might not be the global optimum in the design space. The final design is thus depended on the starting design.

One could try several starting designs to see if noticeable differences appear. This does not necessary lead to a global optimum but to multiple local optima. It is nearly impossible to proof that the converged design is a global optimum. One can try to use engineering sense and experience to judge the design.

TO algorithm presented in this communication uses a distributed starting design. This means that when the volume constrain is 30% that at the initialization step all elements have their density set to $X_e = 0.3$.

Even solving for one global optimum might not result in the requested result, as multiple designs might have the same stiffness. A clear example of that would be a design space under uni-axial tension [54]. One thick bar would perform the same as a group of thinner bars with the same total thickness. This does not only mean that different designs can have the same performance but that even several equally optimal solutions can exist. One design might be better due to manufacturing, maintenance or other reasons. Sadly the algorithm does not allow the user to make such a choice as it only calculates one of the local minima.

This research uses the topology optimization with this drawback in mind. This means that this issue was not resolved and that better solutions to the specific optimization problem might exist. If one is interested in the global optimum one could consider using methods such as genetic algorithms or extend the iterative gradient method with disconnected bifurcation checks [87].

The filtering methods used to set a minimal filter size can cause several problems at the border of the design domain as shown by A. Clausen and E. Andreassen [88]. In their paper they formulate three issues; the first one being that along domain boundaries the minimum feature size is not satisfied, secondly that structural edges are forced to be perpendicular to domain boundaries and lastly that the geometries tend to “stick” to the domain boundaries. They do propose solutions for the discrete design case but because of time constraints they were not implemented in the algorithm.

Chapter 7

Fatigue crack growth life maximization

The proposed stress intensity optimization does not necessary maximize the fatigue crack growth life as it only minimizes the crack growth rate at one specific crack length. The optimization does not care about the crack growth rate at any other crack lengths, it might even cause its fatigue life to be shorter than that of a non optimized design. To tackle this problem an optimization that uses the Paris-Erdogan formula to calculate the fatigue crack growth life is proposed. The algorithm is based upon the stress intensity factor minimization, it uses the same FE method and optimization strategy. The differences are that the objective and the sensitivity equations are replaced and that, per iteration, more FEA need to be solved.

7.1 Method

Fatigue crack growth rate can be predicted with the Paris-Erdogan rule. The fatigue crack growth life can be determined by integrating the inverse of the crack growth rate to the crack length. For the optimization algorithm this would result in a summation, $N = \sum \mathrm{d}N/\mathrm{d}a\ \delta a$. It would need to calculate stress intensity values for the crack at different lengths, i.e. incrementally increasing the crack length. The implementation in this thesis assumes that the crack path is known before the optimization designs the geometry. This assumption is valid for the compact tension specimen with a symmetry condition and simplifies the calculation of the adjoint sensitivities.

Multiple FEA are required to determine the crack growth rate for all these crack increments. As the stress intensity factor and crack growth rate changes with increasing crack length. The algorithm assumes K_I between crack increment l and $l+1$ to be constant and equal to the average, i.e. $(K^l + K^{l+1})/2$. The amount of cycles required to growth the crack from the starting crack length, $l = 0$, to the last crack length ,$l = L$, as the objective:

$$N = \frac{1}{C} \sum_{l=1}^{L-1} \frac{\delta a_l}{\left(\frac{1}{2} \left(K_I^l + K_I^{l+1} \right) \right)^m} \tag{7.1}$$

where δa_l is the difference between the crack length of the current increment and the next one. C and m are constants from the Paris-Erdogan equation.

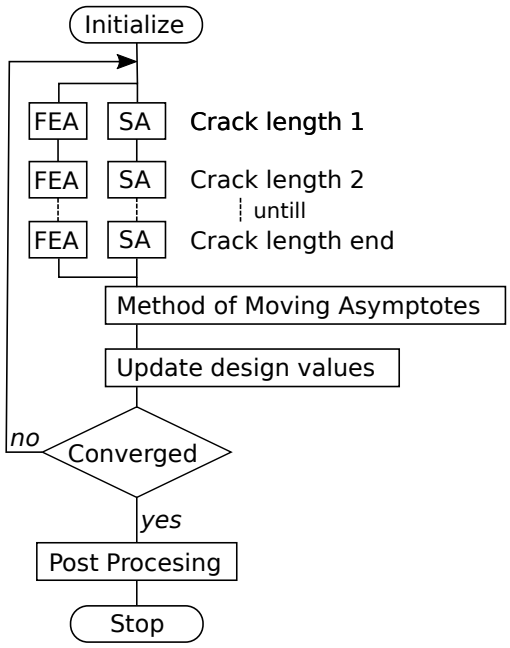

Figure 7.1: Fatigue life topology optimization flowchart, with a FE and sensitivity analysis for every crack increment.

The sensitivity of N to the density distribution can be expressed as:

$$\frac{\partial N}{\partial X_e} = -\frac{m 2^m}{C} \sum_{l=1}^{L-1} \frac{\delta a_l \left(\frac{\partial K_I}{\partial X_e}^l + \frac{\partial K_I}{\partial X_e}^{l+1} \right)}{\left(K_I^l + K_I^{l+1} \right)^{m+1}} \tag{7.2}$$

This formulation does not work however, the optimization converges to a solution that does not satisfy the resource constraint. The method of moving asymptotes requires the sensitivities of the density constraint derivative, dV/dX_e to be in the same order of magnitude as the objective sensitivity dN/dX_e. Assuming that; the geometry is manufactured of titanium (Ti-6Al-4V/ELI), printed with selective laser melting, loaded at room temperature and with a stress ratio $R = 0$, the constants[1] are $m = 4.41$ and $C = 5.05 \times 10^{-16}$ while the Poisson's ratio $\nu = 0.31$ [89]. It becomes clear that the term $m2^m/C$ becomes

[1] The reference paper reports that $C = 2.08 \times 10^{-12}$. However they use other units for stress intensity factors, the value was therefore converted.

large causing the objective sensitivity to be orders of magnitude larger than the volume constraint derivative. This problem was solved by using a mathematical objective that scales exactly linear with the physical objective:

$$O = \frac{1}{m2^m \sum_{l=1}^{L-1} \delta a_l} \sum_{l=1}^{L-1} \frac{\delta a_l}{\left(\frac{1}{2}\left(K_I^l + K_I^{l+1}\right)\right)^m} \tag{7.3}$$

resulting in a sensitivity of:

$$\frac{\partial O}{\partial X_e} = -\frac{1}{\sum_{l=1}^{L-1} \delta a_l} \sum_{l=1}^{L-1} \frac{\delta a_l \left(\frac{\partial K_I}{\partial X_e}^{l} + \frac{\partial K_I}{\partial X_e}^{l+1}\right)}{\left(K_I^l + K_I^{l+1}\right)^{m+1}} \tag{7.4}$$

Maximizing O should maximize N as well, as they are linearly dependent. In real applications one might not be interested in maximizing the overall fatigue live but only a part of it, where for example because of inspectability. One could consider maximizing the size of from the smallest inspectable crack to the failure length. When doing so one might increase the importance of one crack increment over the others for which weighing factors (w_l) were introduced resulting in the following optimization:

$$\begin{aligned} \max_{X_1, X_2, \ldots, X_N} \quad & O = \frac{1}{m2^m} \sum_{l=1}^{L-1} w_l \frac{\delta a_l}{\left(\frac{1}{2}\left(K_I^l + K_I^{l+1}\right)\right)^m} \\ \text{s.t. :} \quad & \boldsymbol{f^l} = \boldsymbol{K^l u^l} \ \forall \ l \in 1, 2, \ldots, L \\ & \sum_{e=1}^{N} v_e X_e \ \leq \ V \\ & X_{\min} \leq X_e \leq X_{\max} \ \forall \ e \in \{1, 2, \ldots, N\} \\ \text{where :} \quad & \boldsymbol{K} = \sum_{e=1}^{N} \boldsymbol{K}_e(X_e, \overline{E}) \end{aligned} \tag{7.5}$$

7.2 Limitations

The limitations of the fatigue crack growth life maximization are inherited from the stress intensity minimization one. Two of these limitations are discussed again, as they have more impact on this FCGL maximization than they had on the SIF minimization.

That the thickness of crack tip elements cannot be changed is a significant problem for fatigue life maximization of variable thickness plates. The fatigue crack growth analysis requires the crack to propagate. In the fatigue maximization all elements around the crack are forced to have unit thickness. Literature shows that creating patterns of varying thickness/stiffness in front and after the crack tip influences the crack growth rate and the overall fatigue live [12, 82]. These kinds of crenelation patterns cannot be created by the optimization algorithm.

That the crack geometry needs to be determined in advance does also have a larger impact in this crack growth life maximization algorithm. The fatigue life optimization assumes a crack path and does not consider that the crack might deviate from it. It might very well be possible that a better design, one in which more load cycles are required for the crack to grow a certain length, can be obtained by “crack steering”. It is recommended to investigate how the method can be expanded such that crack steering becomes possible.

Chapter 8

Validation of the finite element method

To ensure that the FEA results are accurate a validation study was performed. One can argue that the accuracy of the FEA is unimportant because the optimization method depends on the gradient information only. This means that the trend between objective and optimization variables is more critical than the actual accuracy. However, validating that the FEA captures the trend properly is the easiest by ensuring that the stress intensity results are accurate throughout the entire design domain.

The validation exists of two phases, firstly by comparing flat plate FEA to existing empirical fit solutions. And secondly by testing optimized geometries and comparing the test results to the FEA.

Separating the hypothesized weaknesses of the model into different tests allows for more direct recommendations. The flat plate validations, discussed in section 8.1, give an indication about the accuracy of the enriched FE model. While problems related to the density-stiffness model or artificially well performing geometry problems should show up in the variable thickness validation (section 8.2).

To ensure repeatability all the results data generated is available online[1]. This data includes raw data, scrips and graphs of both the simulations and measurements.

8.1 Flat plate validation

For the validation of the enriched FEA three problems have been selected, the compact tension, single edge and double edge crack specimens. Analytical stress intensity equations are available for these geometries and because they are used in a variety of testing procedures the accuracy of these equations

[1]The optimization settings, results and post processing scripts are available on OSF [90].

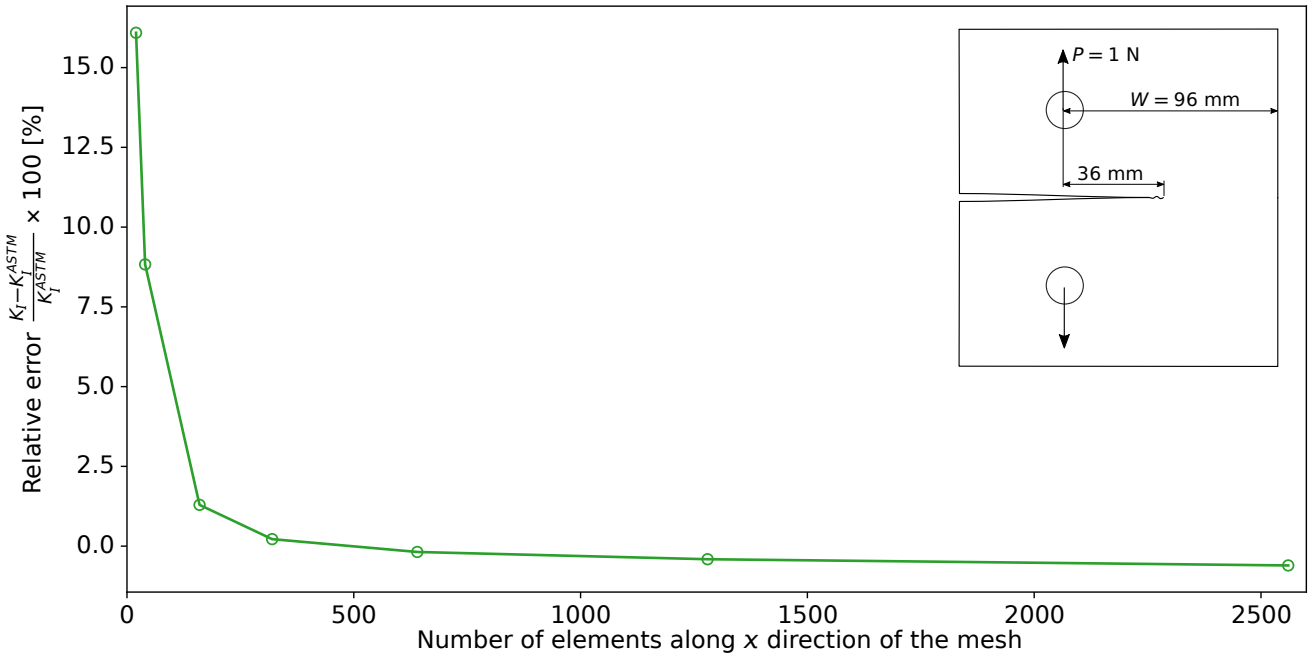

Figure 8.1: Mesh convergence check of a compact tension specimen, where scaled FEA results are compared to an empirical solution of the ASTM standard [76]. For a specimen of unit thickness the empirical solution results in $K_{\text{ASTM}} = 0.697$ MPa$\sqrt{\text{mm}}$, to which the converged FEA differs less than 1%.

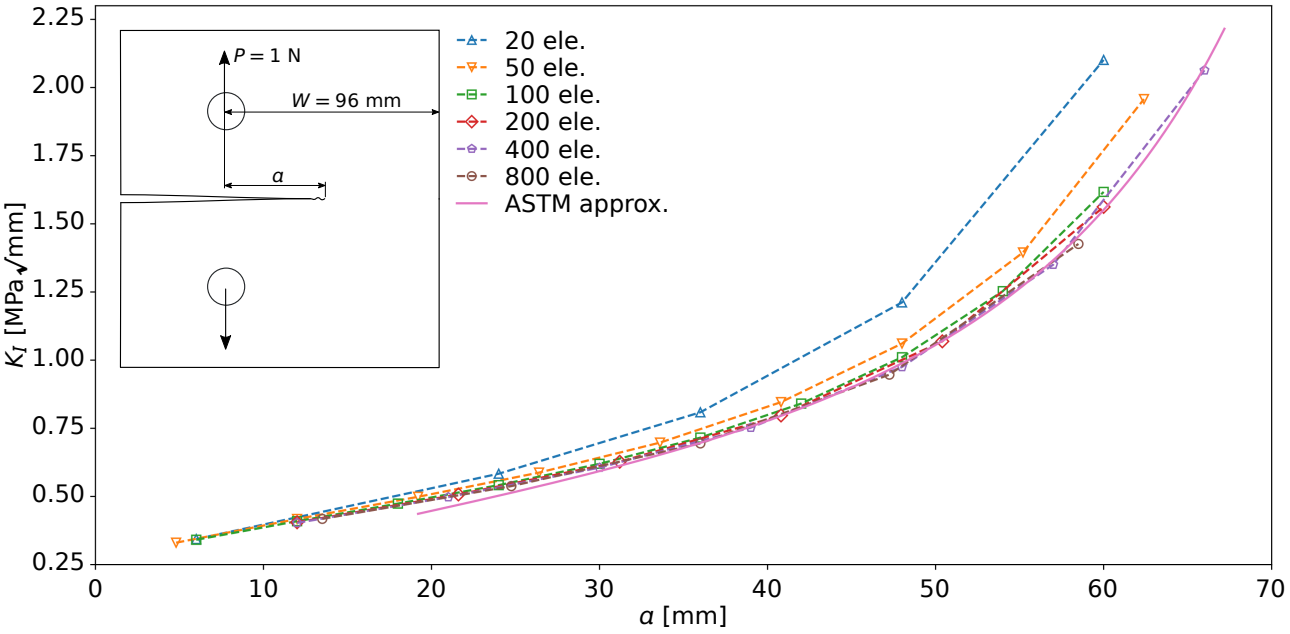

Figure 8.2: Validation where scaled FEA results of several mesh sizes and crack lengths are compared to an empirical solution of the ASTM standard [76], all specimens are of unit thickness.

has been confirmed.

There is a problem with the algorithm that must be solved before the mesh refinement study can be performed. In these simulations every element has a dimension of 2×2, as shown in fig. 6.2. In the code the transformation between the local element and global coordinate system was not implemented. When the mesh is refined, the model will represent a physically larger geometry.

The value of the stress intensity is dependent on the physical size which means that the FEA results need to be scaled to the reference geometry. For each geometry the required scaling factors will be derived.

8.1.1 Compact tension specimen

For the CT geometry, which is defined in ASTM standards [25, 76], the following parameters where used: $W = 96$ mm, $a = 36$ mm, $P = 1$ N, $B = 1$ mm. The stress intensity factor can be calculated with,

$$K_{\text{ASTM}} = \frac{P}{B\sqrt{W}} \frac{2+\frac{a}{W}}{\left(1-\frac{a}{W}\right)^{3/2}} \left[0.886 + 4.64\left(\frac{a}{W}\right) - 13.32\left(\frac{a}{W}\right)^2 + 14.75\left(\frac{a}{W}\right)^3 - 5.6\left(\frac{a}{W}\right)^4\right] \quad (8.1)$$

and results, for the geometry chosen, in a stress intensity factor $K_I = 0.719 \pm 0.65\%$ MPa$\sqrt{\text{mm}}$. The function is empirical, created by least square root fitting to data, and has an uncertainty of $\pm 0.65\%$.

In section 8.1 it was mentioned that the amount of elements directly relates to the dimension of the part. For the CT specimen this means that the values of W and a are directly related to the mesh size, while the ratio a/W, thickness B and load P are independent of the amount of elements used.

The scaling factor, named s, from the FEA to the target size can be defined as,

$$s_W = \frac{W}{W^{\text{FEA}}} \quad (8.2)$$

$$s_a = \frac{a}{a^{\text{FEA}}} \quad (8.3)$$

because eq. (8.1) states that $K_I \propto 1/\sqrt{W}$, a scaling of the stress intensity factor can be derived, resulting in,

$$K_I = K_{\text{FEA}} \frac{1}{\sqrt{s_W}} \quad (8.4)$$

after scaling the stress intensity values they were compared to the empirical solution.

Figure 8.1 shows that the FEA solution does converge to the empirical one for increasingly finer meshes. The solution of the most refined mesh, $K_I = 0.715$ MPa$\sqrt{\text{mm}}$ is less than 1% below the empirical value. Acceptable results, those with an error of <2.5%, are obtained when the amount of elements in x direction is equal or more than 160.

In fig. 8.2 the empirical solution and the scaled finite element results are plotted for various crack lengths. The graph affirms that the FEA solutions become more accurate with increasing mesh size. The FEA model is clearly able to capture the trend of K_I as a function of crack length a, even at coarse resolutions.

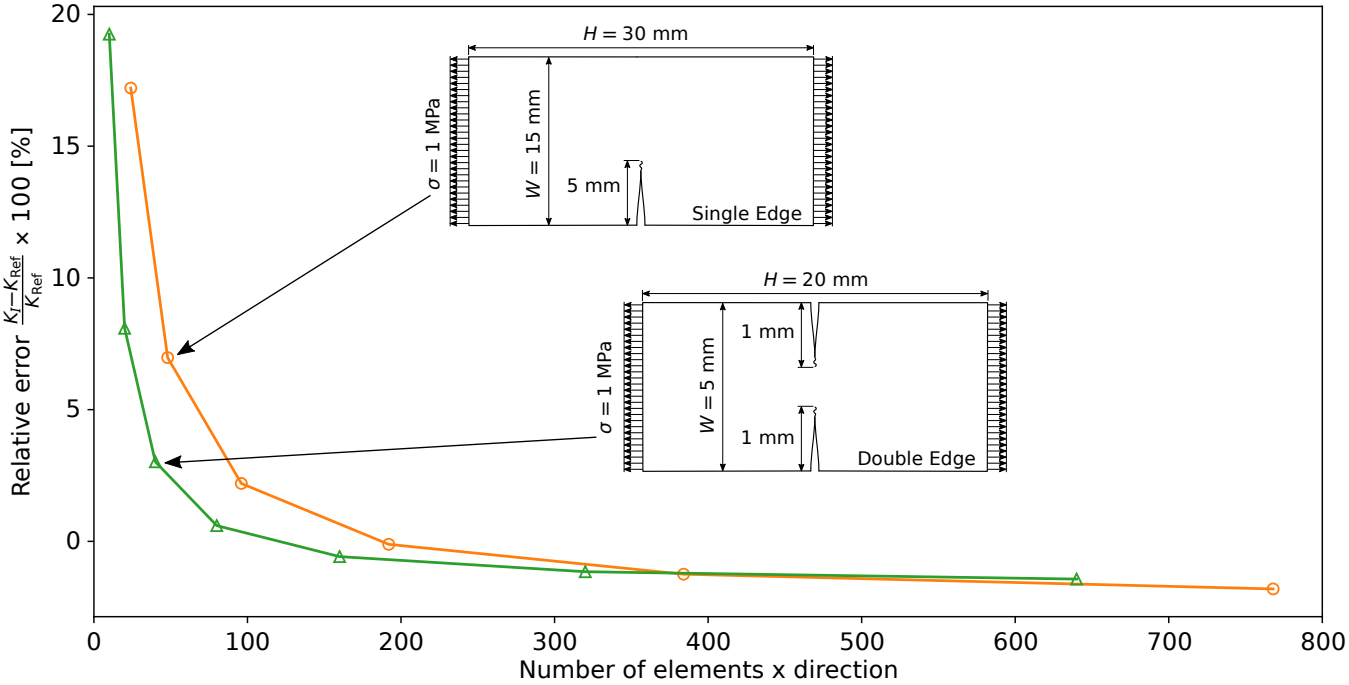

Figure 8.3: Mesh convergence check of a (double) edge crack specimen, where scaled FEA results are compared to an empirical solution obtained from "The Stress Analysis of Cracks Handbook" [24], $K_{Ref} = 7.09$ and $K_{Ref} = 2.00$ MPa$\sqrt{}$mm for the edge crack and double edge crack respectively. In both cases the relative error converges to a difference of less than 2%.

8.1.2 Edge crack specimens

For two other sample geometries, the single and double edge cracks specimens, the same mesh refinement and validation study was performed.

For both geometries the empirical stress intensity equations were obtained from the "The Stress Analysis of Cracks Handbook" [24], for single edge crack specimens given was,

$$K_{Ref} = \sigma\sqrt{\pi a}\left[1.122 - 0.231\left(\frac{a}{W}\right) + 10.55\left(\frac{a}{W}\right)^2 - 21.71\left(\frac{a}{W}\right)^3 + 30.382\left(\frac{a}{W}\right)^4\right] \quad (8.5)$$

and for a double edge crack specimens the equations was,

$$K_{Ref} = \sigma\sqrt{\pi a}\left[1.12 + 0.406\left(\frac{a}{W}\right) - 2.394\left(\frac{a}{W}\right)^2 + 3.860\left(\frac{a}{W}\right)^3\right] \quad (8.6)$$

which for the geometries given in fig. 8.3 results in a stress intensity value of $K_I = 7.09 \pm 0.5\%$ for the single and $K_I = 2.01 \pm 2\%$ MPa$\sqrt{}$mm for the double edge crack specimens.

For both these specimens the stress intensity value $K_I \propto \sqrt{a}$ resulting in a stress intensity scaling factor

$$K_I = K_{FEA}\sqrt{s_a} \quad (8.7)$$

From fig. 8.3, which compares the analytical to the FEA solution, it can be concluded that the FEA solution converges. Although the amount of elements in width direction required for the error to go below 2.5% is different between the geometries, converged results can be obtained at relative low, 300 elements along the width, resolutions.

It should be noted that L. Nash-Gifford and P. Hilton showed that accurate stress intensity factors of the double edge crack specimen can be reached at even with only a couple of elements [32]. They obtain accurate results with fewer elements than what is possible with the implementation used in this thesis.

8.1.3 Conclusion

From the mesh convergence and validation of flat problems four conclusions can be drawn.

Firstly that the stress intensity factor converges stably with increasing mesh refinement. The resolution required to converge differs from geometry to geometry. Of all three problems the mesh required is acceptable in the sense that reasonable computational effort is required to solve the FE problem.

Secondly, the mesh required for converged solutions is finer than those in the paper of L. Nash-Gifford and P. Hilton [32], where they presented the enriched bicubic serendipity elements. The difference in mesh requirement can be explained by the following reasons. They used a local mesh refinement strategy with higher, third, order elements throughout the whole mesh. This in contrast to the algorithm presented in this paper which has constantly sized linear elements. The local refinement they used will allow a coarse mesh further a way from the tip while using

higher order shape functions will result in a more accurate approximation of the displacement field. Furthermore, because they used bicubic serendipity elements throughout the mesh, problems with meshing around the enriched elements does not exist.

Simply using bicubic elements throughout the entire mesh will greatly increase the computational requirement to obtain optimized results at high resolutions, because the mesh is directly linked to the optimization resolution. It is possible implement a multi-resolution optimization where the mesh is courser than the resolution of the optimization variables. This does significantly improve the performance of higher order finite element meshes in topology optimization [81].

Thirdly that the stress intensity factors calculated with the enriched FEA match the empirical solutions for all geometries inspected.

Lastly, that an element-global coordinate transformation should be implemented in the algorithm to avoid the need of scaling FE results. Scaling is possible for the geometries considered as the factors could be derived from empirical equations to calculate the stress intensity, however for more complicated geometries their scaling factors cannot be derived. This means that a mesh refinement study with the current algorithm is impossible for arbitrary geometries.

In the end it can be concluded that, although the current FE implementation works, two improvements to the FEA analysis can be made:

- A element to global coordinate transformation should be implemented.
- The hanging node method must be removed by using bicubic elements throughout the entire mesh as shown in [32].
- A multi-resolution optimization scheme should be implemented to result in high resolution optimized geometries at low computation costs as shown in [81].

8.2 Variable thickness validation

The previous section shows that the FE model can accurately capture cracks in flat specimens. It does not show however, how accurate the model is for variable thickness plates. Adding thickness variation into the model introduce problems, for example the thickness-stiffness problem which was discussed in section 6.4.1.

The test discussed in this section was performed to verify whether the FE model can accurately calculate the displacement field and stress intensity factors for variable thickness geometries. It was assumed that all designs which the optimization algorithm iterates over are in between the initial one, a flat plate, and the optimization results. Since the flat plates where validated already, only geometries resulting from an actual optimization where tested. This reduced the amount of specimens and time significantly.

During the test three different measurements where performed; DIC (Digital Image Correlation) was used to measure how much the crack opens up, an extensometer was used to measure the clamp displacement and the load cell measured the failure strength. The crack opening and clamp displacement can be related to the specimen's stiffness response, while the maximum load can be related to stress intensity factors directly.

For these tests six different samples, one flat compact tension specimen and five optimized CT geometries where used. The optimizations where run with different settings to obtain different geometries, more details about the optimization of CT specimens is discussed in section 9.1.

It was hypothesized that FE results of the specimens with large abrupt changes in thickness are less accurate than their smoother counterparts. The FE method assumes that through the thickness the strains/stresses are constant. But as shown in fig. 6.6, this is not the case at the thickness changes. The more abrupt the change, the larger the stiffness overestimation is.

8.2.1 Specimen

To ensure that some specimens have smoother thickness changes than the others the main difference between the specimens is in the density filter radius, the larger this is, the more smooth the geometry becomes. Another variation between the specimens is the maximum thickness, because a larger maximum thickness allows for larger changes in thickness which was hypothesized to be detrimental for the FEA accuracy. The settings used are shown in table 8.1, all other settings were kept constant, a minimum thickness 1 mm, 500 elements in horizontal direction, and a crack that reaches until the middle ($a/W = 0.375$).

	$r_{\min}$ [elements]	$x_{\max}$ [mm]
CT Flat	1.0	1.0
CT0053	1.5	2.0
CT0054	3.0	2.0
CT0055	7.0	2.0
CT0057	30.0	2.0
CT0058	1.5	1.5

Table 8.1: The differences between the optimization settings.

The thicknesses distributing resulting from these optimizations was transformed into a .stl (steriolithography file format) mesh with the help of a ball pivoting surface reconstruction algorithm [91] in meshlab [92]. The mesh was scaled to the final dimension, shown in fig. 8.4, the minimum thickness was set at 20 mm.

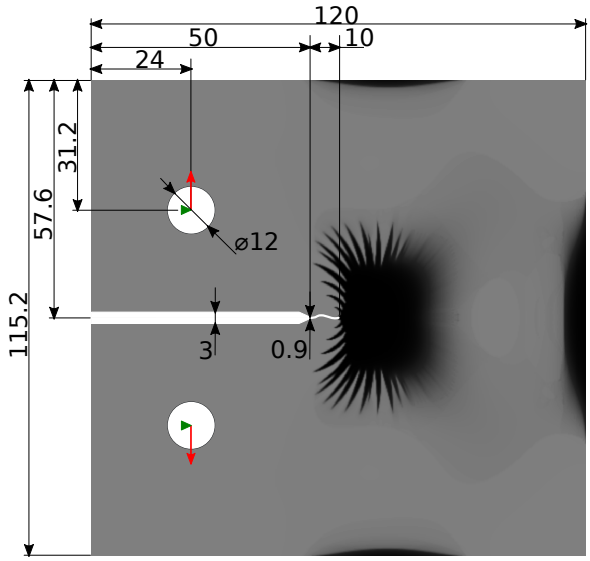

Figure 8.4: The dimension of the specimens, the thickness of the specimen is 20 mm. The dimensions are projected on the geometry of CT0053.

Eventually the parts where manufactured of white resin (FLGPWH04) with a formlabs Form 2 printer. The specimens where cured for 60 minutes in a curing chamber at 60°C. The slit and holes where machined while the precrack was made by hand with a hacksaw and finished with a 0.25mm thick jigsaw. The dimensions of the final specimens was measured and documented.

The final geometry is close to the simulated one, however one important difference was found. The thickness at the cracktip was not manufactured accurately. This thickness was set to 1 in all simulations, 20 mm after scaling, and all surrounding elements where allowed to change. In the optimization the surrounding elements became significantly thicker which resulted in small but deep dimple at the crack tip. Sadly this dimple was barely visible after printing due to the printer resolution and accuracy. This difference is likely to have little effect on the crack opening as the opening is related to stiffness and driven by a global response, on which this local difference has only little effect. However, this difference is likely to increase the failure load significantly as it is dependent on local properties.

8.2.2 Test setup

The first test, which measures the crack opening is a test within the elastic regime. The goal is to plot how much the crack opens at every location along the crack length. The displacement can be linked to the overall elastic response, and assuming the FEA is accurate the model should have a crack opening similar to reality.

To measure this DIC is used. A 3D, two cameras, setup was used and consisted of 5.0 MP FLIR Grosshopper3 cameras with a Sony Pregius IMX250 sensor. The cameras where equipped with 80 mm lenses while a spot was used to ensure a (constant) and light target.

The test was performed on a Zwick 20 kN test bank that was equipped with an extensometer and analog output channel to export the force to the DIC computer (1 V = 200 N). A preload of 20 N was used and a speed of 1 mm/min was set. From testing the flat compact tension specimen till failure, 1118 N, it was decided to load all other specimens to 500 N. As 500 N is far below the expected failure load no damage occurred, which allows for a repeated test if required.

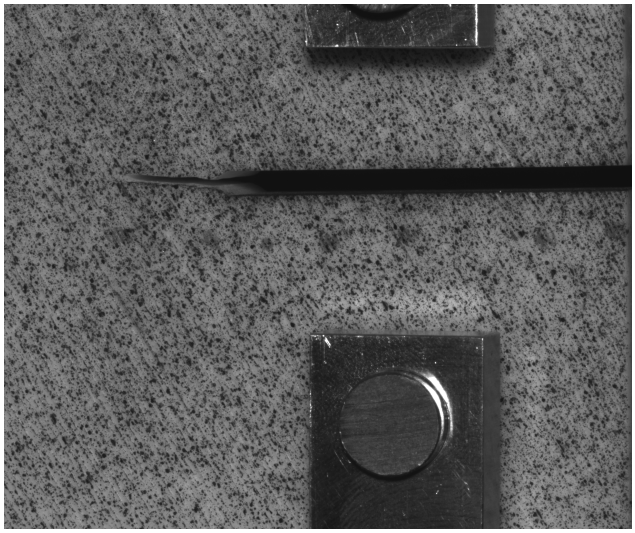

Figure 8.5: In plane rotation of the CT Flat sample. This figure is moving in the digital edition of this thesis.

During the test it was observed that the part rotated a bit. This was probably caused by a (small) misalignment of the bracket holding the specimens. This is made visible in fig. 8.5, which shows the difference between a photo at rest and loaded condition. The other movements visible, crack gap widening and the slight translation downward, are expected. This rotation happened slowly and even at higher loads due to the high friction between the bracket and tensile machines' wedge grips. As the misalignment between the brackets was different per specimen a different amount of rotation was observed per specimen.

The data was processed with Vic-3D which calculated the location and displacement of the surface using the speckle patterns. The subset size and step size where automatically determined and auto calibration was used to obtain accurate and precise results.

Two less usual post-processing steps where required to obtain the required displacement fields. To have the coordinate system of the measurements align with that of the model the coordinate system needed to be set such that the crack aligns with the x-axes. While the rigid body movements where to be removed from the displacement fields as the model excludes those. This removal did also remove the rigid

body rotation resolving all issues related to it.

Python was used to interpolate the results to a structured grid, plot the displacement fields and extract the crack opening as a function of horizontal location. The crack opening is calculated by adding the downward deflection 3 mm below the crack to the upward deformation 3 mm above the crack. Some distance above and below the crack is required as DIC cannot give results at the edge.

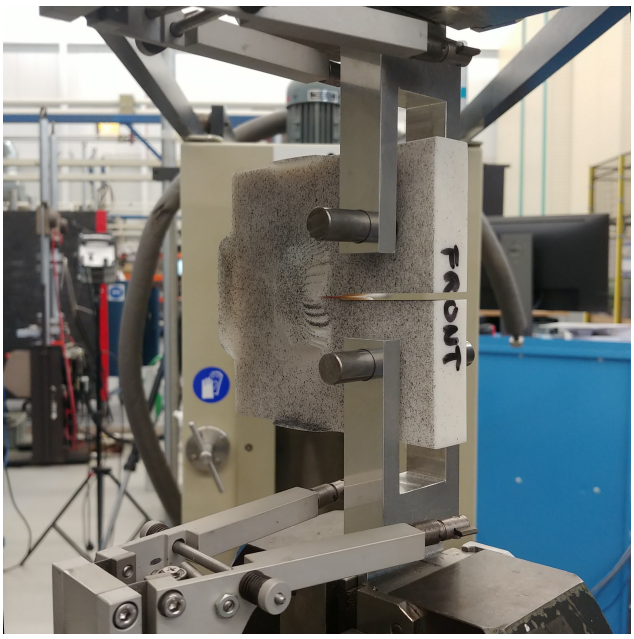

Figure 8.6: Compact tension tensile test setup.

During these elastic tests an extensometer was mounted on the clamps, as shown in fig. 8.6. The idea was to use this to determine the elastic modulus required to make the FEA of the flat CT specimen match that of the measurements. The results where excluded because the rigid body rotation caused the results to be inconsistent and invalid, a part of the extension measured was due to this rotation.

After testing the elastic response, the fracture strength was measured. To do so the specimens where pulled apart in the Zwick 10 kN testing machine. No other sensors then the load cell were used, the only intention was to measure the ultimate strength.

8.2.3 FE setup

A python code to run the FEA and export the crack opening and stress intensity values was derived from the optimization algorithm. This code can import the optimized geometries while it allows one to alter parameters such as the material properties, crack length and even SIMP penalization factor.

Most of the settings used for these FEA are the same as those used in the optimization from which the geometry was obtained. Three differences exist however, material stiffness, crack length and load magnitude. From the manufactured specimens the crack was measured and the actual length was used in the FEA model. As the stiffness influences both the crack intensity value and crack opening magnitude it was required to obtain its actual value.

As it was proofed that the FEA is accurate in predicting the flat plate results, see Section 8.1, the flat specimen was used to tune the model. The flat specimen is the only that was loaded in tension until it broke wile using the DIC setup. A load close to failure (1072 N) was chosen to determine the stiffness from. It is important to notice that this variable plate problem required some sort of running stiffness per unit thickness value (E/t), see eq. (6.2). As the model is run with a thickness of 1 (unity) the goal is simply to find the stiffness required for the model to match measurements.

As the model is linear, all displacements can be scaled inversely with stiffness, which results in $E/t = E_{\text{old}}/t \cdot O_{\text{FEA}}/O_{\text{real}}$. And resulted in a stiffness of 58956.7 MPamm/mm.

	E/t [MPamm/mm]	Opening [mm]
Original	1.0	30740
Scaled	58956.7	0.5214

Table 8.2: FEA crack opening for different stiffness's an $F = 1072$ N. The crack opening was measured to be 0.5214 mm.

As the FEA uses symmetry the crack opening was calculated as twice the y displacement of the elements directly at the crack, while the stress intensity factors were obtained from the FE enrichment.

To predict the fracture strength the fracture toughness (K_{IC} MPa$\sqrt{}$mm) is required. This was again obtained by tuning the FEA of the flat specimen to its measurement. To simplify all calculations the stress intensity factors where used without scaling to the real specimen dimensions. As the stress intensity factor is linear depended on the load the following equation determines the fracture toughness,

$$K_{IC} = F_{\max} K_I(F = 1N) \tag{8.8}$$

resulting in $K_{IC} = 269.9$ MPa$\sqrt{}$mm. Reversing this equation allows for the calculation of the fracture strength of the optimized specimens,

$$F_{\max} = \frac{269.9}{K_I(F = 1N)} \tag{8.9}$$

8.2.4 Results

The crack opening test show good agreement between the FEA and measurements for CT Flat, CT0053, CT0057 and CT0058, as shown in fig. 8.7. The crack opening graphs of the FEA and measurments have similar shapes and the magnitudes.

In fig. 8.7 one can consistently find two differences between the measurements and FE results. Firstly

the crack opening magnitude of the FEA is slightly lower ($\leq$ 1%) and secondly that at the crack-tip the FEA crack opening drops to zero directly, whereas the measurements show a smoother transition.

The specimens, CT0053, CT0054, CT0055 and CT0057 are all very similar in geometry which means that the crack opening calculated with the FEA are all nearly equal. In fig. 8.8, which shows these samples, one can see that the FEA results are overlapping with each other. Surprising is that the measurements of two of these specimens, CT0054 and CT0055, are inconsistent with the simulations.

The failure load test shows that all specimens where stronger than predicted, as shown in fig. 8.9. The differences between measurements and predictions is significant and can be up to 30%.

8.2.5 Discussion of the results

The differences in fig. 8.7 can simply be explained; firstly the FEA seems to be stiffer because the stiffness (E/t) was calculated at a load close to failure (1072 N). Although the material is brittle and shows a near linear stress strain curve it is assumed that the difference of $\leq$ 1% is caused by a bit of non-linear behavior just before failure.

Secondly that the measured crack opening does not drop off to zero directly at the crack tip can be explained by the measurement method. The crack opening was measured by taking the upward displacement 3 mm above the crack and added to the downward displacement 3 mm below the crack, this will have a smoother transition because no singularities exist above or below the crack tip. The FEA uses the displacements directly at the crack, they drop to zero at the crack tip as there is no opening anymore.

No good explanation for the offset between the measurements and FEA of specimen CT0054 and CT0055 have been found. The specimens are created by a simulation with filtersizes (r) between those of CT0054 and CT0057 resulting in geometries that are similar to those. It would be logical to assume that the crack opening would be similar, but it is not. The maximal opening is 0.23 mm, close to that of the flat specimen. Besides the sharp drop at $x = 0$ (fig. 8.8) is not supposed to exist. Such a large drop would locally require an enormous strain, which seems impossible. The test data was processed multiple times to exclude the possibility of mistakes in the processing steps. In the end it was decided to exclude CT0054 and CT0055 as they are assumed to be outliers caused by measurement errors.

That the failure loads where always higher than predicted by the FEA was most likely caused by the manufacturing issues mentioned in section 8.2.1. Firstly was the crack tip not infinity sharp, but made with a 0.25mm jigsaw which reduces the stress magnitudes at the crack tip. Secondly was the thickness at the crack tip larger than modeled due to the printing inaccuracies. A local increase of thickness at the crack tip increases the failure load, mostly easily explained with the concept of strain energy release rate,

$$G = \frac{K_I^2}{E} \tag{8.10}$$

and can be related to the amount of energy required per unit new fracture area. When the part, locally, becomes thicker than expected more energy is required to create the new area increasing the critical load.

In the end it can be concluded that the FE model is able to accurately model deformation but verifying that the stress intensity factors are accurate was impossible because the geometry manufactured was

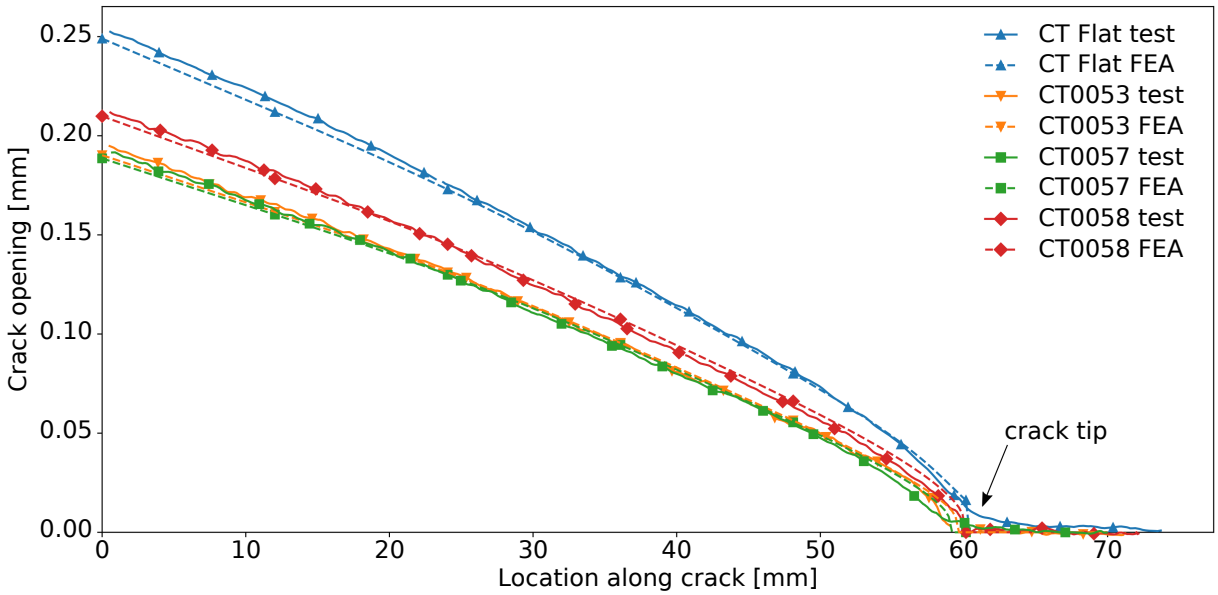

Figure 8.7: The crack opening of the FEA and measurements of CT Flat, CT0053, CT0057 and CT0058.

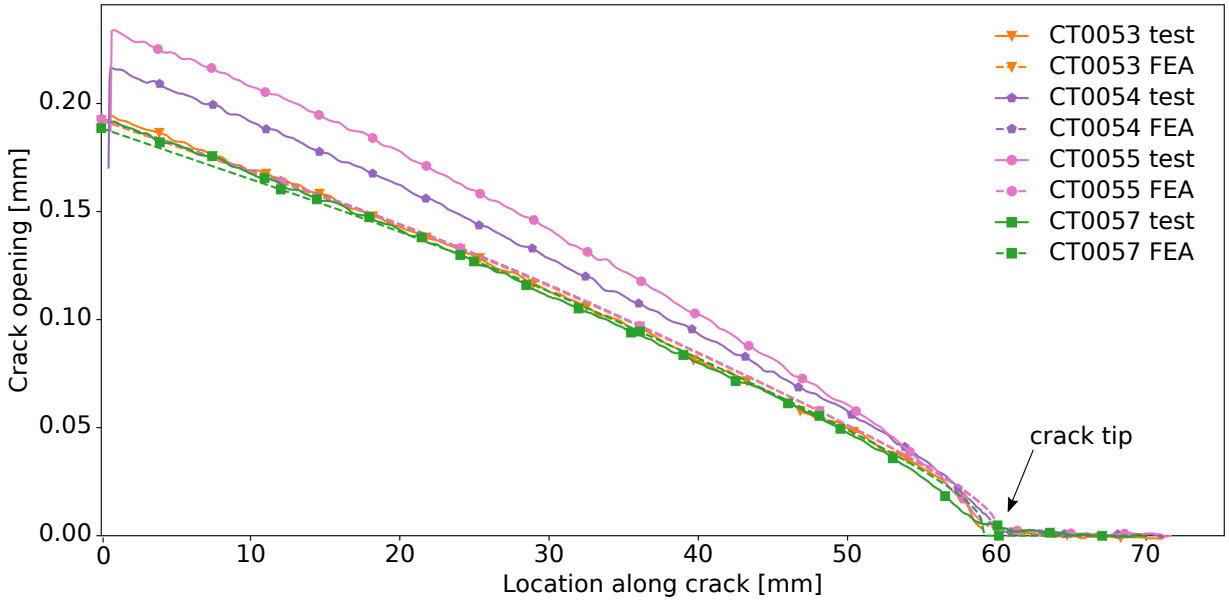

Figure 8.8: The crack opening of the FEA and measurements of CT0053, CT0054, CT0055 and CT0057.

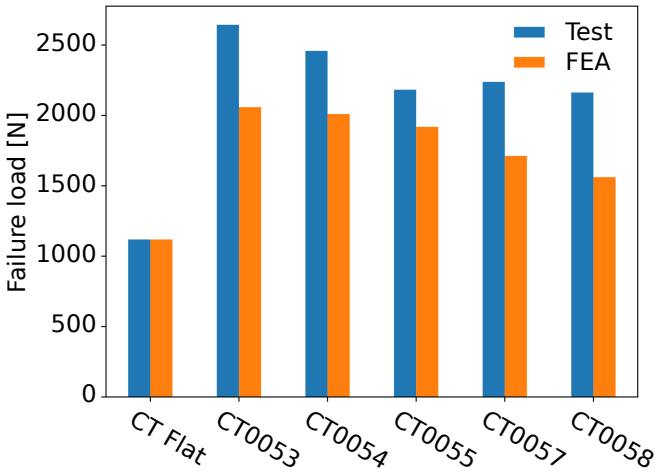

Figure 8.9: Comparison of actual and predicted failure loads.

significantly different from the modeled one. It was also impossible to proof that the filter size has an effect on the accuracy of the FEA model, because of two outliers in the four samples meant to test that hypotheses. It is recommended to improve the code such that:

- The enriched crack tip elements are allowed to change in thickness, which does not only impact the stiffness term but also the enrichment parts. To avoid instabilities in the optimization it is recommended to keep the crack tip elements density linked to that of the surrounding ones.
- Performing tests with more samples to proof, or disprove, the hypotheses that claim that underneath a certain filter size errors caused by the thickness-stiffness equation will invalidate the FEA.

8.2.6 Discussion of the test procedure

Although the crack opening and fracture tests where successfully used to validate the FE model the tests themselves can be improved upon. Several problems where encountered:

- Manufacturing of an infinitely sharp crack tip was impossible with plastics.
- The performance of some specimens was close te equal because the geometries where similar (CT0053 and CT0057), more variation in the design is recommended.

A better test would be a fatigue crack growth speed test. This would allow one to determine the stress intensity values as a function of crack length by using the Paris law. As the crack is formed by growing, the tip will be sharp and the test can return stress intensity factors of as a function of location. The drawback is that such a test would require metal specimens which is relatively expensive and the manufacturing will be time-consuming.

Chapter 9

Designing variable thickness plates

Since the optimization algorithm was developed and its FE method validated it can now be used to design parts. This chapter presents the results of variable thickness plate optimizations. In this optimization a base plate of unity thickness is improved by adding material. Appendix A discusses the settings of this optimization where the design variables are interpreted as the local plate thickness. Similar to the validation study, the focus lies on compact tension specimens because the code to analyze and optimize them is already developed.

The chapter starts with a detailed discussion of the stress intensity minimization of the compact tension specimens in section 9.1. The focus lies on the magnitude of the stress intensity factor reduction, its sensitivity to the simulation settings and the geometries that results from it.

Then a fatigue life optimization of these compact tension specimen will be discussed in section 9.2. Here the computational costs, the resulting geometries and performance will be compared to the stress intensity optimization.

9.1 Minimizing stress intensity

The optimization problem and setup must be discussed before their results are. To reduce the computational cost a symmetry axis is used resulting in a model of the upper half of the CT specimen, as is shown in fig. 9.1. The horizontal symmetry axis creates a boundary condition, which constrains vertical movement at the bottom. At the crack this vertical boundary condition was removed to allow the nodes to move up and down freely.

For all simulations 500 by 240 elements in horizontal direction were used while the problem was initialized with a constant thickness equal to 1. In the area just around the load introduction the plate thickness was constraint to a value of 1 to avoid local thickness spikes to appear due to stress concentrations. The crack extended to half-way the part ($a/W = 0.375$). The minimum thickness (X_{min}) was also set to 1 while settings such as the filter size, maximum thickness and material constraint where varied. Because of time constraints the optimizations where cut off after 5000 iterations, even if the result was not yet converged. A complete overview of the simulations,

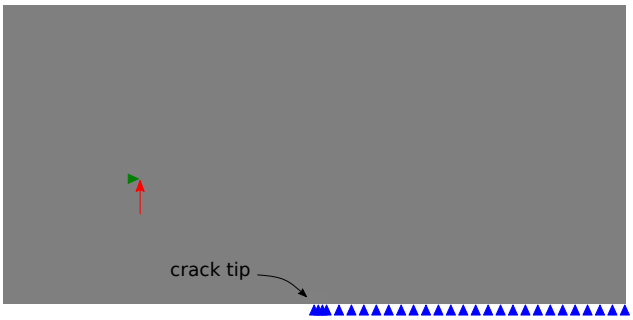

Figure 9.1: Low resolution compact tension specimen initialization and load case. The red arrow is a force, the blue triangle is vertical constraint while the green one is a horizontal constraint.

there settings and the post-processing scripts can be found online[1].

The results will be compared to a flat compact tension specimen of unity thickness. Of these flat plates the stress intensity factors will be calculated with the algebraic approximation of eq. (8.1). The performance will be given as a dimensionless ratio, $K_{\text{SIM}}/K_{\text{Ref}}$. This comparison might be unfair as the mass of the optimized geometry can be more than that of this flat plate, depending on the material constraint. Therefore, the performance of a flat plate of same weight is shown as well.

9.1.1 Sensitivity to optimization settings

The first investigation studied the sensitivity of the density filter size on the stress intensity factor of optimization results. Figure 9.2 does not only show how the final stress intensity is influenced but also shows what the difference is between the resulting geometries.

Clearly the size of the finest features increases with increasing filter size. This is the intended behavior, as the filter is meant to allow for mesh-refinement studies which requires constant smallest feature sizes on different meshes.

One can imagine that an increasing minimal feature size constrains the design spaces, as disallowing

[1] The optimization settings, results and post processing scripts are available on OSF [90].

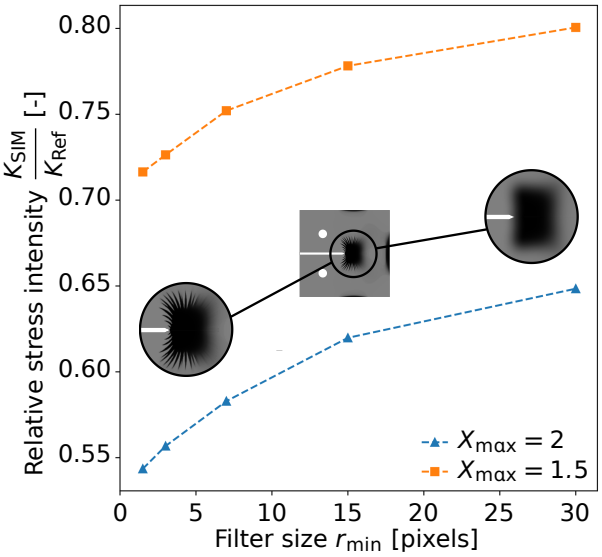

Figure 9.2: Optimization results at different filter sizes, final weight is 110% of the flat reference. A flat plate of same weight would have a relative performance of 0.91.

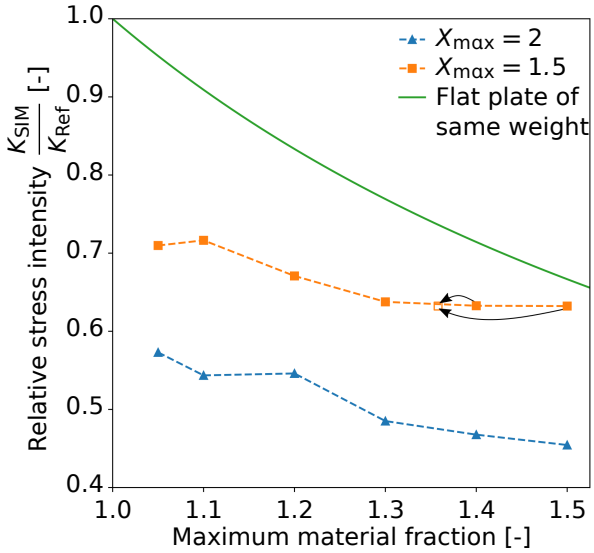

Figure 9.3: Optimization for different volume fractions and flat plate of same weight. Cases with max thickness of 1.5 do never use more than 1.36 volume even if it is available.

small features to appear results in less different designs to choose from. This can cause the designs at larger filter sizes to become less optimal. The graphs in fig. 9.2 clearly show that the most efficient designs are those with small filter sizes.

The filter can not be removed however, as the smallest features should at least be larger than the element size, to avoid the appearance of inaccuracies in the FE algorithm. Unknown is what the minimal filter size is that results in acceptable designs. It was impossible to derive the minimal filter size required to for accurate FE results from the validation study (chapter 8). Currently filters are set such that no checkerboard patterns appear but it is unknown whether other but similar, numerical, problems exist and from which filter size they are removed.

The optimization algorithm distributes the element stiffness such that the stress intensity is minimized. The local thickness constraints X_{min} and X_{max} have a great impact on the performance of the optimal solution, because the element stiffness is related to the local thickness. From fig. 9.2 it can be observed that the samples with a larger maximum thickness perform better.

Due to linearity in the model the absolute magnitudes are not that important, it is the ratio between stiffness of the thickest and thinnest elements that has the most impact. It is therefore hypothesized, that optimizations with double the thickness and volume constraints will simply result in a scaled geometry with the same layout. Doubling the thickness everywhere means that the crack tip elements thickness should be doubled as well. This makes testing of the hypothesis impossible with the current implementation, as it requires the crack tip element thickness to be unity.

Figure 9.3 was produced to verify the impact of the resource (material) constraint. This constrains the amount of material available for distribution, in the code the constraint is reported as the maximum average thickness of the plate. The higher the value, the more material can be used. Using less than available is allowed.

One might simply assume that more material will result in stronger parts, for example the stress intensity factor of flat CT specimens is inversely proportional to the thickness, but for complex geometries it is not that simple. Two exceptions can be found in the graph. Firstly, for low volume fraction some unstable behavior can be found. That the stress intensity is not continuously decreasing for increasing material constraint is attributed to simulation getting stuck in different local minima. Secondly, adding mass might actually be detrimental, because it increases the local stiffness, which then attracts load and results in higher stresses.

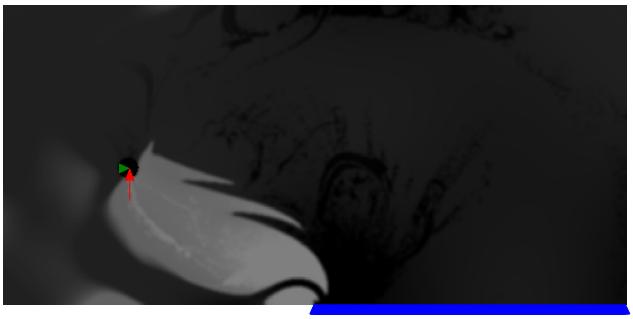

Figure 9.4: Optimization can assign less mass than available. The simulation was set up with a material constraint of one, in the end a fraction of only 0.868 was reached.

In fig. 9.3 it is shown that adding material to the optimization algorithm does indeed improve the performance initially, however, at a certain point it has no effect anymore. For the thin optimizations ($X_{max} = 1.5$) a volume fraction up to 1.5 was allowed, this essentially means that the optimization can distribute material with maximum thickness everywhere. The algorithm did not do this however, it did only use a volume fraction of 1.36, as indicated by the arrows.

An other example of this is given in fig. 9.4, where only 87% of the assigned mass was used. The simulation was run with the local thickness values (X_e) constraint by $X_{max} = 1$ and $X_{min} = 0.5$ and a volume fraction of one. Assigning all the material would result in a geometry equal to the reference design, a flat plate with a thickness of 1 everywhere. The optimization shows that even removing material can result in a stress intensity reduction of nearly 50% ($K_{SIM}/K_{Ref} = 0.54$). The material is removed between the crack tip and the load introduction, which will cause less load to be attracted to the crack and locally result in lower stresses.

In the end it can be concluded that the volume fraction has a smaller impact on the results then expected. It is less important than the ratio between the maximum and minimum thickness. More important is that this shows that adding mass might not be the solution when considering stress intensity optimization. This can cause the biological optimization methods, developed by Jones and Das [68, 69], to work badly. These biological algorithms do namely assume that adding mass locally improves the performance locally.

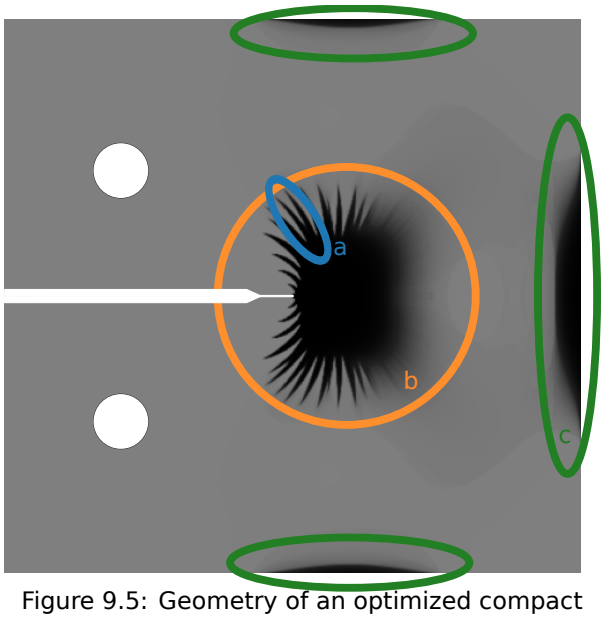

Figure 9.5: Geometry of an optimized compact tension specimen. Geometric features a. fringes, b. plateau and c. edges.

	K_I [MPa$\sqrt{}$mm]	Part of improvement [%]
a, b and c	0.1311	100.0
a and b	0.1357	96.8
b only	0.1521	80.9
c only	0.2336	6.9

Table 9.1: Contribution in stress intensity reduction of the geometric features. It can be derived that the fringes (feature a) contribute for 14.9%.

9.1.2 Characteristic geometric features

The final geometries contains several distinct features that appear in most of these CT optimizations. Some features that appear have a larger impact on the performance than others. In fig. 9.5 three features have been highlighted; the fine fringing patterns, the plateau just behind the crack tip and the increased edge thickness. The fine fringing pattern does not appear in all simulations, as larger filter sizes forces features to become larger which causes fringes to disappear.

Simulations have been run where some of these features have been removed to calculate their individual impact. Of which the results are reported in table 9.1. The impact of the features was given in a percentage of the improvement of the final design with respect to the reference plate. Note that adding the performance of all three features separately does not result in the same as that of a simulation with all features. This is caused by the (minor) interaction between the features.

The impact of the fringes could not be calculated separately because they are dependent on the plateau. The impact can be derived from the difference between the simulations with a & b and b only and resulted in a contribution of 14.9%.

It is hypothesized that these fringes create an anisotropy behavior, as the stiffness in length direction is higher than that along the width. This anisotropy can guide the loads into certain directions, guiding it away from the crack tip. This hypothesis remains however untested.

The impact of the plateau behind the crack tip is the largest, 80.1%, of all the features. The impact is most likely caused because it can reduce the loads of the crack tip stress redistribution. Just behind the crack tip normal stresses are largest, adding material in this region will reduce the stress of the redistribution most significantly.

The impact of the increased edge thickness is most likely caused by a similar reason, reducing stresses of the bending behavior of the CT specimens. The layout of the CT specimen is developed to create a moment around the out of plane axis. This moment causes extra tensile stresses at the crack tip and allows fracture toughness measurements with a small specimen at relative low loads, hence the name compact tension specimen. While the bending stresses cause tension at the crack tip, they cause compression at the back. This means that increasing the thickness at the back will resist the bending more

than adding material halfway between the crack tip and the edge.

Overall, it can be concluded that the plateau at the crack tip has the most impact compared to the other features. The reasons that the features impact the performance can be hypothesized but where not verified. It is recommended to perform a more detailed investigation into the features and the reason that they arise. This might help us understand more about the design of damage tolerant structures.

9.2 Maximizing fatigue life

Fatigue life maximization design geometries that will sustain the most load cycles before the crack grows to a given length. This is different from stress intensity minimization for two reasons.

Firstly, because of scaling, which is caused by the non-linearity of the Paris-Erdogan relation,

$$\frac{\mathrm{d}a}{\mathrm{d}N} = CK_I^m \tag{9.1}$$

where $C = 5.05 \times 10^{-16}$ and $m = 4.41$ are the constants used in this study [89]. Due to the power m a small improvement in K_I, will result in a relatively larger change in da/dN. For example a reduction in stress intensity of 10% will result in a 35% lower crack growth rate.

Secondly because fatigue life maximization takes the performance over a range of crack lengths (increments) in account. This results in the following integral equation,

$$N = \int_{a_{\min}}^{a_{\max}} \frac{\mathrm{d}N}{\mathrm{d}a} \mathrm{d}a \tag{9.2}$$

the maximization of fatigue life is essentially equivalent to maximizing the area underneath the a-dN/da curve. Whereas minimizing K_I will lead to a maximal dN/da value for a crack of one specific length.

Notice that dN/da, the amount of cycles to grow one mm, is non commonly used in literature. Normally the crack growth rate da/dN [mm/cycle] is discussed as it comes from the Paris-Erdogan formula directly. The crack growth rate is logical to use when one wants to illustrate that cracks propagate faster with increasing crack length. It fails however, in the discussion of the optimization algorithm presented, as it has no direct physical relation with the objective[2]. For completeness this thesis will present both the a-da/dN and a-dN/da graphs, as can be seen in figs. 9.9 and 9.10.

It is evident that due to these differences fatigue life maximization will lead to other results than stress intensity minimization. This section explores what these differences are. It will focus on the computational aspect, optimized geometries and their performance.

9.2.1 Computational considerations

In this thesis little attention was payed to the computational efficiency, stress intensity minimization was fast enough to run on a simple laptop anyway. This is different for fatigue life maximization. The difference in computational requirements comes from the fact that information of the stress intensity and its sensitivity are required as a function of crack length. The fatigue growth model requires calculating stress intensity factors for the crack at different values of a. For each stress intensity calculation a mesh needs to be generated on which a FEA and adjoint problem will be solved. Please see the methodology in chapter 7 for more information.

In the current, simple but inefficient, implementation the following steps are taken:

1. During the problem initialization the meshes for the crack at all lengths are generated.
2. During each iteration the following steps are performed for all these meshes:
   (a) Assemble the stiffness matrix.
   (b) Solve both the linear elastic and adjoint problems with a complete Cholesky factorization, which has a computational complexity of $O(n^3/3)$.

All meshes are generated ones and reused throughout all iterations, which compared to regenerating them, reduces the computational requirements. This causes an increase of the memory requirements, because all the meshes generated need to be saved untill they are used. The size of all these arrays becomes significant. The optimizations run for the stress intensity optimization section (section 9.1) with a mesh of 500 by 240 elements required 0.3 GB to store the mesh. For fatigue life maximization many of these meshes need to be saved. For an optimization with a crack that growths from element 220 to 430 around 210 crack length increments are required, just saving the meshes requires 63 GB of RAM already.

No attempt to improve the mesh generation and saving was made because the current implementation is incompatible with any method that allows for crack steering. When the crack path can be changed by the optimization variables, the mesh of the current crack increment can only be determined after finishing the FEA calculation of the previous increment. This means that the mesh can only be generated in each increment.

Besides the memory requirement, the optimization requires a large computational effort as it needs to solve two systems of linear equations per crack length considered. For the problems solved in figs. 9.8 to 9.10 every iteration required around 13

[2] A optimization with a direct relation to crack growth rate can be formulated, where one minimizes the crack length at a certain amount of load cycles: $a = \int_{N_{\min}}^{N_{\max}} \mathrm{d}a/\mathrm{d}N \, \mathrm{d}N$ which relates to the area under the N-da/dN curve which similarly uncommon.

minutes on a pc with a Intel Xeon E5-1620 v2. The optimization required 12 days to converge, this is significantly longer than the 4 to 8 hours which is used in stress intensity minimization at the same resolution.

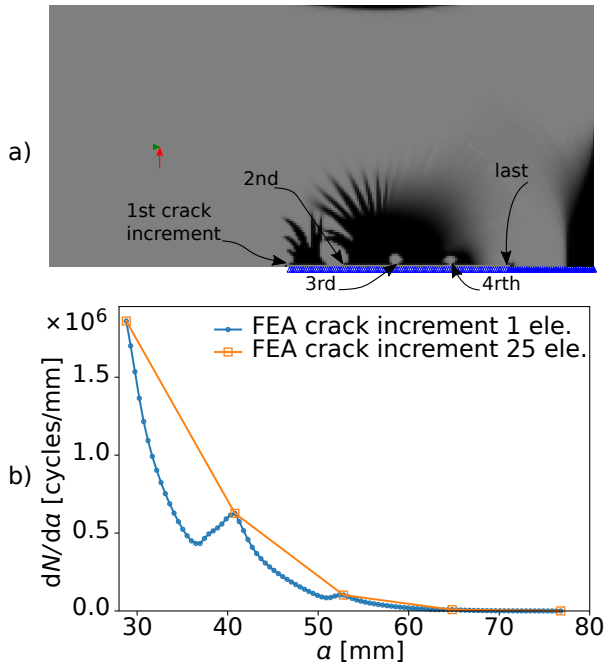

Figure 9.6: Optimization with large crack increments will result in poor designs. The area underneath the dN/da plot is clearly larger for the FEA with larger crack increments which was used in the optimization. The prediction with small increments size is an analysis of the same geometry.

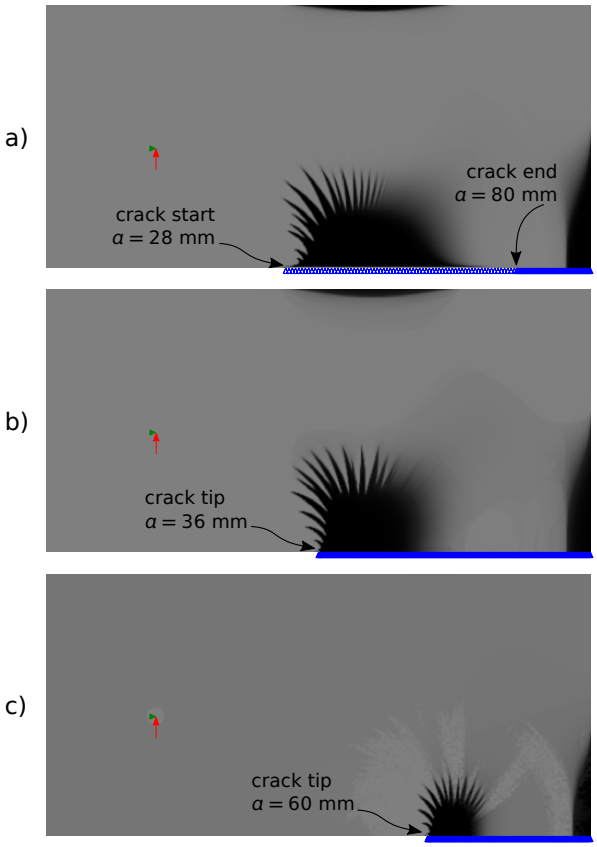

Figure 9.7: Comparing geometries of fatigue life and stress intensity maximization, where a) shows a fatigue life optimization, while b)&c) are results of stress intensity minimization.

To reduce both the memory and computational requirements one could use a crack increment that are larger than one element between every stress intensity calculation. Performing the calculation every two elements will already half the memory and computational requirements.

Taking crack length increments that are far greater than the element size will result in inaccurate fatigue life predictions which has a large effect on the optimization results. An optimization with large increments will design a structure that preforms well at the location where the stress intensity factors are calculated and neglect the rest. Figure 9.6a the result of an optimization with a crack increment of 25 elements is shown. A more accurate FEA with used crack increments of 1 element was run. The area under the dN/da curves in fig. 9.6b of the smaller crack increments is lower. This proves that taking to large increments will lead to degenerate designs of with performance is overestimated by the optimization.

From experience a crack increment of two elements can always be used without any artifacts appearing. This is also why the lines shown in figs. 9.8 to 9.10 are generated by calculating the stress intensity values every two elements.

Improving the computational efficiency should be a major focus before expanding the capabilities to higher resolution or 3D problems. One could consider improving the currently algorithm by using efficient FE problem solvers [49] and creating a parallel implementation [93] with for example the PETSc framework[3]. Another solution to reduce the computational requirement is to reduce the amount of FEA that need to be performed, for example by replacing them with more simple algebraic approximations. B. Herremans showed that an algebraic approximation of the fatigue performance could replace the FE model used in optimization algorithm, wile retaining accuracy. The original model (developed by J. Lu [12]) was to slow for high resolution problem, while the improved version could be run in a matter of seconds [71].

9.2.2 Results and comparison

When comparing a fatigue life maximization to stress intensity minimization results, surprising conclusions can be drawn. The fatigue life optimization result discussed in this section maximizes the amount of cycles required for a crack to grow from 28 to 80 mm. This was compared to a stress intensity minimization for a short crack and a long crack, with a crack

[3] Look for an example at TopOpt_in_PETSc or [94].

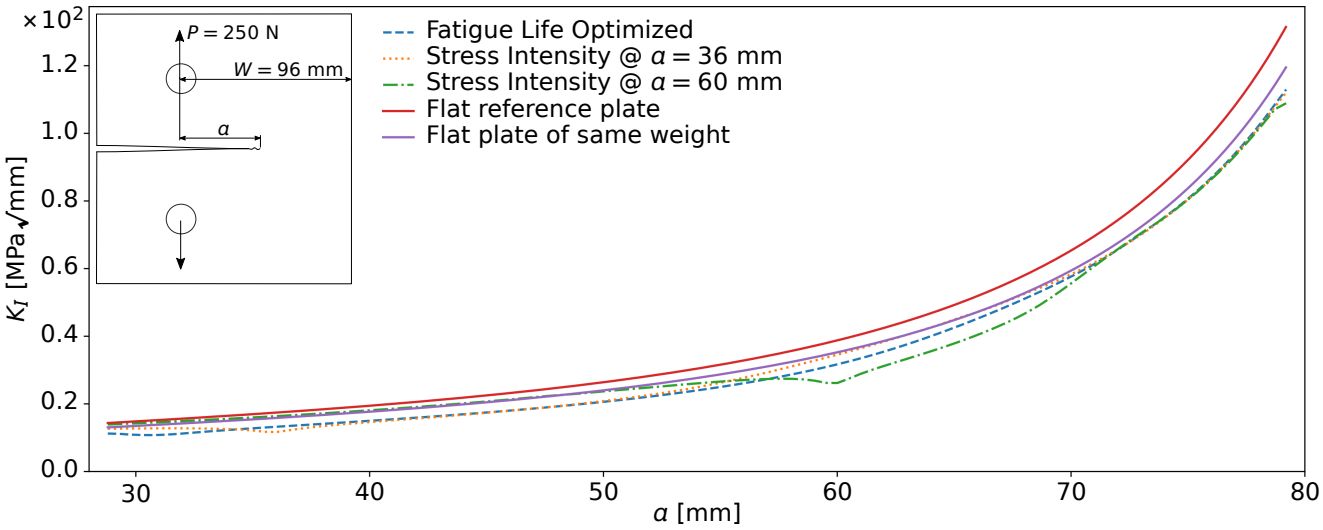

Figure 9.8: Comparing stress intensity as a function of crack length of fatigue life optimization results.

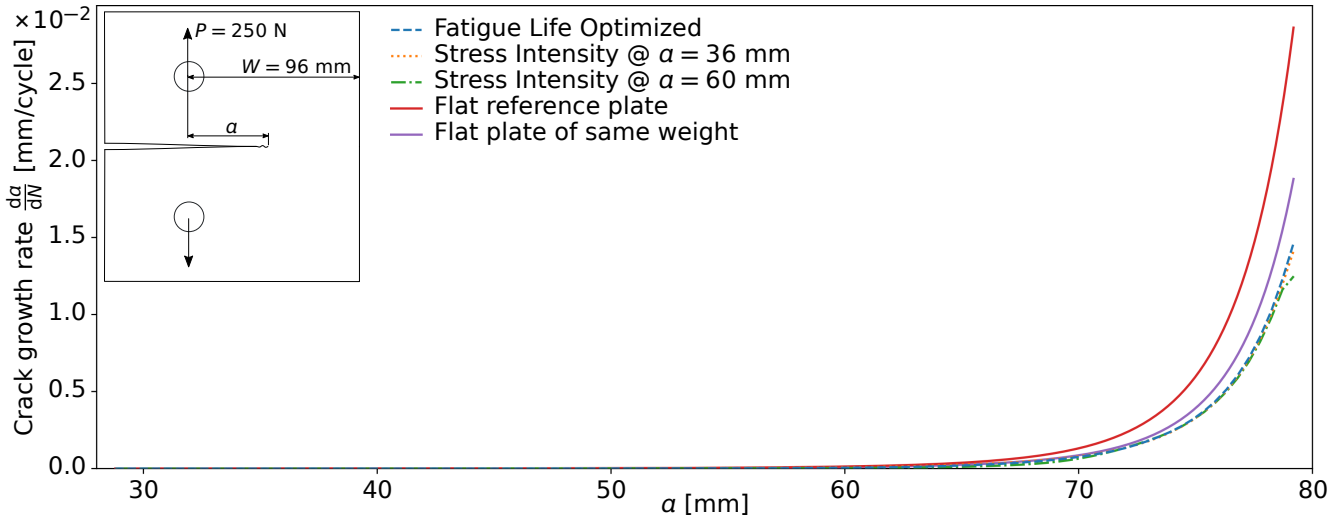

Figure 9.9: Comparing crack growth rate as a function of crack length of fatigue life optimization results.

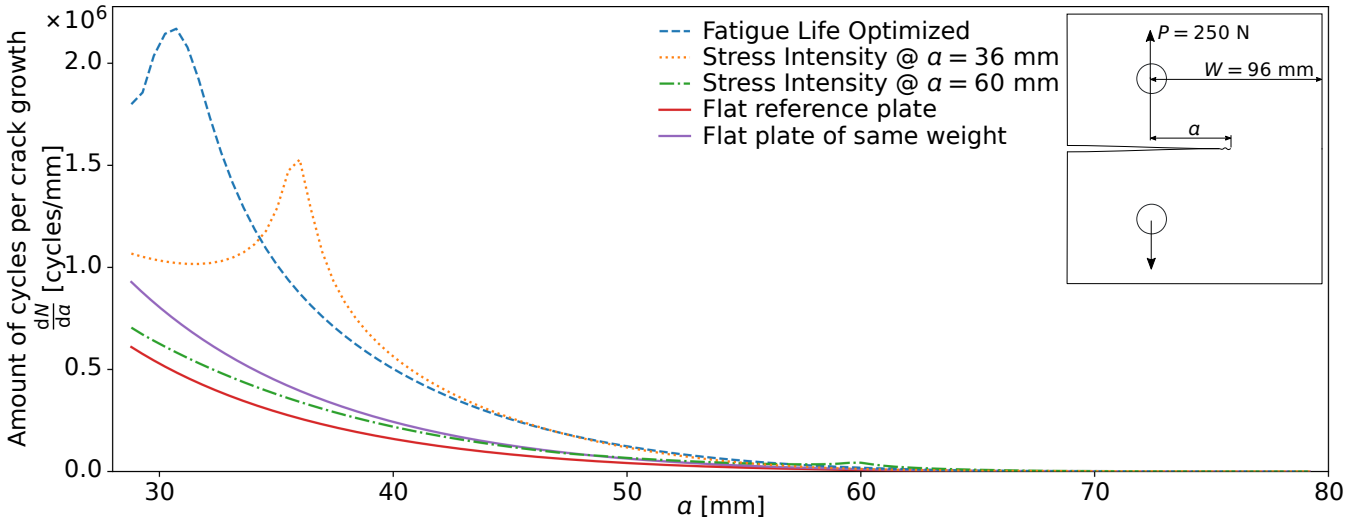

Figure 9.10: Comparing crack growth rate as a function of crack length of fatigue life optimization results.

tip at 36 and 60 mm respectively. For all these optimizations the local thickness was limited between $1 \leq X_e \leq 2$ with a resource constrain of 1.1. The geometries that where obtained from these optimizations are shown in fig. 9.7.

The final geometry of a fatigue life optimization has the same type of features that were observed in stress intensity minimization results. The fringing patterns, plateau and increased edge thickness do appear, although the plateau is a bit more stretched out. The plateau starts approximately 31 mm from the load introduction. A location close to that of the crack tip at the first increment. In the dN/da graph, fig. 9.10, this is also the location where a peak is observed.

The optimization seems to favor increasing fatigue resistance of the first crack increments over improving the performance for longer cracks. This causes the fatigue life maximized geometry in fig. 9.7a to be most similar to the stress intensity minimization with the short crack $a = 36$ mm of fig. 9.7b. The only clear difference between the stress intensity or dN/da graphs, figs. 9.8 and 9.10, is that the fatigue life optimization has the minimal stress intensity at an even shorter crack length.

Fatigue life is impacted more by the performance of the first crack length increments because the crack growth is slowest when a is small. This means that the crack tip stays longer in the area influenced by a feature such as a plateau. Besides reducing a low stress intensity factor has more impact that a relatively equal reduction for a higher stress intensity value, the difference is caused by the power in the Paris-Erdogan formula. This difference can be observed when the stress intensity graph, fig. 9.8, and dN/da graph, fig. 9.10, are compared. These effects are both amplified by the combined tension-bending behavior of the CT specimen. This causes the driving force and stress intensity factor to more steeply with crack length than for a load case that is tension dominated only.

These arguments do also explain the difference in fatigue life of the stress intensity minimization of short and long cracks (geometries shown in fig. 9.7b and fig. 9.7c). Figure 9.11 clearly shows that the fatigue life of the geometry with the stress intensity minimized for a crack of 36 mm is larger than that of the one optimized with the crack length $a = 60$ mm.

Most surprising is that the fatigue life of a geometry with a minimal stress intensity for $a = 36$ mm is comparable to the fatigue life optimized one. A stress intensity maximization with the crack tip placed 31 mm from the load introduction performed even better. Its fatigue life was just a couple of percentage smaller than that of the fatigue life maximized design. While the fatigue life of the stress intensity minimization with the long crack, $a = 60$ mm, is almost comparable to that of the flat reference plate. Even a flat plate of the same weight performs better.

It is hypothesized that crack steering needs to be allowed before fatigue life maximization outperforms stress intensity minimization significantly. Because the increase in computational effort, it is recommencement to not use the fatigue life maximization implementation. Running a stress intensity optimization with the crack tip positioned at the first increment will lead to a structure that performs well for a fraction of the computational time.

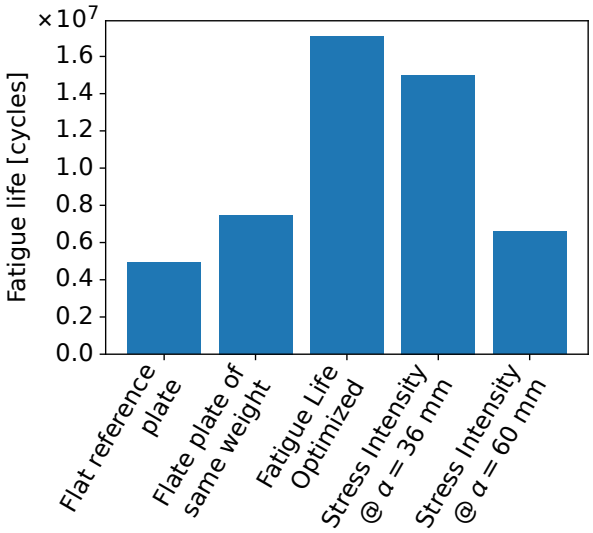

Figure 9.11: Performance comparison between fatigue life and stress intensity optimization.

Chapter 10

Designing discrete parts

The algorithm can design discrete parts such that the stress intensity at the crack tip is minimized. The difference with the previous chapter on variable thickness plate optimization is that the final geometries of this chapter are discrete, locally either having material or no material. Forcing the optimization into a discrete design was done by setting the SIMP penalization factor to $p = 3$, while the local density was constraint with $0 \leq X_e \leq 1$. When interpreting the results a 1 means that material is present and a 0 that the location is void.

To avoid checkerboard patterns a density filter was used. This causes gray scale areas to appear there where material borders empty areas. Because discrete designs are the objective, these gray areas have to be removed. This was achieved by altering the optimization settings in the last 200 iterations, the filter size was gradually reduced while the penalisation factor was increased to 4.

Two different cases are optimized for; the free and the infill design case. A description of the optimization settings for both cases is available in appendix A, which does also explain how the two cases are different. After sections 10.1 and 10.2 on stress intensity minimization, a small discussion about the difficulties of fatigue life maximization for discrete geometries will follow in section 10.3.

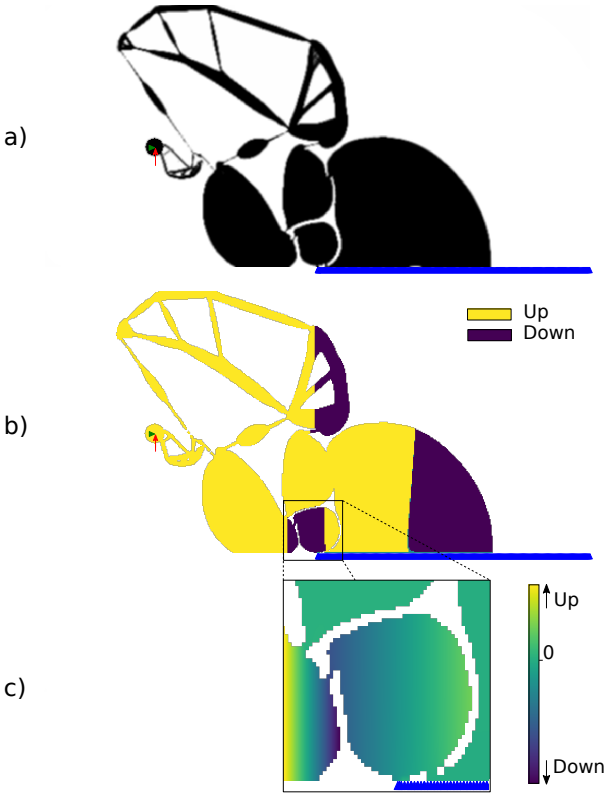

Figure 10.2: Optimized geometry without a base structure resulting in compliance mechanisms, where a) shows a optimized geometry for b) the displacement direction and c) the area where around the crack tip.

10.1 Free design

In the free design case the algorithm can distribute the mass throughout the entire design domain. The main problem of this optimization is that the final design deviates far from the initial one, which is a flat plate. This means that the stress state without crack will also change. If the stress state of the design without crack is different from the initial one the crack might initiate at another location making the optimization obsolete. The results of this optimization is interesting, because it gives insight to what the model determines as optimal in these extremely unconstrained conditions.

The optimizations in this section are following the compact tension specimen load case extensively discussed in the previous chapters. Some differences do exist, the SIMP penalization factor $p = 3$ and the local density is constraint between 0 and 1

These discrete optimizations without a base geometry results in a design with characteristics of compliance mechanisms. In fig. 10.2 an optimized geometry is shown, of this geometry the y displacement just before the crack tip is negative. This means that it moves down, 'closing' the crack. This mechanism operates by elastic deformation instead of rigid body movement, in which it is similar to compliance designs, discussed by T. Bruns and D. Tortorelli [60], or tHIhe MEMS actuator optimization examined by O. Sigmund [64, 65].

Before running the optimizations, the hypothesis was that the optimized geometry would disconnect the crack tip from the load introduction. As creating an alternative load path would reduce the stress inten-

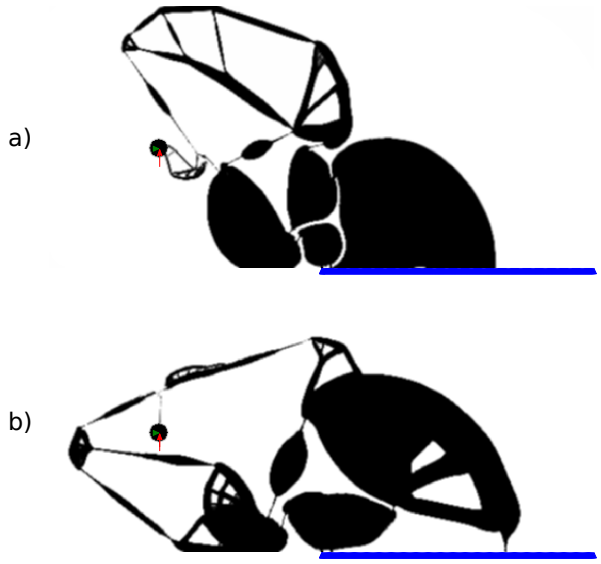

Figure 10.3: Optimized geometries without a base structure are sensitive to changes in the moving limit. The optimizations had a limit set to a) 1 and b) 0.125 which result in different designs.

sity at the crack tip to zero. These geometries did not appear however as these compliance mechanisms perform even better. The downward movement just before the crack tip will cause negative stress intensity factors.

A downward displacement along the crack is impossible, the material will come in contact with what is on the opposite side of the crack/symmetry axis. The model allows for these downward displacements because it lacks contact laws.

Nevertheless, these geometries would still perform well when contact is included. The contact causes the stresses around the crack tip to be compressive, which means that the crack tip is closed. In a closed crack purely compressive stresses will not cause any fatigue propagation, as the stress can be transferred from one side of the crack to the other without any effect of the singularity.

This does not mean that the designs obtained are optimal, as several weaknesses can be found in the model. Solutions to these problems need to be found before optimizing discrete structures that should be used in reality:

1. The crack might not initiate at the assumed location, because the stresses in the final design are very different from the initial one. This causes the optimization maximize the wrong objective.
2. These compliance mechanisms violate the assumption of small deformation because the geometry is designed to have large displacements. A geometrically non-linear FEA should be used.

Besides these issues it was surprising to see that the choice of moving limit has a large effect on the results. Its affect can be seen in fig. 10.3 where the resulting geometry of two simulations is shown. The only difference between them is the moving limit, a property which has no influence on the physical meaning of the problem. Its impact is on the implementation of the update-scheme only. The effect of moving limit changes on variable thickness plate optimization was small.

This setting limits the density change within an iteration. For large moving limits, not the moving limit but the asymptotic behavior of the MMA or the maximum/minimum density will be limiting the density changes. This means that a simulation with a tight moving limit will require more iterations to converge as smaller changes can be made per iteration. Sometimes optimization with differing moving limits will converge to solutions in different local minima. Surprising is, that the impact of this is much larger on the discrete optimizations than the variable thickness ones.

No investigation into why the optimization becomes so sensitive to the moving limit was performed, as it did not fall within the scope of this thesis. An investigation in this matter could lead to better understanding of the optimization method, its limitations and its interaction with the physical problem at hand.

10.2 Honeycomb infill

Designing an infill that is within an existing structure will have less of an impact on the stresses of the design. This makes infills less likely to violate the assumption that a crack initiates at the predicted location than the free design version.

Topology optimization is commonly used at the start of the design process to obtain concepts. The optimization results are then processed by an engineer so that it satisfies all requirements which where not taken in account by the algorithm.

This is different from the reinforcement method presented in this section. Here discussion is about reinforcing an existing design by adding extra features with an extra mass budget. The base geometry can be anything, for example, an existing part or a stress minimization result. Similar to normal topology optimization, the optimal design needs to be post processed. An engineer needs to alter the design so that it meets other requirements or manufacturing constraints.

This means that before running any optimization the base structure needs to be generated. A compact tension specimen with a honeycomb meta-material was used as a base design where the performance was improved by the optimization algorithm. Converting the honeycomb base geometry to a discrete version causes not only raged edges but also a change in volume fraction. This can also be observed when comparing figs. 10.4a and 10.4b. The courser the discretization the larger the differences with respect to the original base structure are. This was why a mesh of a high resolution, 1000 by 480 el-

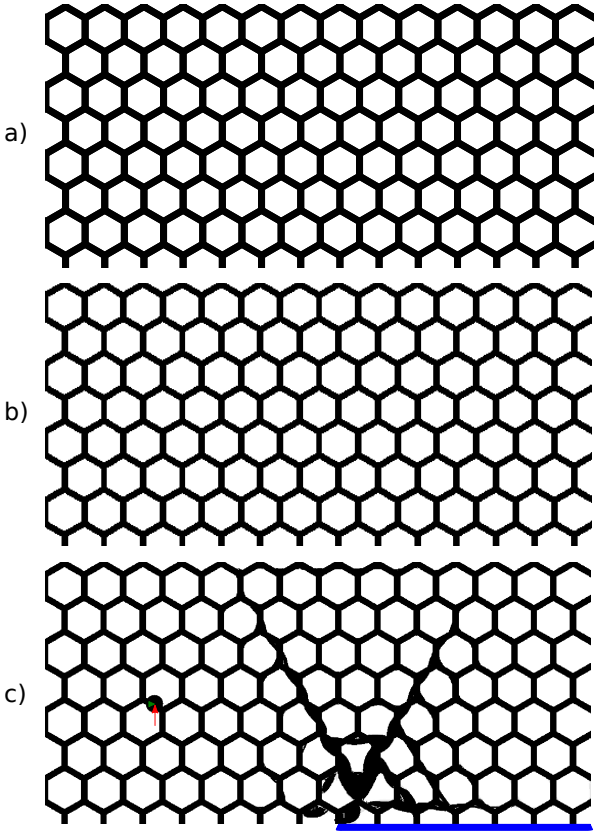

Figure 10.4: A honeycomb infill optimization and its base geometry. a) a base structure with volume fraction of 0.33, b) the discretized one, which due to rounding has a fraction of 0.30 and c) the optimization result shown has a fraction of 0.33.

ements, was used. The crack tip was moved a bit further away as the tip should be placed at a location with material. The tip was positioned there were the first ligament of the honeycomb was found after $a = 60$ mm ($a/W = 0.375$).

Honeycomb structures are anisotropic and multiple directions can be found. Two basic orientations were distinguished in this thesis, one with struts horizontal and one with struts vertical. Other orientations and its impact on fracture toughness are discussed by F. Lipperman, M. Rynvkin and M. B. Fuchs [95]. Figure 10.5 shows optimization results for these different orientations. The geometry in the top figure causes crack tip compression whereas the bottom one results in a stress intensity value that is close to zero. This demonstrate that orientation of honeycombs has an impact on the damage tolerance of the structure, even after infill optimization.

Significant improvements can be obtained, not only for the honeycombs designs discussed here, but for cellular solids in general. Compliance mechanisms that close the crack tip are observed. Adding a bit of mass is already enough, just increasing the volume fraction from 0.3 to 0.33, will cause the crack tip to close. Little extra material is required because these structures are very flexible on a local scale. These

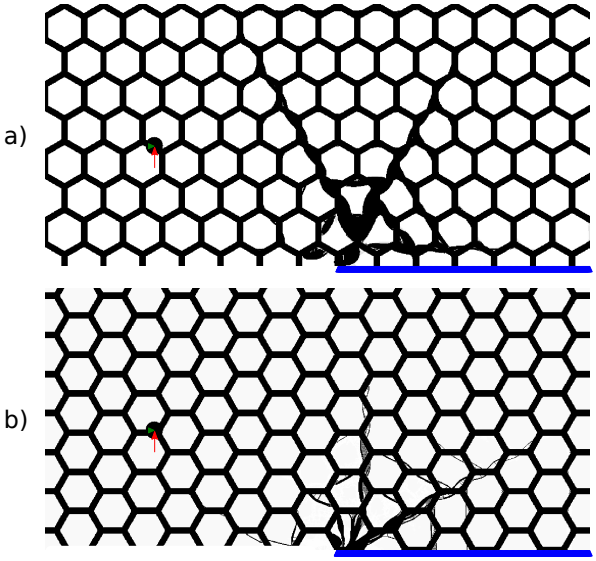

Figure 10.5: Optimization of honeycomb infill with different base structure orientation, a) one with vertical struts and b) one with horizontal struts.

cellular solids might be strong and stiff when looking at a large scale, but on a small scale the structure is compliant. This means that the stress intensity factor, a property of the local response around the crack tip, can be changed significantly.

This crack closure will increase the loads of the ligaments further in front, which will cause them to break before the crack tip ligament. This is similar to crack bridging which is known to improve the fracture toughness of materials such as bone [96], nacre [97], metal matrix composites [98], fiber composites [99] and many others.

10.3 Fatigue life problems

Fatigue life maximization of discrete structures is not possible with the current algorithm. Because of two reasons; stress intensity values at less than dense areas and crack initiation.

If the elements around the crack tip have a density value other than zero, the values of stress intensity cannot be calculated. This is caused by one of the current implementation limitations of these enriched elements. As mentioned in section 6.4, the thickness of an element at the crack tip must be unity. A discrete fatigue life optimization algorithm will try to place or remove material, also along the crack path. This would create voids or intermediate density values at a location where stress intensity calculations are performed which results in errors.

This problem does not exist when the optimization tries to reinforce a part were the crack path stays within an area with material. This is clearly not the case for the fully free and honeycomb designs discussed in this section.

The second problem is that the model presented cannot predict fatigue crack initiation, as that is not based upon stress intensity factors. The crack needs to reinitiate at every void it encounters, which can greatly increase the fatigue life. This initiation period can be quite significant and is the reason that honeycomb geometries are so fatigue resistant. The good fatigue performance of the cellular solids lay in the fact that reinitiation of the crack is required at every ligament.

A honeycomb infill optimization for fatigue life maximization should be based upon stress concentration instead of stress intensity factor minimization. The formulation of the algorithm could be similar to the one presented in this thesis, where the objective is to maximize the amount of cycles for the crack to propagate. For each ligament the amount of cycles for failure needs to be calculated by:

1. Calculating the stresses of the critical ligament.
2. Using the Wöhler curve equation to calculate the amount of cycles the ligament holds.
3. Breaking the ligament in question.

An attempt to maximizing the fracture resistance, not fatigue life, of honeycomb infill typologies can be made by altering the algorithm proposed by L. Xia, D. Ba and J. Yvonnet [75]. Their “Topology optimization for maximizing the fracture resistance of quasi-brittle composites” maximizes the fracture energy of the bi-material composite by distributing an inclusion material. Changing it from a bi-material model to an algorithm that considers one material with voids should be possible.

Part III

Conclusion, Discussion & Recommendations

Chapter 11

Discussion and conclusion

This thesis explored the opportunities that topology optimization (TO) offers to design fatigue crack growth resisting geometries. Hence, algorithms for stress intensity factor minimization and fatigue crack growth life maximization were developed. Physical tests were performed to verify the accuracy of the algorithms. While the performance of the algorithms was explored with examples.

The novelty of the method presented in this thesis is the combination of a FE crack tip enrichment technique and a topology optimization algorithm. The crack tip element enrichment method allows one to calculate the stress intensity factors directly from the FEA. This reduces the complexity of the optimization which results in a shorter the computational time and cost.

This method and the way it was implemented in a python program required several assumptions. The most important assumptions will be introduced before discussing the results,

- the crack path is known beforehand,
- the crack path will not cross elements,
- the crack tip is positioned at a node, and
- the enriched crack tip element thickness cannot change.

11.1 Finite element enrichment

The enriched FEA was based upon the method presented by S.E. Benzley [31] and L.N. Gifford [32]. It can model the discrete behavior at the crack tip by enriching a bicubic serendipity element, where the crack tip displacement field was derived with the Westergaard function method [33]. As a result the stress intensity factors K_I and K_{II} become degrees of freedom in the FEA. This means that solving the linear elastic FE problem directly calculates the stress intensity factors.

The implementation in this thesis assumes that the crack path is along element borders and that the crack tip is positioned on a node. The benefit of this method is that no mesh refinement around the crack tip is required. Little remeshing is needed when the crack increases in length. The only change required is shifting the degrees of freedom that are related to the enrichment.

In this thesis the implementation of this enriched FEM was simplified. All elements beside those at the crack tip were bilinear quadrilaterals. The higher order elements were connected to the surrounding ones with hanging nodes. This means that the mesh is non-conform and that the displacement field could potentially become discontinuous.

To validate the FEM, its enrichment and implementation, two steps were performed: Firstly, the results of the FE method were compared to algebraic results obtained from literature. Secondly, final geometries from optimizations were physically tested.

From the first step it was concluded that the stress intensity results of the FE enrichment method were accurate. At a converged mesh, the stress intensity factors of the compact tension, single and double edge crack specimens, were within 2 percent of their algebraic solutions.

In the second step the elastic response of the optimized geometries was predicted accurately. The fracture load was not, the FEA underestimated it. This fracture load is inversely proportional to the stress intensity factor. That specimens outperformed the predictions was most likely caused by a manufacturing inaccuracy. The stereolithography printer that build the part, made the thickness at the crack tip too large.

During these two validation steps, the following problems were encountered:

- Refining the mesh causes the model to represent a physically larger part, because the model does not transform from a local element to the global system. This changes the stress intensity factor as it is dependent on specimen size.
- The stress intensity factors required a finer mesh to converge in the implementation used in this thesis than in the enriched crack tip element literature. This is most likely caused by the hanging nodes in the mesh.
- The fracture load inaccuracy was caused by the crack tip element thickness. In the model this thickness was constraint to one while all surrounding elements where thicker, manufacturing this was impossible.

Despite these problems the enriched crack tip FE method could be used to calculate the stress intensity factors.

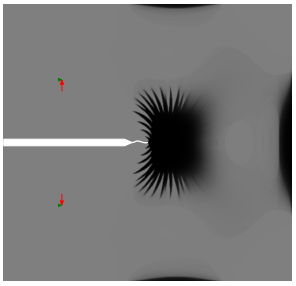

a) Variable thickness problem.

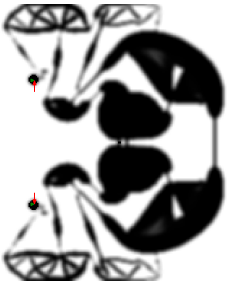

b) Discrete problem.

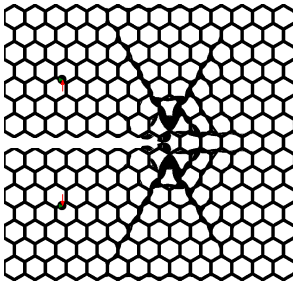

c) Honeycomb infill problem.

Figure 11.1: Three diferent types of optimizations were used for the evaluation and validation.

11.2 Stress intensity factor minimization

A stress intensity factor (SIF) minimization algorithm was developed. It used the enriched FEM to calculate the stress intensity factors. The sensitivity of the SIF to the design variables was calculated with an adjoint formulation. The local approximation and update scheme were based upon the method of moving asymptotes and a density filter was used to enforce checkerboard free designs.

The SIF minimization was performed with three different kinds of compact tension specimens.

- A variable thickness plate optimization where the design variables are the local thicknesses. The local thickness is constraint between a minimum and maximum. The result of such an optimization can be found in fig. 11.1a.
- A discrete optimization in which material is distributed throughout the design space. Here the SIMP penalization method is used to obtain a design that is discrete, as is shown in fig. 11.1b
- An infill optimization case which is similar to the discrete optimization problem. Here material is added to an existing geometry, while the existing geometry cannot be altered. Figure 11.1c shows how extra mass is distributed in a honeycomb base structure.

The evaluation of the optimization started with the variable thickness plate optimization. When the algorithm calculates the local plate thickness the results have a 20 to 40 percent lower stress intensity factor than plates of the same weight.

It was shown that increasing the amount of material available did not always result in better performing structures. This was already hypothesized and invalidates some reference studies. In those reference studies an algorithm was described, which assumed that (localy) adding material will result in better performance. This assumption is incorrect, because the optimization did not always use all material available. In those cases the resulting geometry reduced the thickness between the crack tip and load introduction. This will attract less load to the crack tip, reducing the stress intensity factor.

When designing discrete geometries, it was observed that the optimized geometries cause crack closure. The designs that appear are compliant mechanisms, which cause the crack tip to be compressed as much as possible, resulting in negative stress intensity factors. These compliance designs are more optimal than a geometry that avoids the crack tip and creates an alternative load path.

The assumed crack tip location, which was determined in advance, is most likely violated however. The stress distribution of these discrete designs is vastly different from the flat plate from which the crack tip location was derived. It is therefore unlikely that the crack would initiate at the location originally assumed. This means that the optimization minimizes the SIF of a crack that will not initiate and appear. Optimizing geometries this way will not lead to fracture resilient designs.

The third kind of SIF minimization attempted to design a discrete infill that would increase the fracture resistance of a honeycomb meta-material. It became apparent that these optimization techniques can cause great changes in the fracture mechanisms of these meta-materials. The algorithm utilizes that the local (deformation) behavior, that of one ligament, can easily be changed. The honeycomb material might be strong or stiff on a large scale, but reducing tension in the one ligament at the crack tip does not require much change to the overall geometry. For some cases increasing the volume fraction from 0.3, honeycomb only, to 0.33, honeycomb with infill, could cause crack closure mechanisms to appear already.

11.3 Fatigue crack growth life maximization

The fatigue crack growth life (FCGL) predictions were based upon a discrete summation of the Paris-Erdogan rule. This means that stress intensity factors need to be calculated for the crack at different lengths (crack increments). The design sensitivities were then derived and expressed in some summation of the stress intensity factor sensitivities.

The current implementation of the algorithm requires

the crack path to be known in advance. In general the crack path depends on the actual topology, causing it to change every iteration when the design is updated. This makes it impossible to determine the crack path before running the optimization, limiting the applicability of this optimization algorithm. The crack path for the symmetric compact tension specimen can be determined before running the FEA, as it is straight. Hence, optimizing the variable thickness compact tension specimen was possible.

The FCGL of optimized variable thickness plates outperform flat specimens of the same weight by two times. That improvements of 100 percent can be reached, is caused by the power in the Paris rule. A small reduction in a stress intensity factor will cause the crack growth to slow down significantly.

The computational effort required to perform this fatigue life maximization is large. To determine the FCGL, several FEA have to be run, namely one to determine the stress intensity factor of each crack increment. The optimization algorithm requires the sensitivity values, which adds an extra FEA per crack increment. As a result, the maximization of the FCGL requires a multitude of the number of computations when comparing it to stress intensity factor minimization.

The FCGL maximization offers little improvement compared to the stress intensity minimization. This was shown by comparing the FCGL of a stress intensity minimized and a FCGL maximized part. Here the crack length of the stress intensity minimization was set equal to that of the starting crack length of FCGL analysis. The difference in FCGL was small.

It was hypothesized that large improvements in FCGL will only be obtained when crack steering is implemented. However, this would require an optimization algorithm that considers the crack path direction. Making such an algorithm would require the implementation of a FEM where the crack path and tip can be anywhere and a sensitivity expression that includes the crack path dependency.

11.4 Discussion

The goal of this research was to explore the combination of topology optimization and the design of fatigue tolerant structures. It is the authors believe that better structures can be designed with the support of this type of algorithm. The resulting designs will outperform those that were designed with the traditional methods. Optimization leads to lighter constructions and longer inspection intervals, reducing the costs and environmental footprint.

Optimization is not so simple that a good design appears with the push of a button. The optimization needs to be set up carefully, putting rubbish in results in rubbish coming out. These algorithms do not produce final designs. Interpreting the results into a real design is required because the topology has; ragged edges and areas where it is unclear whether material is assigned or not. Optimization results can be used as inspiration or an initial design.

Two points need special attention when the results of the algorithms discussed in this thesis are processed; the crack tip location assumption and the existence of other failure modes.

It can be difficult to identify the crack tip location before starting the optimization, because the initiation and crack growth direction are influenced by the actual topology, which is still unknown beforehand. After running the optimization, the user is required to verify that the crack initiates at the assumed location.

The algorithm uses stress intensity factors only, no other requirements or failure modes are considered. The resulting designs might fail in failure modes, long before fatigue becomes critical. The design must be improved such that it will satisfy all other requirements. Example requirements are ultimate strength, stiffness and manufacturability.

11.5 Conclusion

The stess intensity minimization algorithm developed in this thesis performs well. It was proven that the crack tip enrichment method is accurate and that implementing it into topology optimization schemes is possible.

The method works best for the design of variable thickness plates, even when considering the assumptions mentioned before. It was proven that stress intensity factors can be reduced by 30 to 40 percent by using the TO algorithm. Designing discrete parts, allowing material do be distributed anywhere, is problematic. These geometries are so different from the original design that the crack will not initiate at locations originally assumed. This is in conflict with the crack path and crack tip assumptions. Using the algorithm to design an infill geometry of a honeycomb meta-material is very promising. Because of flexibility on a local scale, large improvements can be made for a very low weight penalty.

The fatigue crack growth life maximization algorithm works, but only for very specific cases. That the crack path needs to be predetermined does limit the applicability. This means that the optimization is unable to steer the crack. Crack steering could force the crack into a direction of reduced growth, resulting in better performing designs.

The potential of fatigue crack growth life maximization algorithms is large. It was show that, even in its current state, a variable thickness compact tension specimen can easily resist double the amount of load cycles than a flat specimen of the same weight. An improved formulation that can steer the crack might prove to be even more effective.

Chapter 12

Recommendations and future work

This thesis showed that it is possible to optimize structures to be fatigue resilient from a damage tolerance perspective. The algorithms developed for this thesis were used to explore the possibilities that this type of optimization offers. The algorithms and implementations are imperfect and several improvements can be made. These improvements would allow for the optimization of a larger variety of structures, resulting in an increase of the computational efficiency and a better optimization framework. Issues for with the solutions are straight forward or readily available, can be found in section 12.1.

Exploring the opportunities of topology optimization resulted in the discovery of several new research opportunities. These opportunities, discussed in section 12.2, differ from the recommendations because it is yet unclear how to reach their objectives. They could prove to greatly improve current damage tolerance optimization algorithms and result in more resilient designs.

12.1 Recommendations

The recommendations presented here should improve the capabilities of the algorithms when optimizing variable thickness plates. It shortly discusses its importance followed by a possible solution.

12.1.1 Improving the FEA

A coordinate system transformation between the local element and the global coordinates would simplify FEA mesh refinement studies. At the moment all elements have a size of 2×2 length units. Refining the mesh will increase the physical size of the part that is represented by the model. As stress intensity factors are dependent on the actual size, the results need to be scaled. The scaling method that is currently used, see section 8.1, cannot be used when the geometries are too complex. Adding a coordinate system transformation would be a more fundamental solution. Implementing this transformation would require one to perform actual (reduced Gaussian) integration when calculating the transformed element stiffness matrix.

Bicubic elements throughout the entire mesh will solve the hanging node issue, creating a conforming mesh. This would increase the accuracy of the FEA, reducing the amount of elements required for the stress intensity to converge with mesh size. The increased computational cost related to the increasing element order can be countered with the multi resolution optimization algorithm discussed below.

Crack(tip) inside elements would allow for a more flexible calculation of stress intensity values. Currently, the crack must be along element borders and the tip at a nodal location. Combining the crack tip enrichment method [31, 32, 80, 86, 100, 101] and XFEM [102] is proposed. An example of such a combination was developed by X.Y. Liu, Q.Z. Xiao and B.L. Karihaloo [35].

An efficient FE solver will reduce the computational time required by the optimization. The current solver is fast enough for the stress intensity minimization, which is optimized in a couple of hours, but is too slow for high resolution images, 3D problems or fatigue crack growth life optimizations. Implementing a multigrid conjugate gradient method will significantly reduce the amount of computations required [50]. Adopting iterative solvers for topology optimization specifically [51], can improve the efficiency even more. Such an efficient MG-cg method for topology optimization is discuses by O. Amir, N. Aage and B.S. Lazarov [49]. Other methods to improve the computational efficiency include, using a parallel framework [93, 103] such as PETSc [94] or approximations instead of the FEA [52, 71].

12.1.2 Improving the optimization

Higher order multi resolution optimization will increase the computational efficiency [104–106]. It has a finer design variables mesh than the FE mesh does [107, 108]. J. Groen, M. Langelaar, O. Sigmund and M. Ruess [81] found that using bicubic Legendre elements combined with 5×5 design variables per element is most efficient for 2D problems. This improvement can be used in combination with the one that proposed to use bicubic elements throughout the entire mesh. Be aware that in this thesis serendipity elements were used, whereas this multi-resolution scheme requires the use of Legendre elements.

Better filtering strategies will remove some artifacts that appear because of the density filtering

technique that the algorithms uses. A. Clausen and E. Andreassen criticized the basic sensitivity or density filter because of the use of homogeneous Neumann boundary conditions. They propose to use a padding around the design domain to get rid of these boundary effects [88].

A variable crack tip thickness could significantly improve the results of the FCGL maximization of variable thickness plates. It was shown that patterns of increased and decreased thickness on the crack path can increase the fatigue crack growth life of plates [12, 71]. Implementing variable crack tip thickness requires deriving $\partial K_e/\partial X_e$ for the enriched crack tip element suffices. But there is a high risk that the optimization results in invalid or unwanted geometries. Allowing the crack tip to be optimized might result in the total removal of material at the crack tip element. Properly constraining the crack tip thickness can solve this.

Adding a compliance constraint to the discrete optimization problems can be used to obtain more rigid designs. The discrete designs obtained in this thesis are not useful in normal design cases, they are to compliant. Z. Kang, P. Liu and M. Li [13] showed that stiffer designs can be obtained when the optimization considers the compliance. Adding (end-)compliance to the optimization can most easily be achieved by adding it as a constraint to the MMA update scheme.

Constraining the crack initiation location would eliminate the need to verify whether the crack initiated at the assumed location. This could be achieved by constraining the stresses locally [109–112]. This constraint is imposed on the topology without a crack. Relaxing the constraint at one location will lead to a design where the crack initiates at that location, because of the locally increased stresses.[1] Difficulties can be expected during the implementation of these constraints. Due to the local behavior these stress constraints are notoriously computational demanding and can even be unstable.

12.2 Future work

Based upon the experience obtained during this thesis three topics which require further investigation were identified. Their objective and need will be described in detail. The proposals will, if possible, advice on methods and point to literature available to solve problems that are likely to be encountered.

[1] Regarding stress minimization in general, these algorithms cause fatigue crack initiation to be equally unlikely in all places. Hence, the entire part has to be inspected instead of just the critical location. This would cause the duration of the inspection to increase, resulting in higher inspection costs and vehicle unavailability.

12.2.1 Extensive validation

One of the most obvious spin-offs would be to study the performance of this algorithm when optimizing for real design cases. This thesis focused on compact tension specimens solely. Working on other structures could provide new insights. Performing this extensive validation on SIF minimized variable plates is recommended. Because the SIF algorithm for variable thickness plates is most mature of all options presented in this thesis.

Special attention should be given to the validation of the fatigue crack initiation location. The algorithm has the crack set at a predetermined location. Its solution would be meaningless if in reality the optimized geometry will not have a crack propagate over that location. One could perform tests or calculate the stress field of optimized geometries without a crack and determine where the crack initiated. See for example the work of Z. Kang, P. Liu and M. Li [13].

The work of Z. Kang [13] describes an algorithm that minimizes both compliance and strain energy release rate for the discrete designs. Including compliance in the optimization causes the final designs to be more useful for structural applications. Adding compliance as an objective or constraint to the SIF minimization could result in similar designs. Due to the isotropic linear elastic fracture mechanics assumptions, the strain energy release rate and SIF are related to each other by material properties. That the goal is physically equivalent does not necessarily mean that the same results are obtained. Comparing the results of a SIF algorithm that considers compliance to those of Z. Kang could provide valuable insight. It would show the impact of a different mathematical representation for optimization with a physically equivalent objective.

Studying how sensitive the SIF would be if the crack tip were to deviate a bit from where it was assumed is advised. In two structures of the same design (small) variations in initiation and propagation of cracks can exist. This variation can come from; use, manufacturing differences and up to a certain extent even from stochastic phenomena. Hence, it would be unlikely for a crack to end up exactly there were predicted.

Using the optimization on real parts will also provide feedback to what improvements should be made. This will not only cause the algorithm to mature faster but also provide us with better understanding on its performance and capabilities.

12.2.2 Path independent formulation

One of the main drawbacks of the fatigue crack growth life maximization algorithm for variable thickness plates presented in this thesis, is that it is not crack-path independent. The results would be invalid if the crack path does not propagate through the optimal geometry as was originally assumed. This also means that it does not consider any crack steering

features. Allowing this crack steering could result in designs that perform significantly better.

There are two main directions leading to an algorithm that takes the path dependency into account. Both options have one thing in common; the entire fracture process needs to be seen as one problem. This in is contrast with the implementation of this thesis, where the FCGL problem is seen as a summation of the inverse crack growth rate.

The first option is using a non-local damage model. This is most similar to examples of topology optimization that solve the path dependency problem. Both the algorithms of K.A. James and H. Waisman [66] and that of L. Xia, D. Da and J. Yvonnet [75] use some type of local damage model. The main difficulty is in the calculation of the adjoint formulation of the sensitivities, but it is shown that it can be derived [113–115].

Another method would be to consider a local damage model, such as the Paris rule. One could try to maximize the amount of load cycles, before the stress intensity or strain energy release rate reaches a critical value. This type of implementation would require a FEA that allows cracks to cross elements and a crack tip that can be positioned anywhere. To reduce the complexity, it is recommended to use a model that can calculate the crack growth magnitude and direction with a formulation that is as concise as possible. For example, one could think of an XFEM formulation with a direct stress intensity calculation [35] and a mixed-mode crack propagation criterium [116, sec. 5.2]. Similar to the non-local damage methods, the main difficultly would be the adjoint equation derivation which allows for an efficient calculation of the sensitivities.

Implementing some of the recommendations presented in the previous section would be beneficial to both the local and non-local methods. Both methods will cause the computational effort to rise. Reducing the computational complexity can be achieved by implementing an efficient FE solver and higher order elements with a multi-resolution optimization method. Besides, creating a code where the thickness at the crack(tips) can vary is required as the crack tip can be positioned anywhere in this improved FCGL maximization algorithm.

12.2.3 Meta-material infill optimization

One of the problems studied in this thesis was stress intensity factor minimization for the infill of a honeycomb meta-material. The optimization results were promising. Changing the local behavior requires little extra material, while it had a large impact on the stress intensity factor. The problem was that the fatigue crack growth of these mata-materials cannot be described with the Paris rule. The fatigue resistance of these structures comes from the fact that reinitiation is required when the crack grows through a ligament.

Fatigue crack growth life optimization for infill design of these meta-materials should be based upon a repeated reinitiation process. A simplified and limited algorithm that requires the crack path to be known in advance could be developed relatively quickly, and would be similar to what this thesis presented. The Paris crack growth equation should be substituted by the Wöhler-curve, while stress intensity values need to be replaced by the stress at the current 'crack tip' ligament. The amount of cycles required to break one ligament can be calculated from the stress state and an equation from the Wöhler-curve, for example $N_i = W(\sigma_i)$. As the ligament is now broken, one needs to compute the number of cycles that the next ligament, crack increment, can withstand. In the end, the total fatigue life can be calculated with a summation of these ligaments breaking $N = \sum N_i$, the sensitivities can be derived from some type of summation of the sensitivities to the stresses at the different crack increments.

This method has the same problem as the FCGL maximization, namely the crack path needs to be predetermined and crack steering is not allowed. Creating a path independent method would be an improved formulation that is applicable to more (complex) design cases. One could consider an accumulative damage progressive failure model. An example of this is using a combination of Wöhler curve equations and the Miner's rule. The stiffness of an element should be reduced when the Miner's equation reaches one.

Bibliography

[1] C. Myant, J. Li, and B. Wu, "The Current Landscape for Additive Manufacturing Research," Imperial College London, Londen (UK), Tech. Rep., 2016, p. 83. [Online]. Available: http://hdl.handle.net/10044/1/39726.

[2] I. Gibson, D. Rosen, and B. Stucker, "Applications for Additive Manufacture," in *Additive Manufacturing Technologies*, 2nd, New York (NY): Springer, 2015, ch. 19, pp. 400–141, ISBN: 9781493921133.

[3] ProtoCAM, *Optimized 3D Print Production with Generative Design*, 2018. [Online]. Available: https://www.protocam.com/learningcenter/blog/generative-design/ (visited on 04/13/2019).

[4] M. Radny and D. Elbracht, *Additive Layer Manufacturing: A new Perspective in Structural Design*, 2012. [Online]. Available: http://www.3d-printing-additive-manufacturing.com/media/downloads/145-d2-14-30-a-radny-matthias-airbus.pdf (visited on 05/08/2019).

[5] M. Tomlin and J. Meyer, "Topology optimization of an Additive Layer Manufactured (ALM) aerospace part," in *Proceeding of the 7th Altair CAE Technology Conference*, Gaydon (UK), 2011, pp. 1–9. [Online]. Available: https://www.mmsonline.com/cdn/cms/uploadedFiles/Topology-Optimization-of-an-Additive-Layer-Manufactured-Aerospace-Part.pdf.

[6] M. P. Bendsøe and O. Sigmund, *Topology Optimization*. Berlin, Heidelberg: Springer Berlin Heidelberg, 2004, ISBN: 978-3-642-07698-5.

[7] O. Sigmund, "A 99 line topology optimization code written in matlab," *Structural and Multidisciplinary Optimization*, vol. 21, no. 2, pp. 120–127, 2001, ISSN: 1615147X.

[8] S. Turteltaub, "Optimal control and optimization of functionally graded materials for thermomechanical processes," *International Journal of Solids and Structures*, vol. 39, no. 12, pp. 3175–3197, Jun. 2002, ISSN: 00207683.

[9] M. P. Bendsøe and A. R. Díaz, "A method for treating damage related criteria in optimal topology design of continuum structures," *Structural Optimization*, vol. 16, no. 2-3, pp. 108–115, Oct. 1998, ISSN: 0934-4373.

[10] M. Seabra, J. Azevedo, A. Araújo, L. Reis, E. Pinto, N. Alves, R. Santos, and J. Pedro Mortágua, "Selective laser melting (SLM) and topology optimization for lighter aerospace componentes," *Procedia Structural Integrity*, vol. 1, pp. 289–296, 2016, ISSN: 24523216.

[11] D. Brackett, I. Ashcroft, and R. Hagues, "Topology optimization for additive manufacturing," in *Proceedings of the solid freeform fabrication symposium*, Austin (TX), 2011, pp. 348–362. [Online]. Available: http://sffsymposium.engr.utexas.edu/Manuscripts/2011/2011-27-Brackett.pdf.

[12] J. Lu, N. Kashaev, and N. Huber, "Crenellation Patterns for Fatigue Crack Retardation in Fuselage Panels Optimized via Genetic Algorithm," *Procedia Engineering*, vol. 114, pp. 248–254, 2016, ISSN: 18777058.

[13] Z. Kang, P. Liu, and M. Li, "Topology optimization considering fracture mechanics behaviors at specified locations," *Structural and Multidisciplinary Optimization*, vol. 55, no. 5, pp. 1847–1864, May 2017, ISSN: 1615-147X.

[14] R. P. Reed, J. H. Smith, and B. W. Christ, "The Economic Effects of Fracture in the United States," National Bureau of Standards, Washington (DC), Tech. Rep., 1983, p. 19. [Online]. Available: https://www.gpo.gov/fdsys/pkg/GOVPUB-C13-f4e5346c0d18781656463ed637910e99/pdf/GOVPUB-C13-f4e5346c0d18781656463ed637910e99.pdf.

[15] L. Faria, "The Economic Effects of Fracture in Europe," European Atomic Energy Community & Sticht-ing Voor Toepassing van Materialen, Delft (NL), Tech. Rep., 1991.

[16] J. Schijve, *Fatigue of Structures and Materials*, 1st. Dordrecht (NL): Springer, 2009, ISBN: 978-1-4020-6807-2.

[17] A. F. Blom, A. Hedlund, W. Zhao, and A. Fathulla, "Short fatigue crack growth behaviour in Al2024 and Al7475," in *The Behaviour of Short Fatigue Cracks*, K. J. Miller and E. R. de los Rios, Eds., EGF Pub.1, Londen (UK): Mechanical Engineering Publications, 1986, pp. 37–66. [Online]. Available: http://www.gruppofrattura.it/ocs/index.php/esis/EGF1/paper/download/9682/6393.

[18] L. Trško, M. Guagliano, O. Bokůvka, and F. Nový, "Fatigue life of AW 7075 Aluminium Alloy after Severe Shot Peening Treatment with Different Intensities," *Procedia Engineering*, vol. 74, pp. 246–252, 2014, ISSN: 18777058.

[19] C. R. Rice, J. L. Jackson, J. Bakuckas, and S. Thompson, *Metallic materials properties development and standardization (MMPDS-01)*, Washington (DC), 2003.

[20] G. R. Irwin, "Analysis of Stresses and Strains Near the End of a Crack Traversing a Plate," *Journal of Applied Mechanics*, vol. 24, pp. 361–364, 1957, ISSN: 04306252.

[21] P. C. Paris, M. Gomez, and W. Anderson, "A Rational Analytic Theory of Fatigue," *The trend in Engineering*, vol. 13, pp. 9–14, 1961, ISSN: 0742-4795.

[22] P. C. Paris and F. Erdogan, "A Critical Analysis of Crack Propagation Laws," *Journal of Basic Engineering*, vol. 85, no. 4, p. 528, 1963, ISSN: 00219223.

[23] D. L. Steadman, R. L. Carlson, and G. A. Kardomateas, "On the form of fatigue crack growth formulae," *International Journal of Fracture*, vol. 73, no. 4, R79–R81, Dec. 1995, ISSN: 0376-9429.

[24] H. Tada, P. C. Paris, and G. R. Irwin, "Stress Analysis Results for Common Test Specimen Configurations," in *The Stress Analysis of Cracks Handbook*, 3rd, New York (NY): ASME Press, 2000, pp. 39–80, ISBN: 0791801535.

[25] ASTM Standard E-1820, "E1820-18 Standard test method for measurement of fracture toughness," ASTM International, West Conshohocken (PA), Tech. Rep., 2018, pp. 1–55.

[26] S. K. Chan, I. S. Tuba, and W. K. Wilson, "On the finite element method in linear fracture mechanics," *Engineering Fracture Mechanics*, vol. 2, no. 1, pp. 1–17, 1970, ISSN: 00137944.

[27] G. Qian, V. F. González-Albuixech, M. Niffenegger, and E. Giner, "Comparison of KI calculation methods," *Engineering Fracture Mechanics*, vol. 156, pp. 52–67, 2016, ISSN: 00137944.

[28] A. F. Bower, "Modeling Material Failure," in *Applied Mechanics of Solids*, 1st, Baton Rouge (LA): CRC Press, 2009, pp. 547–613, ISBN: 9781439802489.

[29] G. Cherepanov, "Crack propagation in continuous media," *Journal of Applied Mathematics and Mechanics*, vol. 31, no. 3, pp. 503–512, Jan. 1967, ISSN: 00218928.

[30] J. R. Rice, "A Path Independent Integral and the Approximate Analysis of Strain Concentration by Notches and Cracks," *Journal of Applied Mechanics*, vol. 35, no. 2, p. 379, 1968, ISSN: 00218936.

[31] S. E. Benzley, "Representation of singularities with isoparametric finite elements," *International Journal for Numerical Methods in Engineering*, vol. 8, no. 3, pp. 537–545, 1974, ISSN: 0029-5981.

[32] L. Nash Gifford and P. D. Hilton, "Stress intensity factors by enriched finite elements," *Engineering Fracture Mechanics*, vol. 10, no. 3, pp. 485–496, Jan. 1978, ISSN: 00137944.

[33] H. M. Westergaard, "Bearing pressures and cracks," *Journal of Applied Mechanics*, vol. 6, A49–53, 1939.

[34] P. D. Hilton and B. V. Kiefer, "The Enriched Element for Finite Element Analysis of Three-Dimensional Elastic Crack Problems," *Journal of Pressure Vessel Technology*, vol. 102, no. 4, p. 347, 1980, ISSN: 00949930.

[35] X. Y. Liu, Q. Z. Xiao, and B. L. Karihaloo, "XFEM for direct evaluation of mixed mode SIFs in homogeneous and bi-materials," *International Journal for Numerical Methods in Engineering*, vol. 59, no. 8, pp. 1103–1118, Feb. 2004, ISSN: 0029-5981.

[36] M. P. Bendsøe, "Optimal shape design as a material distribution problem," *Structural Optimization*, vol. 1, no. 4, pp. 193–202, Dec. 1989, ISSN: 0934-4373.

[37] B. S. Lazarov and O. Sigmund, "Filters in topology optimization based on Helmholtz-type differential equations," *International Journal for Numerical Methods in Engineering*, vol. 86, no. 6, pp. 765–781, May 2011, ISSN: 00295981.

[38] E. Andreassen, A. Clausen, M. Schevenels, B. S. Lazarov, and O. Sigmund, "Efficient topology optimization in MATLAB using 88 lines of code," *Structural and Multidisciplinary Optimization*, vol. 43, no. 1, pp. 1–16, Jan. 2011, ISSN: 1615-147X.

[39] J. Wu, N. Aage, R. Westermann, and O. Sigmund, "Infill Optimization for Additive Manufacturing—Approaching Bone-Like Porous Structures," *IEEE Transactions on Visualization and Computer Graphics*, vol. 24, no. 2, pp. 1127–1140, Feb. 2018, ISSN: 1077-2626.

[40] T. Y. Chen and Y. H. Chiou, "Structural Topology Optimization Using Genetic Algorithms," *World Congress on Engineering*, vol. 3, 2013.

[41] M. Beckers, "Topology optimization using a dual method with discrete variables," *Structural Optimization*, vol. 17, no. 1, pp. 14–24, Feb. 1999, ISSN: 0934-4373.

[42] A. J. J. Lagerweij, *TopOpt 2D testing v0.10 @ github.com*, 2018. [Online]. Available: github.com/AJJLagerweij/topopt/releases/tag/v0.10 (visited on 08/20/2004).

[43] W. Li-Yi, *TopOpt @ github.com*, 2017. [Online]. Available: https://github.com/1iyiwei/topopt (visited on 08/20/2004).

[44] N. Olhoff and J. E. Taylor, "On Structural Optimization," *Journal of Applied Mechanics*, vol. 50, no. 4b, p. 1139, 1983, ISSN: 00218936.

[45] G. Strang and R. V. Kohn, "Optimal design in elasticity and plasticity," *International Journal for Numerical Methods in Engineering*, vol. 22, no. 1, pp. 183–188, Jan. 1986, ISSN: 0029-5981.

[46] R. V. Kohn and G. Strang, "Optimal design and relaxation of variational problems, I," *Communications on Pure and Applied Mathematics*, vol. 39, no. 1, pp. 113–137, 1986.

[47] M. P. Rossow and J. E. Taylor, "A Finite Element Method for the Optimal Design of Variable Thickness Sheets," *AIAA Journal*, vol. 11, no. 11, pp. 1566–1569, Nov. 1973, ISSN: 0001-1452.

[48] K. Svanberg, "The method of moving asymptotes - a new method for structural optimization," *International Journal for Numerical Methods in Engineering*, vol. 24, no. 2, pp. 359–373, Feb. 1987, ISSN: 10970207.

[49] O. Amir, N. Aage, and B. S. Lazarov, "On multigrid-CG for efficient topology optimization," *Structural and Multidisciplinary Optimization*, vol. 49, no. 5, pp. 815–829, May 2014, ISSN: 1615-147X.

[50] Y. Saad, "Multigrid Methods," in *Iterative methods for sparse linear systems*, 2nd, Society for Industrial and Applied Mathematics, 2003, ch. 13, pp. 423–464, ISBN: 9780898715347.

[51] O. Amir, M. Stolpe, and O. Sigmund, "Efficient use of iterative solvers in nested topology optimization," *Structural and Multidisciplinary Optimization*, vol. 42, no. 1, pp. 55–72, Jul. 2010, ISSN: 1615-147X.

[52] O. Amir and O. Sigmund, "On reducing computational effort in topology optimization: how far can we go?" *Structural and Multidisciplinary Optimization*, vol. 44, no. 1, pp. 25–29, Jul. 2011, ISSN: 1615-147X.

[53] K. Svanberg, "MMA and GCMMA – two methods for nonlinear optimization," KTH Royal Institute of Technology, Stockholm, Sweden, Tech. Rep., 2007, pp. 1–15.

[54] O. Sigmund and J. Petersson, "Numerical instabilities in topology optimization: A survey on procedures dealing with checkerboards, mesh-dependencies and local minima," *Structural Optimization*, vol. 16, no. 1, pp. 68–75, Aug. 1998, ISSN: 0934-4373.

[55] J. R. Smith, "Designing Biomorphs with an Interactive Genetic Algorithm," in *Proceedings of the 4th International Conference on Genetic Algorithms (ICGA-91)*, San Diego (CA): Morgan Kaufmann Publishers Inc., 1991, pp. 535–538. [Online]. Available: https://sensor.cs.washington.edu/pubs/biomorphs%7B%5C_%7Dnofigs.pdf.

[56] C. C. Lai and Y. C. Chen, "A User-Oriented Image Retrieval System Based on Interactive Genetic Algorithm," *IEEE Transactions on Instrumentation and Measurement*, vol. 60, no. 10, pp. 3318–3325, Oct. 2011, ISSN: 0018-9456.

[57] O. Sigmund, "Morphology-based black and white filters for topology optimization," *Structural and Multidisciplinary Optimization*, vol. 33, no. 4-5, pp. 401–424, Feb. 2007, ISSN: 1615-147X.

[58] ——, "Design of Material Structures Using Topology Optimization," PhD thesis, Technical University of Denmark, Dec. 1994.

[59] ——, "On the design of compliant mechanisms using topology optimization," *Mechanics of structures and machines*, vol. 25, no. 4, pp. 493–524, 1997, ISSN: 0890-5452.

[60] T. E. Bruns and D. A. Tortorelli, "Topology optimization of non-linear elastic structures and compliant mechanisms," *Computer Methods in Applied Mechanics and Engineering*, vol. 190, no. 26-27, pp. 3443–3459, Mar. 2001, ISSN: 00457825.

[61] B. Bourdin, "Filters in topology optimization," *International Journal for Numerical Methods in Engineering*, vol. 50, no. 9, pp. 2143–2158, Mar. 2001, ISSN: 0029-5981.

[62] A. R. Díaz and O. Sigmund, "Checkerboard patterns in layout optimization," *Structural Optimization*, vol. 10, no. 1, pp. 40–45, Aug. 1995, ISSN: 0934-4373.

[63] S. Turteltaub, "Functionally graded materials for prescribed field evolution," *Computer Methods in Applied Mechanics and Engineering*, vol. 191, no. 21-22, pp. 2283–2296, Mar. 2002, ISSN: 00457825.

[64] O. Sigmund, "Design of multiphysics actuators using topology optimization – Part I: One-material structures," *Computer Methods in Applied Mechanics and Engineering*, vol. 190, no. 49-50, pp. 6577–6604, Oct. 2001, ISSN: 00457825.

[65] ——, "Design of multiphysics actuators using topology optimization – Part II: Two-material structures," *Computer Methods in Applied Mechanics and Engineering*, vol. 190, no. 49-50, pp. 6605–6627, Oct. 2001, ISSN: 00457825.

[66] K. A. James, J. S. Hansen, and J. R. R. A. Martins, "Structural topology optimization for multiple load cases using a dynamic aggregation technique," *Engineering Optimization*, vol. 41, no. 12, pp. 1103–1118, 2009, ISSN: 0305215X.

[67] E. Nutu, "Multiple load case topology optimization based on bone mechanical adaptation theory," *UPB Scientific Bulletin, Series D: Mechanical Engineering*, vol. 77, no. 4, pp. 131–140, 2015, ISSN: 14542358.

[68] R. Jones, D. Peng, P. Chaperon, S. Pitt, D. Abramson, and T. Peachey, "Structural optimisation with damage tolerance constraints," *Theoretical and Applied Fracture Mechanics*, vol. 43, no. 1, pp. 133–155, Mar. 2005, ISSN: 01678442.

[69] R. Das, R. Jones, and D. Peng, "Optimisation of damage tolerant structures using a 3D biological algorithm," *Engineering Failure Analysis*, vol. 13, no. 3 SPEC. ISS. Pp. 362–379, 2006, ISSN: 13506307.

[70] M. Ayatollahi, S. Razavi, and H. Chamani, "Fatigue Life Extension by Crack Repair Using Stop-hole Technique under Pure Mode-I and Pure mode-II Loading Conditions," *Procedia Engineering*, vol. 74, pp. 18–21, 2014, ISSN: 18777058.

[71] B. Herremans, "Thickness distribution optimisation in flat panels for damage tolerance using genetic algorithms," Unpublished Master Thesis, Technical University of Delft, 2019.

[72] L. Li, G. Zhang, and K. Khandelwal, "Failure resistant topology optimization of structures using nonlocal elastoplastic-damage model," *Structural and Multidisciplinary Optimization*, Apr. 2018, ISSN: 16151488.

[73] M. Jansen, G. Lombaert, M. Schevenels, and O. Sigmund, "Topology optimization of fail-safe structures using a simplified local damage model," *Structural and Multidisciplinary Optimization*, vol. 49, no. 4, pp. 657–666, Apr. 2014, ISSN: 1615-147X.

[74] K. A. James and H. Waisman, "Failure mitigation in optimal topology design using a coupled nonlinear continuum damage model," *Computer Methods in Applied Mechanics and Engineering*, vol. 268, pp. 614–631, Jan. 2014, ISSN: 00457825.

[75] L. Xia, D. Da, and J. Yvonnet, "Topology optimization for maximizing the fracture resistance of quasi-brittle composites," *Computer Methods in Applied Mechanics and Engineering*, vol. 332, pp. 234–254, Apr. 2018, ISSN: 00457825.

[76] ASTM Standard D5045, "D5045-14 Standard Test Methods for Plane-Strain Fracture Toughness and Strain Energy Release Rate of Plastic Materials," ASTM International, West Conshohocken (PA), Tech. Rep., 2014, pp. 1–10.

[77] ASTM Standard E647-15e1, "Standard Test Method for Measurement of Fatigue Crack Growth Rates," ASTM International, West Conshohocken (PA), Tech. Rep., 2015, pp. 1–49.

[78] A. J. J. Lagerweij, *TopOpt 2D MSc thesis release v1.0 @ github.com*, 2019. [Online]. Available: https://github.com/AJJLagerweij/topopt/releases/tag/v1.0.

[79] O. Sigmund, N. Aage, and E. Andreassen, "On the (non-)optimality of Michell structures," *Structural and Multidisciplinary Optimization*, vol. 54, no. 2, pp. 361–373, 2016, ISSN: 16151488.

[80] O. C. Zienkiewicz, *The Finite Element Method In Engineering Science*. New York (NY): McGraw-Hill, 1971, ISBN: 0070941386.

[81] J. P. Groen, M. Langelaar, O. Sigmund, and M. Ruess, "Higher-order multi-resolution topology optimization using the finite cell method," *International Journal for Numerical Methods in Engineering*, vol. 110, no. 10, pp. 903–920, Jun. 2017, ISSN: 00295981.

[82] C. D. Rans, R. Rodi, and R. Alderliesten, "Analytical prediction of mode I stress intensity factors for cracked panels containing bonded stiffeners," *Engineering Fracture Mechanics*, vol. 97, no. 1, pp. 12–29, 2012, ISSN: 00137944.

[83] W. Wang, C. Rans, R. C. Alderliesten, and R. Benedictus, "Predicting the influence of discretely notched layers on fatigue crack growth in fibre metal laminates," *Engineering Fracture Mechanics*, vol. 145, pp. 1–14, 2015, ISSN: 00137944.

[84] K. S. Ravi Chandran and I. Barsoum, "Determination of stress intensity factor solutions for cracks in finite-width functionally graded materials," *International Journal of Fracture*, vol. 121, no. 3-4, pp. 183–203, 2003, ISSN: 03769429.

[85] A. Radman, X. Huang, and Y. M. Xie, "Maximizing stiffness of functionally graded materials with prescribed variation of thermal conductivity," *Computational Materials Science*, vol. 82, pp. 457–463, 2014, ISSN: 09270256.

[86] T. Belytschko and T. Black, "Elastic crack growth in finite elements with minimal remeshing," *International Journal for Numerical Methods in Engineering*, vol. 45, no. 5, pp. 601–620, Jun. 1999, ISSN: 0029-5981.

[87] P. E. Farrell, C. H. L. Beentjes, and Á. Birkisson, "The computation of disconnected bifurcation diagrams," pp. 1–20, Mar. 2016. arXiv: 1603.00809.

[88] A. Clausen and E. Andreassen, "On filter boundary conditions in topology optimization," *Structural and Multidisciplinary Optimization*, vol. 56, no. 5, pp. 1147–1155, Nov. 2017, ISSN: 1615-147X.

[89] V. Cain, L. Thijs, J. Van Humbeeck, B. Van Hooreweder, and R. Knutsen, "Crack propagation and fracture toughness of Ti6Al4V alloy produced by selective laser melting," *Additive Manufacturing*, vol. 5, pp. 68–76, Jan. 2015, ISSN: 22148604.

[90] A. J. J. Lagerweij, *Fatigue & Damage Tollerance in Topology Optimization @ OSF*, 2019. [Online]. Available: https://osf.io/psr5m/ (visited on 05/06/2019).

[91] F. Bernardini, J. Mittleman, H. Rushmeier, C. Silva, and G. Taubin, "The ball-pivoting algorithm for surface reconstruction," *IEEE Transactions on Visualization and Computer Graphics*, vol. 5, no. 4, pp. 349–359, 1999, ISSN: 10772626.

[92] P. Cignoni, M. Callieri, M. Corsini, M. Dellepiane, F. Ganovelli, and G. Ranzuglia, *MeshLab: an open-source mesh processing tool*, Pisa (Italy), 2008.

[93] N. Aage and B. S. Lazarov, "Parallel framework for topology optimization using the method of moving asymptotes," *Structural and Multidisciplinary Optimization*, vol. 47, no. 4, pp. 493–505, Apr. 2013, ISSN: 1615-147X.

[94] N. Aage, E. Andreassen, and B. S. Lazarov, "Topology optimization using PETSc: An easy-to-use, fully parallel, open source topology optimization framework," *Structural and Multidisciplinary Optimization*, vol. 51, no. 3, pp. 565–572, Mar. 2015, ISSN: 1615-147X.

[95] F. Lipperman, M. Ryvkin, and M. B. Fuchs, "Design of crack-resistant two-dimensional periodic cellular materials," *Journal of Mechanics of Materials and Structures*, vol. 4, no. 3, pp. 441–457, May 2009, ISSN: 1559-3959.

[96] R. O. Ritchie, M. J. Buehler, and P. Hansma, "Plasticity and toughness in bone," *Physics Today*, vol. 62, no. 6, pp. 41–47, Jun. 2009, ISSN: 0031-9228.

[97] F. Barthelat and H. D. Espinosa, "An Experimental Investigation of Deformation and Fracture of Nacre–Mother of Pearl," *Experimental Mechanics*, vol. 47, no. 3, pp. 311–324, May 2007, ISSN: 0014-4851.

[98] J. K. Shang and R. O. Ritchie, "Crack bridging by uncracked ligaments during fatigue-crack growth in SiC-reinforced aluminum-alloy composites," *Metallurgical Transactions A*, vol. 20, no. 5, pp. 897–908, May 1989, ISSN: 0360-2133.

[99] F. Zok and C. Hom, "Large scale bridging in brittle matrix composites," *Acta Metallurgica et Materialia*, vol. 38, no. 10, pp. 1895–1904, Oct. 1990, ISSN: 09567151.

[100] G. Heppler and J. S. Hansen, "Mixed mode fracture analysis of rectilinear anisotropic plates by high order finite elements," *International Journal for Numerical Methods in Engineering*, vol. 17, no. 3, pp. 445–464, Mar. 1981, ISSN: 0029-5981.

[101] P. R. Heyliger and R. D. Kriz, "Stress intensity factors by enriched mixed finite elements," *International Journal for Numerical Methods in Engineering*, vol. 28, no. 6, pp. 1461–1473, Jun. 1989, ISSN: 0029-5981.

[102] N. Moës, J. Dolbow, and T. Belytschko, "A finite element method for crack growth without remeshing," *International Journal for Numerical Methods in Engineering*, vol. 46, no. 1, pp. 131–150, 1999, ISSN: 00295981.

[103] S. Balay, S. Abhyankar, M. F. Adams, J. Brown, P. Brune, K. Buschelman, L. Dalcin, A. Dener, V. Eijkhout, W. Gropp, D. Kaushik, M. Knepley, D. May, L. C. McInnes, R. T. Mills, T. Munson, K. Rupp, P. Sanan, B. F. Smith, S. Zampini, H. Zhang, and H. Zhang, "PETSc Users Manual," Argonne National Laboratory, Lemont (IL), Tech. Rep. ANL-95/11 - Revision 3.11, 2019. [Online]. Available: http://www.mcs.anl.gov/petsc.

[104] J. Parvizian, A. Düster, and E. Rank, "Finite cell method," *Computational Mechanics*, vol. 41, no. 1, pp. 121–133, Sep. 2007, ISSN: 0178-7675.

[105] A. Düster, J. Parvizian, Z. Yang, and E. Rank, "The finite cell method for three-dimensional problems of solid mechanics," *Computer Methods in Applied Mechanics and Engineering*, vol. 197, no. 45-48, pp. 3768–3782, Aug. 2008, ISSN: 00457825.

[106] D. Schillinger and M. Ruess, "The Finite Cell Method: A Review in the Context of Higher-Order Structural Analysis of CAD and Image-Based Geometric Models," *Archives of Computational Methods in Engineering*, vol. 22, no. 3, pp. 391–455, Jul. 2015, ISSN: 1134-3060.

[107] T. H. Nguyen, G. H. Paulino, J. Song, and C. H. Le, "A computational paradigm for multiresolution topology optimization (MTOP)," *Structural and Multidisciplinary Optimization*, vol. 41, no. 4, pp. 525–539, Apr. 2010, ISSN: 1615-147X.

[108] J. Parvizian, A. Düster, and E. Rank, "Topology optimization using the finite cell method," *Optimization and Engineering*, vol. 13, no. 1, pp. 57–78, Mar. 2012, ISSN: 1389-4420.

[109] P. Duysinx and M. P. Bendsøe, "Topology optimization of continuum structures with local stress constraints," *International Journal for Numerical Methods in Engineering*, vol. 43, no. 8, pp. 1453–1478, Dec. 1998, ISSN: 0029-5981.

[110] Y. Luo, M. Y. Wang, and Z. Kang, "An enhanced aggregation method for topology optimization with local stress constraints," *Computer Methods in Applied Mechanics and Engineering*, vol. 254, pp. 31–41, Feb. 2013, ISSN: 00457825.

[111] H. Emmendoerfer and E. A. Fancello, "Topology optimization with local stress constraint based on level set evolution via reaction–diffusion," *Computer Methods in Applied Mechanics and Engineering*, vol. 305, pp. 62–88, Jun. 2016, ISSN: 00457825.

[112] D. Yang, H. Liu, W. Zhang, and S. Li, "Stress-constrained topology optimization based on maximum stress measures," *Computers & Structures*, vol. 198, pp. 23–39, Mar. 2018, ISSN: 00457949.

[113] J. Sobieszczanski-Sobieski, "Sensitivity of complex, internally coupled systems," *AIAA Journal*, vol. 28, no. 1, pp. 153–160, Jan. 1990, ISSN: 0001-1452.

[114] P. Michaleris, D. A. Tortorelli, and C. A. Vidal, "Tangent operators and design sensitivity formulations for transient non-linear coupled problems with applications to elastoplasticity," *International Journal for Numerical Methods in Engineering*, vol. 37, no. 14, pp. 2471–2499, Jul. 1994, ISSN: 0029-5981.

[115] S. Cho and H.-S. Jung, "Design sensitivity analysis and topology optimization of displacement–loaded non-linear structures," *Computer Methods in Applied Mechanics and Engineering*, vol. 192, no. 22-24, pp. 2539–2553, Jun. 2003, ISSN: 00457825.

[116] M. Malekan, L. L. Silva, F. B. Barros, R. L. Pitangueira, and S. S. Penna, "Two-dimensional fracture modeling with the generalized/extended finite element method: An object-oriented programming approach," *Advances in Engineering Software*, vol. 115, no. October 2017, pp. 168–193, 2018, ISSN: 18735339.

Appendix A

Optimization settings

The differences between the variable thickness plate, discrete and infill stress intensity factor minimization problems are discussed in this appendix. The objective of these problems are introduced and the settings of example optimizations will be discussed. Attention will be given to the differences between the problems, as they are caused by small changes in the settings.

A.1 Variable thickness plate

As the name suggests the goal is to obtain the design of a plate. It considers how to reinforce a flat reference plate. It will add material to the plate to improve its performance, by increasing the thickness locally. The local thicknesses are the design and optimization variables.

The model assumes that the element stiffness is directly proportionality to the local thickness. It will add material to an element to increase its stiffness. The local thickness can not be thinner than the reference plate, hence the minimum thickness is constraint with $X_{\text{min}} = 1$. A maximum local thickness constraint (X_{max}) was introduced to ensure that the part cannot become too thick. Setting the maximum thickness to two will allow the algorithm to design parts that are locally twice as thick as the reference plate.

In this optimization the volume fraction is used as a material constraint. It is relative to the amount of material of the reference plate. For the example case, table A.1, a volume fraction of 110% and a maximum thickness of 2 were used. The designs are allowed to use 10% more mass that the reference design. The optimization could decide to increase the local thickness to 1.1 everywhere. It could also increase the thickness of ten percent of the elements to 2 while keeping all other elements at a thickness of 1.

Figure A.1: Variable thickness plate optimization CT0053 result.

	Name	**Symbol**	**Python**	**Value**
Material	Young's modulus	E	`young`	1
	Zero stiffness	$E_{\min}$	`Emin`	1×10^{-9}
	Poisson's ratio	ν	`poisson`	0.3
Constraints	Volume fraction	V	`volfrac`	110%
	Minimum thickness	$X_{\min}$	`density_min`	1
	Maximum thickness	$X_{\max}$	`density_max`	2
	MMA moving limit	n.a.	`move`	0.25
Mesh	Reslution x direction	n.a.	`nelx`	500
	Resolution y direction	n.a.	`nely`	n.a.
	Crack length (elements)	n.a.	`crack_length`	250
Optimization	SIMP penalty factor	p	`penal`	1
	Filter type	n.a.	`filt`	'density'
	Filter radius	$r_{\min}$	`rmin`	1.5
	Max. number iterations	n.a.	`loopy`	5000
	Convergence limit	n.a.	`delta`	0.001
Output	Stress intensity itr. 1	$K_{I,1}$	`n.a`	0.2412
	Stress intensity itr. 100	$K_{I,10}$	`n.a.`	0.14
	Stress intensity end	K_I	`ki`	0.13
	Iteration end	n.a.	`itr`	1900
	Change of last itr.	n.a.	`n.a.`	0.001
	Time (seconds)	n.a.	`n.a.`	14479

Table A.1: Input and output variables for the variable thickness plate optimization CT0053.

A.2 Free discrete part

The discrete part optimization tries to improve the material distribution. It solves the problem where the design variables are binary either 0 (no-material) or 1 (material).

To steer the optimization to a discrete material distribution a penalization scheme is used. This method (SIMP) makes intermediate values perform unfavorable, hence these intermediate values are removed by the optimization. This SIMP method requires a penalization factor of 3 or higher, while the design variables are constraint between 0 and 1.

Figure A.2 shows gray areas between the white and black. There gray areas indicate that the design variables are in between 0 and 1. This behavior is caused by the density filter and is unwanted. Changes in settings were made during the optimization to reduce the impact of the filters. Table A.2 shows how the penalization factor was increased and the filter radius was decreased for the last 200 iterations. This should reduce the amount of intermediate density elements and results in a more clear design, as can be seen by comparing figs. A.2 and A.3.

Figure A.2: Discrete optimization CT Extreme 8 at the end of the first optimization (5000 itr.).

Figure A.3: Final result of CT Extreme 8 where the filter radius is incrementally decreased.

	Name	**Symbol**	**Python**	**Value**
Material	Young's modulus	E	`young`	1
	Zero stiffness	$E_{\min}$	`Emin`	1×10^{-9}
	Poisson's ratio	ν	`poisson`	0.3
Constraints	Volume fraction	V	`volfrac`	25%
	Minimum thickness	$X_{\min}$	`density_min`	0
	Maximum thickness	$X_{\max}$	`density_max`	1
	MMA moving limit	n.a.	`move`	1
Mesh	Reslution x direction	n.a.	`nelx`	500
	Resolution y direction	n.a.	`nely`	n.a.
	Crack length (elements)	n.a.	`crack_length`	250
Optimization 1	SIMP penalty factor	p	`penal`	3
	Filter type	n.a.	`filt`	'density'
	Filter radius	$r_{\min}$	`rmin`	8
	Max. number iterations	n.a.	`loopy`	5000
	Convergence limit	n.a.	`delta`	0.001
Optimization 2	SIMP penalty factor	p	`penal`	4
	Filter type	n.a.	`filt`	'density'
	Filter radius	$r_{\min}$	`rmin`	4
	Max. number iterations	n.a.	`loopy`	+100
	Convergence limit	n.a.	`delta`	0.001
Optimization 3	SIMP penalty factor	p	`penal`	4
	Filter type	n.a.	`filt`	'density'
	Filter radius	$r_{\min}$	`rmin`	2
	Max. number iterations	n.a.	`loopy`	+100
	Convergence limit	n.a.	`delta`	0.001
Output	Stress intensity itr. 1	$K_{I,1}$	`n.a`	4.54
	Stress intensity itr. 100	$K_{I,10}$	`n.a.`	-544.70
	Stress intensity end	K_I	`ki`	-7296.39
	Iteration end	n.a.	`itr`	5200
	Change of last itr.	n.a.	`n.a.`	0.164
	Time (seconds)	n.a.	`n.a.`	50681

Table A.2: Input and output variables for the discrete optimization CT Extreme 8.

A.3 Honeycomb infill

The honeycomb infill optimization will try to reinforce the honeycomb base structure. The settings are similar to the discrete optimization, because it considers the same material or no-material distribution problem.

To ensure that the honeycomb background structure remains intact they are introduced as passive elements. To find the location of the passive elements a python script[1] has been made. This script designs the honeycomb background in terms of cell size, orientation and volume fraction.

The only other difference is that the amount of elements was increased. This was required to have the algorithm design features inside the honeycomb cells.

[1] This scrip is available on OSF [90].

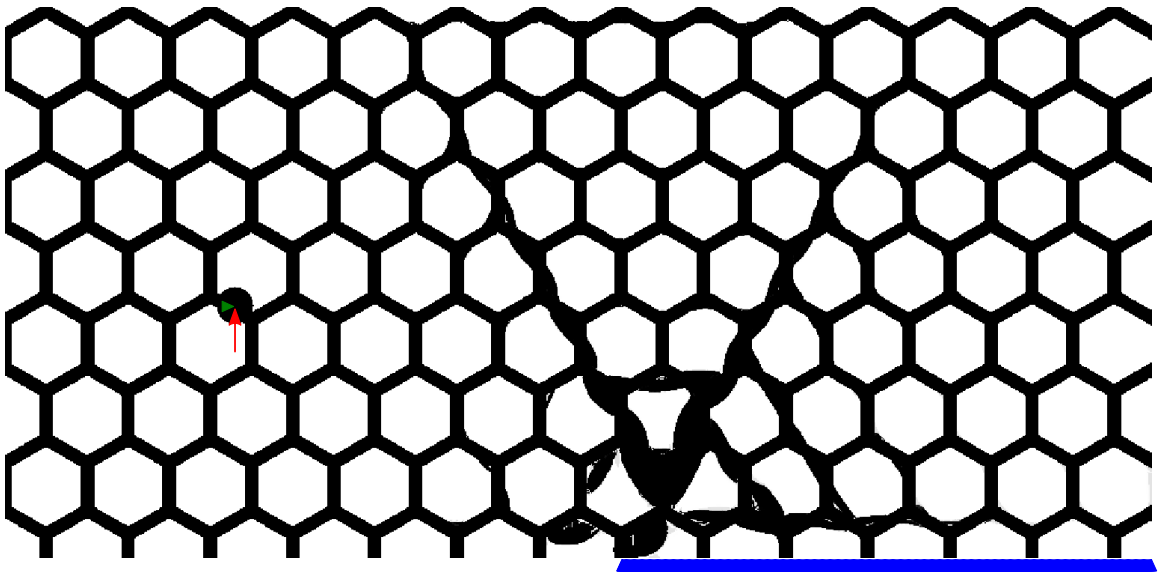

Figure A.4: Honeycomb infill result.

	Name	**Symbol**	**Python**	**Value**
Material	Young's modulus	E	`young`	1
	Zero stiffness	E_{min}	`Emin`	1×10^{-9}
	Poisson's ratio	ν	`poisson`	0.3
Constraints	Volume fraction	V	`volfrac`	25%
	Minimum thickness	X_{min}	`density_min`	0
	Maximum thickness	X_{max}	`density_max`	1
	MMA moving limit	n.a.	`move`	1
Mesh	Reslution x direction	n.a.	`nelx`	10000
	Resolution y direction	n.a.	`nely`	n.a.
	Crack length (elements)	n.a.	`crack_length`	538
Optimization 1	SIMP penalty factor	p	`penal`	3
	Filter type	n.a.	`filt`	'density'
	Filter radius	r_{min}	`rmin`	6
	Max. number iterations	n.a.	`loopy`	5000
	Convergence limit	n.a.	`delta`	0.001
Optimization 2	SIMP penalty factor	p	`penal`	3
	Filter type	n.a.	`filt`	'density'
	Filter radius	r_{min}	`rmin`	1
	Max. number iterations	n.a.	`loopy`	+500
	Convergence limit	n.a.	`delta`	0.001
Output	Stress intensity itr. 1	$K_{I,1}$	`n.a`	1.26
	Stress intensity itr. 100	$K_{I,10}$	`n.a.`	1.04
	Stress intensity end	K_I	`ki`	-0.02
	Iteration end	n.a.	`itr`	2489
	Change of last itr.	n.a.	`n.a.`	0.050
	Time (seconds)	n.a.	`n.a.`	95888

Table A.3: Input and output variables for the honeycomb infill optimization.

Appendix B

Background information of the figures

To ensure repeatability the optimization settings and their results where uploaded to OSF[1]. Table B.1 clarifies what scripts were used to generate each of the figures.

[1] See: https://osf.io/psr5m/.

Figure	Optimizations	Folder	Scrips
8.1	T0044-CT0055	CT_mesh_convergence.py	/mesh convergence/
8.2	CT0002-CT0043	Flat CT Validation.py	/Flat CT Validation/
8.3	DEC001-DEC008 & EC002-EC008	EC_DEC_mesh_convergence.py	/mesh convergence/
8.7, 8.8 & 8.9	CT0053-CT0055, CT0057, CT0058 & CT Flat	FEA: example.py	/Test Comparison/FEA/Python/
		Test data: process.py	/Test Comparison/Measure/
		Plotting: Graphs.py	/Test Comparison/
9.2	CT0053-CT0062 & CT Flat	Sensitivity.py	/Sensitivity study/
9.3	CT0053, CT0058 & CT0079-CT0088	Sensitivity.py	/Sensitivity study/
9.6	CT FL Stepsize1 & CT FL Stepsize2	Fatigue Life crack increments.py	/Fatigue Life crack increments/
9.8, 9.9, 9.10 & 9.11	CT0053, CT0090, CT Flat & CT Fatigue Life	Fatigue Life plots.py	/Fatigue Life Post Processing/
10.2	CT Extreme 8	example.py	/Displacemet Field/

Table B.1: The scripts used to generate the figures in this thesis.